Universidad Autónoma de Barcelona

Departamento de Física

Electrical Impedance of Normal and Ischemic Myocardium. Role on the Genesis of ST Segment changes and Ventricular Arrhythmias.

Tesis doctoral realizada por: Mark Warren Rodríguez

Co-directores: Juan Cinca Cuscullola, Profesor Titular del Departamento de Medicina de la Universidad Autónoma de Barcelona.

José Millán Gómez, Profesor de Investigación del Consejo Superior de Investigaciones Científicas

Septiembre de 1999

Juan Cinca Cuscullola, Profesor Titular del Departamento de Medicina de la Universidad Autónoma de Barcelona, y José Millán Gómez, Profesor de Investigación del Consejo Superior de Investigaciones Cientificas,

CERTIFICAN: Que la tesis doctoral "Electrical Impedance of Normal and Ischemic Myocardium. Role on the Genesis of ST Segment Changes and Ventricular Arrhythmias", presentada por Mark Warren Rodríguez para aspirar a grado de Doctor en Fisica, ha sido realizada bajo nuestra dirección.

Dr. Juan Cinca Cuscullola

Dr. José Millán Gómez

Barcelona, 17 de Septiembre de 1999

To Papa and Mama

Some thoughts on science and existence…

Al formular cualquier filosofia primera consideración siempre debe ser: ¿Qué podemos saber? Es decir, qué podemos estar seguros de saber, o seguros de que sabemos que sabíamos, si realmente es de algun modo "cognoscible". ¿O lo habremos olvidado todo y tenemos demasiada vergüenza de decir algo? Descartes insinuó el problema cuando escribió: "Mi mente jamás puede conocer mi cuerpo, aunque se ha hecho bastante amiga de mis piernas". Por "cognoscible", dicho sea de paso, no quiero decir aquello que pueda ser conocido por medio de la percepción de los sentidos o que puede ser comprendido por la mente, sino más bien aquello que puede decirse que es Conocido o que posee un Conocimiento o una Conocibilidad, o algo que al menos puedas mencionar a un amigo.

¿Podemos en realidad "conocer" el universo? Dios santo, no perderse en Chinatown ya es bastante difícil. Sin embargo, el asunto es el siguiente: ¿Habrá algo allá fuera? ¿Y por qué? ¿Por qué tendrán que hacer tanto ruido? Por útimo, no cabe duda de que la característica de la "realidad"es que carece de esencia. Esto no quiere decir que no tenga esencia, sino simplemente que carece de ella. (La realidad a la que me refiero es la misma que describió Hobbes, pero un poco más pequeña.) Por lo tanto, el *dictum* cartesiano, "Pienso, luego existo", podría expresarse mejor por "¡Eh, alli va Edna con el saxofón!". Así pues, para conocer una sustancia o una idea, debemos dudar de ella y así, al dudar, llegamos a percibir las cualidades que posee en su estado finito, que estan en, o son realmente "la misma cosa", o "de la misma cosa", o de algo, o de nada. Si esto está claro, podemos dejar por el momento la epistalmología.

"*Como acabar de una vez por todas con la cultura***"**

Woody Allen

Agraïments

Voldria agrair al Dr. Cinca i al Dr. Millán per haver-me introduït en aquest apassionant món de la recerca. Han sigut moltes hores de discussions, experiments, abstracts i articles... He après molt, i estic segur de que les duré sempre amb mi.

Un record molt especial per tota (i han sigut molts) la gent que hi és o ha passat pel laboratori A de Cardiologia Experimental. Amb tots vosaltres he après ciència, i molt més! Com sou molts, us poso amb ordre anti-cronològic: Ana Carreño, Antonio Rodríguez, Bea Rodrigo, Maria Durán, Cora Verduyn, Miquel Coll, Dr. Anivarro Màrius Tresànchez, Josep Mª Bis, Juan Masdeu, Mª Angeles Yáñez, Jordi López Ayerbe, Cristina Moure, Pilar Gómez, Anton Soler, Jordi Merçè, Xavi Gironés, Pere Blanch, Lluís Mont, Alfredo Soldevilla, Alfons Tàpies, Josep Rodés, Bernat Romero, Josep Guiu, Mª Dolres Alvarez, Jordi Ribó, Toni Nicolás, Alfredo Bardají.

A la gent que tot i no sent del laboratori han estat per aquí (al laboratori) d'alguna manera o un altre: Bernardo Pollo, Dani Chillida, Javier de la Torre, Elisabeth Gutierrez, Xavi Gomis, Ramón Bosch.

Al Ramón Bragós, Oscar Casas, Xavi Rosell, Miguel Angel Garcia, i Pere Riu de la UPC. Gràcies per portar-me fins a les fronteres més llunyanes del mon de la impedància elèctrica.

A la gent del CNM i del projecte MicroCard per l'esforç que estan fent per a que tot això s'apliqui algun dia al món real.

Gràcies també a la gent del Laboratori B de Cardiologia Experimental per tenir les seves portes sempre obertes, i al Servei de Cardiologia i al Dr. Soler per fer que tota aquesta aventura hagi sigut possible.

Al Dr Juan Muñoz li voldria agrair haver-me transmès la seva passió pel món de l'electricitat ja des de segon de carrera.

Finalment, m'agradaria agrair a la Kate Leigh per haver-se llegit i corregit l'estil d'una tesi que no te absolutament rès que veure amb lo que ella estudia, i també als membres del tribunal per fer l'esforç de llegir-la en anglès.

Index

Publications and abstracts presented in international congresses related to the thesis:

Chapter 3: Cinca J., Warren M., Carreño A., Tresànchez M., Armadans L., Gómez P., Soler-Soler J. Changes in myocardial electrical impedance induced by coronary artery occlusion in pigs with and without preconditioning. Correlation with local ST segment potential and ventricular arrhythmias. *Circulation*. 1997; 96:3079-3086

M. Warren, J. Cinca, A. Carreño, P. Gómez, P. Blanch, J. Soler-Soler. Ischemic preconditioning delays cellular uncoupling and phase Ib arrhythmias during acute coronary occlusion in swine. *European Heart Journal*, 1997:18 (abstract supplement);164

M. Warren, O. Casas, R. Bragós, M. Tresànchez, A. Carreño, A. Rodríguez-Sinovas, A. Yáñez, J. Rosell, P. Riu, J. Cinca. Timecourse of myocardial tissue electrical impedance during ischemia and reperfusion in in vivo pig hearts. *Proceedings of the X International conference on electrical bio-impedance in Barcelona* 1998, p. 81-82

Chapter 4: Cinca J., Warren M., Tresànchez M., Rodríguez-Sinovas A., Carreño A., Bragós R., Casas O., Domingo A., Soler-Soler J. Passive transmission of ischemic ST segment changes in low electrical resistance myocardial infarct scar in the pig. *Cardiovascular Research* 1998;40:103-112

M. Warren, J. Cinca, R. Bragós, O. Casas, M. Tresànchez, A. Rodriguez-Sinovas, A. Carreño, J. Soler-Soler. Electrical properties of transmural infarct scar in swine. *European Heart Journal*, 1997:18 (abstract supplement);164

M. Warren, M. Tresànchez, J. Cinca, A. Carreño, A. Rodríguez-Sinovas, P. Gómez, J. Soler-Soler. The role of the low resistive myocardial infarct scar on the ST segment potential transmission during periinfarction ischemia; its potential role on arrhythmogenesis. *Medical & Biological Engineering & Computing*, 1997: 35 (Supplement I), p 335

Chapter 5: Mark Warren, Ramón Bragós, Oscar Casas, Antonio Rodríguez-Sinovas, Javier Rosell, Inocencio Anivarro, Juan Cinca. Percutaneous Electrocatheter Technique for On-line Detection of Healed Transmural Myocardial Infarction. (submitted)

List of abbreviations and symbols used throughout the thesis

ANOVA: Analysis of variance
APD: Action potential duration
ATP: Adenosine triphosphate.
AV: Atrio-ventricular
bmp: Beats per minute
cAMP: Cyclic adenosine monophosphate
cGMP: Cyclic guanosine monophosphate
DAD: Delayed afterdepolarisation
DC: Direct current
EAD: Early afterdepolarisation
ECG: Electrocardiogram
IM: Intramyocardial
IV: Intraventricular
LAD: Left anterior descending
LV: Left ventricle
NMR: Nuclear magnetic resonance
PR: Interval between the P deflection and the R deflection of the ECG
QRS: Deflection of the ECG composed by the Q, R, and S deflections
SA: Sino atrial
ST: Interval between the S deflection and the T deflection of the ECG
TQ: Interval between the T deflection and the Q deflection
VF: Ventricular fibrillation
VPB: Ventricular premature beat
VT: Ventricular tachycardia
Ca^{2+}: Calcium ion
Cl^{-}: Chloride ion
K^{+}: Potassium ion
Na^{+}: Sodium ion
pH_e: Extracellular proton concentration
pH_i: Intracellular proton concentration
E_{Na}: Nernst equilibrium potential of sodium
E_K: Nernst equilibrium potential of potassium
E_{Ca}: Nernst equilibrium potential of calcium
E_{Cl}: Nernst equilibrium potential of chloride
E_p: Nernst equilibrium potential of ionic species p
I_p: ionic current of ionic species p
g_p: Conductance of ionic channel of ionic species m
$m(t,V_m)$: scalar parameter describing sodium channel dynamics
$h(t,V_m)$: scalar parameter describing sodium channel dynamics

$j(t,V_m)$: scalar parameter describing sodium channel dynamics
$x(t,V_m)$: scalar parameter describing sodium channel dynamics
$d(t,V_m)$: scalar parameter describing sodium channel dynamics
$f(t,V_m)$: scalar parameter describing sodium channel dynamics
c_m: Membrane capacitance
r_n: Nexal resistance in the two isolated myocytes experimental model
r_e: Extracellular resistance
r_i: Intracellular resistance
r_m: Membrane resistance
V_m: Transmembrane potential
V_r: Resting membrane potential
V_e : Extracellular voltage
V_i : Intracellular voltage
V_{max}: Transmembrane action potential maximum upstroke velocity
V_{eq}: Nernst equilibrium potential
I_i: Intracellular current
I_e: Extracellular current
I_c: Transmembrane capacitative current
λ: Length constant
τ: Time constant
Θ: Velocity of propagation of the excitation wavefront
τ_{foot}: Time constant of exponentially rising action potential
σ: Conductivity
ε: Permitivitty
μ: Permeability
$\mathbf{E}$: Electric field
$\mathbf{B}$: Magnetic field
$\mathbf{D}$: Displacement vector
$\mathbf{J}$: Electric current density
ω: Frequency of the electromagnetic field
I: Electric current
V: Voltage
Z: Electric impedance
R: Resistance
X: Reactance
M: Modulus of electrical impedance
Φ: Phase angle of electrical impedance
R_e: Equivalent extracellular resistance
R_i: Equivalent intracellular resistance
C_m: Equivalent membrane capacitance
ε_s: Low frequency limit of complex dielectric constant

List of abreviations

ε_∞: High frequency limit of complex dielectric constant
α: Empirical parameter of the Cole-Cole equation
R_o: Resistance at 0 Hz
R_∞: Resistance at a frequency approximating ∞
σ_e: Extracellular conductivity tensor of the bidomain model
σ_i: Intracellular conductivity tensor of the bidomain model
g_{el}: Effective extracellular longitudinal conductivity
g_{et}: Effective extracellular transversal conductivity
g_{il}: Effective intracellular longitudinal conductivity
g_{it}: Effective intracellular transversal conductivity
G: Gap junction conductance
k: Fraction of the cross sectional area of the intracellular space withg respect to the extracellular space

GENERAL INTRODUCTION AND OUTLINE OF THE THESIS

Mortality caused by cardiovascular diseases represented 37% of the overall mortality in Catalonia in 1994. Among these deaths, 27% were due to ischemic heart disease [1]. Myocardial ischemia results in four basic clinical syndromes which are angina pectoris, myocardial infarction, heart failure, and sudden cardiac death [2]. Ischemia is defined as a desiquilibrium between the oxygen required for the normal cellular metabolic function and that supplied by the coronary blood flow [3]. In the past few years other ischemia related syndromes have been characterised such as: myocardial stunning, hibernation, preconditioning, or silent ischemia [4].

From the basic pathophysiology point of view acute myocardial ischemia causes a series of metabolic, ionic, neurohumoral, and structural alterations that result in changes in the electrophysiological and mechanical function of the heart. These changes are manifested in membrane patches, single cells, isolated fibres, or intact hearts as alterations in the functional characteristics of ionic channels and pumps. The electrophysiological consequences are alterations in resting membrane potential, action potential, conduction, refractoriness, automaticity, in the electrical passive properties, and finally the development of arrhythmias. Knowledge of the basic alterations taking place during acute and chronic infarction is mandatory for development of new diagnostic and therapeutic targets.

The main objective of this thesis is to study the alterations of the passive electrical properties of the myocardium during coronary artery occlusion. More specifically, their role on the pathogenesis of arrhythmias and on the transmission of injury currents during the acute and chronic stages of infarction. Since myocardial infarction is a dynamic process that spans various weeks or even months, the thesis focuses on two time windows, namely: a) the acute stages of infarction -i.e. the first 4 hours after the onset of myocardial ischemia, and b) the chronic stages of myocardial infarction -one to two months after the onset of coronary occlusion.

Due to the interdisciplinary character of this thesis, the first chapter is a broad review of the basic concepts of cardiac electrophysiology. A special effort is made in distinguishing between the active and passive electrical properties of the myocardium, giving emphasis on the role of the passive electrical properties in the normal cardiac function. Finally, the electrophysiological alterations taking place during the acute and chronic stages of myocardial infarction are reviewed in detail.

In the second chapter a description of the materials and methods used throughout the thesis is provided. However, the experimental protocol followed in each of the studies which form the thesis is detailed in each corresponding chapter.

The third chapter is dedicated to the study of the alterations of tissue electrical impedance that take place during the acute stages of myocardial infarction. An analysis of the biological meaning of both the resistivity and the phase angle components of tissue impedance measured at 1 kHz is made. The alterations of both these parameters during the initial stages of the ischemic insult are correlated with the incidence of ventricular arrhythmias occurring during this period. Moreover, a correlation with the changes in the epicardial electrical potentials is performed. Specifically, the changes in ST segment elevation which have been related to the circulation of injury currents during acute ischemia are considered.

In the fourth chapter, the passive electrical properties of the chronic transmural myocardial infarction are studied. For a more complete characterisation of the passive electrical properties of normal and infarcted myocardium, tissue impedance is measured in a broad range of frequencies. The biological meaning of the impedance spectrum of both tissues is discussed. The role of the characteristic impedance of necrotic tissue in determining the transmission of injury currents during acute peri-infarction is studied in detail in vivo and in vitro. In view of the results, the possible role of the infarct scar in the genesis of arrhythmias during either chronic infarction or during acute peri-ischemia is discussed.

In view of the distinct impedance spectra which characterise normal and chronically infarcted tissues, in chapter five a catheter based system is developed for the distinction of these tissues by intracavitary recording of the endocardial tissue impedance spectrum.

Chapter six deals with the clinical application of the results obtained in the acute infarction model. The study is conformed by a series of experiments designed to asses the performance of a silicon based impedance sensor in detecting the onset of myocardial ischemia by measurement of tissue impedance.

Finally, in chapter seven the overall conclusions of the thesis are drawn.

REFERENCES

1 Departament de Sanitat i Seguretat Social. Anàlisi de la mortalitat de Catalunya, 1994. Barcelona: DSiSS, Generalitat de Catalunya, 1997

2 Fuster V, Badimon L, Badimon JJ, Chesebro JH. The pathogenesis of coronary artery disease and the acute coronary syndromes. New Engl J Med 1992;326:310

3 Hearse D. Myocardial ischemia and metabolic changes associated with the genesis of ventricular arrhythmias. *In* Parrat JR (Ed). Early arrhythmias resulting from myocardial ischemia. Mcmillan Press. London 1982

4 Stunning, hibernation, and preconditioning: *In* Heyndrickx GR, Vatner SF, Wijns W (Ed). Clinical pathophysiology of myocardial ischemia. Lippincott-Raven. Philadelphia 1997

Chapter 1

Background

Contents

ELECTRIC IMPEDANCE BACKGROUND

Propagation of the electric -**E**(ω)- and magnetic -**B**(ω)- fields of a given frequency (ω) through a medium is determined by the conductivity -σ(ω)-, the permittivity -ε(ω)-, and the permeabilty -μ(ω)- of the medium at the given frequency.

The total electric current density ($\mathbf{J}_{tot}$) in a medium with static conductivity σ, and dielectric constant ε is given by equation 1.1 [1].

$$\mathbf{J}_{\mathrm{Tot}} = \sigma \mathbf{E} + \frac{\partial \mathbf{D}}{\partial \mathrm{t}} = (\sigma + \mathrm{j}\omega\varepsilon)\mathbf{E} \tag{1.1}$$

Where **E** is electric field, **D** is the displacement vector, and ω is the frequency of the sinusoidal electromagnetic field. The total current density has an ohmic component which describes the transport of free charges within the material and a displacement component which describes the movement of bound charges. The complex conductivity of the medium ($\tilde{\sigma}$) is defined as $\mathbf{E}/\mathbf{J} = -\tilde{\sigma} = \sigma + \mathrm{j}\omega\varepsilon$. Alternatively, the medium may be characterised by a complex dielectric constant defined as $\tilde{\varepsilon} = \tilde{\sigma}/\mathrm{j}\omega$.

From this equation three types of electrical behaviour may be defined: a) the displacement current (jωε**E**) is much larger than the conduction current (σ**E**), therefore the medium behaves like a dielectric; b) the conduction current is greater than the displacement current, therefore the medium may be classified as a conductor; c) both currents are of the same order of magnitude and the medium is considered as a quasi-conductor. Biological materials show marked conductive properties due to their high ionic composition as well as a dielectric behaviour caused by both the presence of induced and permanent dipoles (charged molecules) and the capacitative nature of the cell membranes.

Measurement of tissue electrical impedance (Z) may be used for determining the conductivity and permittivity of biological tissues. Electrical impedance is defined as the voltage (V) measured across the tissue divided by the sinusoidal current (I) of a given frequency applied through it (Z=V/I). Since the cell membranes have capacitative properties [2] the voltage and the current are complex phasors. Consequently, impedance (Z) will be a complex number (Z=R+jX) where R is the resistance (in phase component of V respect to I) and X is the reactance (in quadrature component of V respect to I). Alternatively, impedance may be

expressed in terms of the modulus (M) and phase angle (ϕ): $Z=M(\cos(\phi) + j\sin(\phi))$. Tissue electrical impedance is not an intrinsic property of the tissue since the applied current distribution depends on the geometrical configuration of the electrodes and on the boundary conditions of the sample under measurement. The relationship between the conductivity and permitivitty and the macroscopic electrical impedance is a geometrical factor named the cell constant. The cell constant can be determined experimentally by measuring the resistance of a medium of known resistivity with the same experimental set up, or may be determined theoretically by solving Laplaces equation with the appropriate boundary conditions [3].

ANATOMICAL BACKGROUND

Myocardial tissue anatomy: Myocytes are roughly cylindrical in shape with a diameter of 15 to 20 μm and a length of 100 μm. A more detailed analysis of the cells reveals a complex three-dimensional geometry with multiple columnar end processes [4]. Through these end processes a single cell is connected to as many as ten other myocytes. The coupled cells form fibre-like arrays that are referred to as cardiac fibres. Throughout the whole heart, the fibres may be organised to form discrete layers or sheets [5]. Measurement of transmural fibre orientation shows that the fibres rotate about 180º from endocardium to epicardium [5,6]. The elongated form of myocytes as well as their organisation into fibres has as a result that cardiac tissue exhibits an anatomical [7] and functional anisotropy [8-11]. Consequently, there are differentiated electrophysiological properties in the longitudinal and transversal cell axis directions.

Until the 1950's myocardial tissue was thought to be a syncytium (i.e. a cellular structure whose intracellular space formed a continuous medium) [12]. However, in 1954 Sjostrand and Anderson proved by means of high resolution microscopy, that cardiac muscle is composed of well defined individual cells separated by specialised zones known as intercalated discs [13-15]. In addition, from the electrophysiologic point of view, Wiedmann had observed that intracellular subthreshold pulses injected in Purkinje fibres could be recorded in the intracellular space of myocytes which were various cell lengths away [16]. This study, and further experiments in which radioactive K^+ ions injected in the intracellular space diffused along various cell lengths gave evidence for the low-resistance connection of cardiac cells [17]. In summary, both the structural and the

electrical series of experiments founded the concept that myocardial cells are electrically connected by specialised junctions.

The structure responsible for intracellular communication is the gap junction. Gap junctions are one of the three types of intercellular junction linking cardiac muscle cells [18]. The other two types of junctions, fascia adherens and desmosomes, are concerned with cellular adhesion. The intercalated disk is a specialised cell organelle which contains the intercellular junctions and is located in the blunted step like ends of the myocytes. Gap junctions are a specialised location were membranes of neighbouring cells meet within 3 nm and are linked by hydrophilic channels that connect the intracellular spaces of the two cells. Their function is related to the transfer of ions and small molecules. A characteristic of gap junction channels is that they are minimally ion selective. In fact, the pore is large enough to allow the passage of low molecular weight dyes and adenosine triphosphate (ATP).

The molecular structure of gap junction channels consist of hexameric assemblies of a protein named connexin. Connexin-43 is the principal junctional protein in mammalian myocardium, but connexin-40 and connexin-45 are also present in the gap junction connections of the specialised conduction tissues. Connexins group to form a hexameric structure containing a central pore. This structure is termed a connexon or connexin hemichannel. A working gap junction channel is formed when a connexon in one cell becomes localised in a cell membrane and matches sterically with a connexon from a neighbouring cell [18].

Cell membrane: Cells are surrounded by a plasma membrane whose main function is to control the passage of ions and molecules into and out of the cell. Observations performed with electron microscopy reveal that the membrane is a heterogeneous structure of about 75 Å in thickness composed mainly (about 70%) of lipids, phospholipids, glicolipids and cholesterol.

The membrane lipids are organised in two hydrophobic lipid layers that are orientated such that the polar groups face the intracellular or extracellular aqueous media. This orientation is thermodynamically favourable, and as a consequence, the hydrophobic lipid tails constitute the membrane interior that behaves like a dielectric of about 30 Å in thickness [19]. The capacitance of the structure formed by the lipid bilayer can be calculated by considering the membrane dimensions and by assuming that the relative dielectric constant is three (i.e. the same value as for oil). Values of cell membrane capacitance (c_m) calculated in this manner range from 0.9 $\mu F/cm^2$ to 12 $\mu F/cm^2$ [20,21]. The electrical resistance of the cell membrane (r_m) is in the order of 1000 Ωcm^2. This relatively low value, as compared to the

resistance of other lipid bilayers, is attributed to the presence in biological membranes of other composites such as proteins, water molecules, ions, and carbohydrates [22]. Of these composites, the proteins determine the function of the membrane in each particular type of cell. More specifically, the membrane proteins determine the active transport of ions and metabolites between intracellular and the extracellular spaces, the intracellular communication by means of specialised unions, etc.

The fluid-mosaic model was proposed in 1966 by Singer and Nicolson to describe the dynamics of the proteins in the cell membrane [22]. According to this model, the proteins float within the membrane bilayer as if they were immersed in a fluid, and in some instances are capable of rotating. Some large proteins such as the (Na, K)-ATPase, the Ca-ATPase and various ion channel proteins inserted in the lipid bilayer protrude through the entire membrane thickness. Other smaller proteins such as the G proteins or the adenylate cyclase enzyme are inserted in only the inner or outer leaflet of the lipid bilayer.

ACTIVE ELECTRICAL PROPERTIES OF THE MYOCARDIUM

Cellular electrophysiology

Resting membrane potential: When a microelectrode is inserted into an quiescent cardiac cell, a DC potential between 50 and 100 mV is found between the intracellular and extracellular compartments [23]. Specifically, in ventricular and atrial cells the resting membrane potential (V_r) is between -80 and -90 mV, in the sinoatrial nodal cells between -50 and -60 mV, and in the Purkinje cells between -90 and -95 mV [24].

The origin of this transmembrane potential difference lies in both the different ionic composition of the intracellular and extracellular spaces, and in the selective permeability of the cell membrane to the various types of ions. As shown in Fig 1.1, the extracellular space has a high Na^+ and Cl^- concentration (145 mM and 120 mM, respectively) and a low concentration of both K^+ (about 4 mM) and of Ca^{2+} (about 2 mM). By contrast, the intracellular space of ventricular cells has a high K^+ concentration (150 mM), and low concentrations of Na^+ (about 15 mM) and Cl^- (about 4 mM). The free intracellular Ca^{2+} concentration is about 10^{-7} M, however, it may reach values as high as 10^{-5} M during contraction. Furthermore, the total intracellular Ca^{2+} is much higher, but most of it is bound to molecules or is sequestered by the mitochondria and the sarcoplasmatic reticulum.

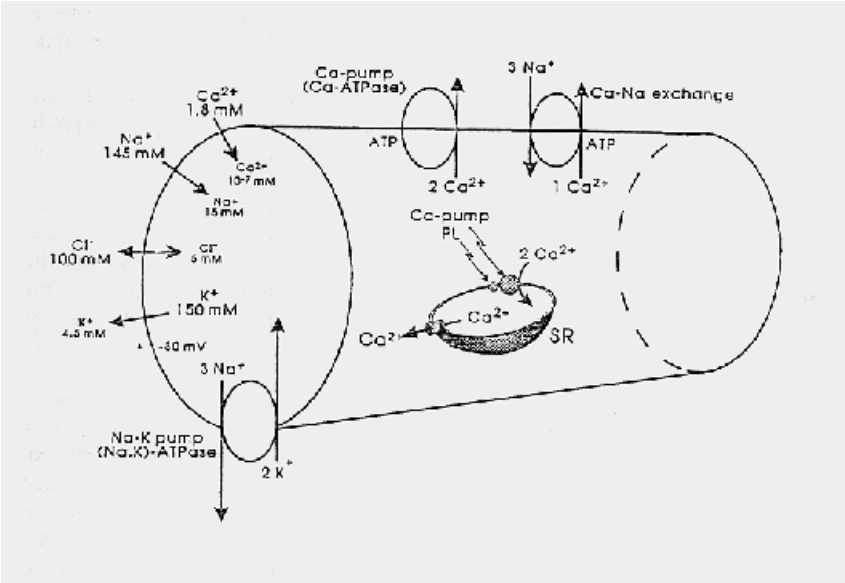

Fig1.1 Intracellular and extracellular ion distributions in a myocardial cell. Polarity and magnitude of the resting potential are also given. Arrows give direction of the net electrochemical gradient. The Na+-K+ pump and the Ca-Na exchanger are located in the cell surface. The Ca-ATPase/Ca pump is located in the sarcoplasmatic reticulum (SR) and on the cell membrane.

The ionic concentration gradients between intracellular and extracellular spaces are maintained by the action of ion-transport mechanisms located in the cell membrane at the expense of metabolic energy. The major transport mechanism is the sodium pump that extracts Na^+ out of the cell against the Na^+ electrochemical gradient (Fig 1.1). This pump is normally linked to K^+ so that while Na^+ is removed from the cell, K^+ is introduced into the cell. Thus, the pump is a Na^+-K^+ coupled pump, which means that in the absence of K^+ ions, Na^+ ions cannot be extracted out of the cell. The coupling ratio between the amount of Na^+ pumped out and the amount of K^+ pumped in, can theoretically vary from 3:3, to 3:2, to 3:1. However, in normal conditions the rate is three to two, and thus, the pump directly

creates a transmembrane potential. The enzyme associated to the Na^+-K^+ pump is the (Na, K)-ATPase and has been identified in virtually all types of tissue [25].

The mechanisms by which the transmembrane gradients of Cl^- and Ca^{2+} are maintained are less well known. Evidence seems to support that Cl^- is not actively transported, i.e. there is no Cl^- pump, which means that it is distributed passively in accordance with the existing membrane potential [26].

The mechanisms responsible for the removal of the positively charged Ca^{2+} ion from the myoplasm are not unique. The sarcoplasmatic reticulum membrane contains a Ca^{2+} -activated ATPase that actively pumps two Ca^{2+} ions from the myoplasm to the sarcoplasmatic reticulum lumen at the expense of one ATP [27]. This pump ATPase is capable of pumping down the intracellular calcium ion concentration to less than 10^{-7} M. Sequestration of Ca^{2+} by the sarcoplasmatic reticulum is an essential mechanism for muscle relaxation.

Another mechanism involved in homeostasis is the Ca/Na exchange reaction [28]. This exchange reaction exchanges one internal Ca^{2+} ion for three external Na^+ ions via a membrane carrier molecule. ATP facilitates this reaction but is not hydrolysed. The energy consumed for the pumping of the Ca^{2+} against its large electrochemical gradient is obtained from the Na^+ electrochemical gradient. By this mechanism, the energy that is required for the Ca^{2+} ion movement is derived from the (Na, K)-ATPase. Thus, the Na-K pump that uses ATP to maintain the Na^+ electrochemical gradient, indirectly helps to maintain the Ca^{2+} electrochemical gradient.

Given an unequal distribution of ions (p) across a membrane, the two factors that influence the distribution of the ions are chemical concentration gradients (∇C_p) and electric field ($\nabla \Phi$). To quantitatively analyse the genesis of the resting membrane potential, the Nernst-Plank equations (equation 1.2) which describe the ionic flux (j_p) when both types of forces are present must be considered.

$$\bar{j}_p = -D_p\left(\nabla C_p + \frac{Z_p C_p F}{RT}\nabla \Phi\right) \tag{1.2}$$

Where T is the absolute temperature, R is the gas constant, F is Faraday's constant, Z_p is the valence of the ion p, and D_p is Fick's constant. The first term of this equation is Fick's law which describes the ion flux due to the existence of ionic concentration gradients. The second term gives the ionic flux in the presence of an electric field.

To understand how the interaction of both concentration gradients and electric

fields give rise to an equilibrium potential when there is an unequal distribution of ions, the Nernst-Plank equations should be solved in the following simplified situation in which only two types of ion exist. If one considers that there is a different intracellular and extracellular concentration of a given salt (e.g.: NaCl) and the membrane is only permeable to one of the ions (e.g. Na^+), then a diffusion of Na^+ will occur from the compartment of highest concentration to that of lowest concentration. The result will be that an electric field will begin to build up across the membrane which will tend to oppose the concentration gradient. When equilibrium is reached, both the electric field force and the force due to the concentration gradient will be exactly opposed, and the net ionic flux across the membrane will be zero. If this condition is imposed to the Nernst-Plank equations, the electric field at which equilibrium occurs can be calculated from Nernst potential (V_{eq}):

$$V_{eq} = \frac{58}{Z_p} \log_{10}\left(\frac{[C_p]_e}{[C_p]_i}\right) \tag{1.3}$$

Where $[C_p]_e$ and $[C_p]_i$ are the extracellular and intracellular concentrations of the ion p.

The ions which have high enough concentrations, high enough diffusional potentials, and high enough membrane conductances to be able to significantly influence the membrane resting potential under normal conditions are Na^+, K^+, Ca^{2+}, and Cl^-. By applying the Nernst equation, the following equilibrium potentials can be calculated for each type of ion: E_{Na} = 60 mV; E_K = -94 mV; E_{Ca} = 129 mV; and E_{Cl} = -80 mV, respectively. Any ion whose equilibrium potential is different from the cellular resting potential is not in equilibrium, and must therefore be pumped at the expense of metabolic energy.

The selective permeability of the membrane to the different types of ions is the other characteristic that determines the resting membrane potential, and is caused by the fact that each ion flows through specialised channels. Therefore, there is a tendency for the ions more permeable to the membrane to move along their concentration gradient, whereas those with lower permeability to remain. At a given membrane potential -V_m- each ionic species (p) is submitted to a driving force which is the difference between its equilibrium potential (E_p) and the membrane potential: (V_m -E_p). In the particular case of Na^+ which has an equilibrium potential of 60 mV, the driving force considering a resting potential of

-80 mV is 140 mV. Similarly, the driving force for potassium is 14 mV. This calculation can be performed in the same manner for the rest of the ions. The electric current transported by each ion (I_p) can be calculated from Ohm's law, i.e. the product of the membrane conductance for that specific ion (g_p) times the driving potential ($V_m - E_p$).

$$I_{Na} = g_{Na} (V_m - E_{Na}) \quad (1.4a)$$

$$I_K = g_K (V_m - E_K) \quad (1.4b)$$

$$I_{Ca} = g_{Ca} (V_m - E_{Ca}) \quad (1.4c)$$

The following example illustrates how the combination of the transmembrane ionic gradient and the selective permeability of the membrane to the different ions determines the resting potential. If Cl^-, Ca^{2+}, and other minor ions are neglected, the maintenance of a constant transmembrane potential requires that the K^+ current is equal and opposite to the Na^+ current. Since in resting conditions the membrane is mainly permeable to K^+, the resting potential approaches the value of the Nernst equilibrium potential of the potassium ion (i.e. -94 mV).

Finally, a modified version of the Nernst potential known as the Goldman-Hodgkin-Katz equation (equation 1.5) must be used to accurately determine the value of the resting potential in terms of the intracellular and extracellular ionic concentrations and the respective ionic channel permeabilities.

$$V_r = \frac{RT}{F} \ln \frac{P_k [K]_o + P_{Na} [Na]_o + P_{Cl} [Cl]_i + \ldots}{P_k [K]_i + P_{Na} [Na]_i + P_{Cl} [Cl]_o + \ldots} \quad (1.5)$$

Where P_p is the membrane permeabilty to each ionic species defined as $D\eta RT/F\Delta x$, in which D is the mobility in the membrane, η is the membrane solution partition coefficient, and Δx is the membrane thickness. For a more precise calculation of the resting potential, the contribution of the pumps has to be included in the Goldman-Hodgkin-Katz equation. Mullins Noda performed this calculation in 1963 [29].

Transmembrane action potential and propagation of excitation: One of the main characteristics of myocardial cells is that they are excitable [30]. Specifically, when a constant current is applied to the intracellular space the membrane

electrical capacitance begins to charge up and this brings the resting transmembrane potential to a less negative value. At a given value of transmembrane potential, named the threshold potential, there is an abrupt change in the membrane properties. The sequence of changes in the transmembrane potential occurring from there on are what is defined as the transmembrane action potential (Fig 1.2).

The action potential is characterised by a very rapid shift of intracellular potential to a positive value known as overshoot potential. This phase of depolarisation is known as phase 0 of the action potential and takes place in about 2-3 ms. Some cardiac cells (Purkinje system and ventricular myocytes) have a second phase of partial repolarisation denominated phase 1. There is then a plateau phase of maintained depolarisation or of very slow repolarisation called phase 2, followed by a fast repolarisation of transmembrane potential named phase 3. Phase 4 is the interval during which transmembrane potential remains at resting potential values.

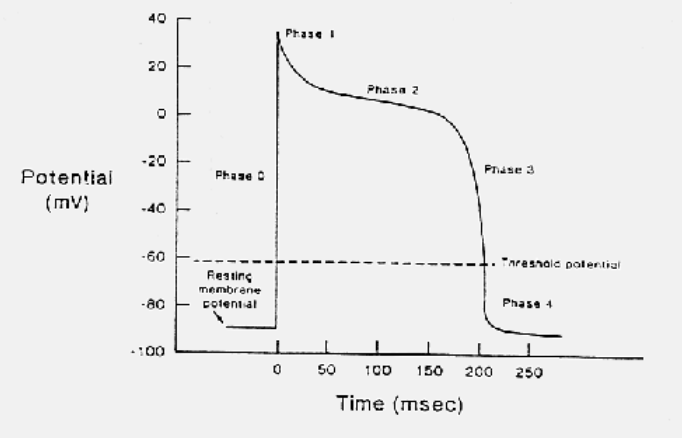

Fig 1.2 Phases of the action potential.

In addition to eliciting action potentials at certain degrees of stimulation, some cells have the ability to initiate an electrical impulse spontaneously [31,32]. This characteristic is referred to as automaticity and is the basis of impulse generation within the cells that form the sinoatrial (SA) node. In these types of cells, phase 4 of the action potential just described is characterised by a slow depolarisation that lasts until the threshold potential is attained.

Another fundamental characteristic of excitable cell membranes is the refractory period of the cell. This concept is defined as the time interval during which the cell membrane does not allow reexcitation [33]. From the onset of the action potential, ventricular myocardial cells in normal conditions remain in refractory state about 90% of the total action potential duration.

The underlying molecular mechanisms responsible of the generation of the action potential are the ionic channels and pumps that reside in the cell membrane. The generation of the action potential is the consequence of abrupt sequential changes in the conductance of the ionic channels which results in large movements of ions between the intracellular and extracellular spaces [34-36]. The initial alterations of these channel conductances may be brought about by changes on the ionic composition of both intra-extracellular spaces (voltage dependant conductances) or may depend on time (time dependant conductances). Once the channel conductances have been activated, the ionic currents are determined by the instantaneous driving force for each particular ion as well as the channel conductance. The driving force for each ion (p) at a time t, is the difference between the transmembrane voltage at that time ($V_m(t)$) minus the Nernst equilibrium potential for that ion (E_p). Since the conductance of each particular ion is a complex function of the transmembrane potential at that time t, as well as of time, the ionic currents are given by equations (1.6a-1.6b) [37].

$$I_{Na} = g_{Na} \cdot m^3(t, V_m(t)) \cdot h(t, V_m(t)) \cdot j(t, V_m(t)) \cdot (V_m(t) - E_{Na}) \qquad (1.6a)$$

$$I_K = g_K \cdot x(t, V_m(t)) \cdot (V_m(t) - E_K) \qquad (1.6b)$$

$$I_{Ca} = g_{Ca} \cdot d(t, V_m(t)) \cdot f(t, V_m(t)) \cdot (V_m(t) - E_{Ca}) \qquad (1.6c)$$

Where g_{Na} , g_K , and g_{Ca} are the maximal conductances of each ion, and m, h, j, x, d, and f are variable scalar parameters (ranging from 0 to 1) that depend on voltage and time which determine the dynamics of activation and inactivation of each ionic channel. These conductance parameters do not have a firm physical basis and have to be found empirically by use of the voltage clamp technique.

At a microscopic level, the sequence of events that occurs once the action potential is triggered is the following (Fig 1.3). The sodium channels open and permit sodium ions to rush down the electrochemical gradient into the cell. Activation of the sodium channel takes place in fractions of a millisecond. The inrushing positive Na^+ ions displace the negative charges stored in the inside of the membrane with the result of transmembrane depolarisation. Since Na conductance -g_{Na}- increases as voltage becomes less negative, g_{Na} is increased regeneratively. As a consequence of the inrushing cations, the intracellular voltage (V_i) in that localised region is more positive than in the neighbouring intracellular parts, so there is a longitudinal voltage difference that generates an intracellular longitudinal current down the voltage gradient. In normal conditions, this longitudinal current depolarises adjacent regions of membrane and brings them to threshold potential, therefore causing sodium channels to open in the contiguous areas of membrane.

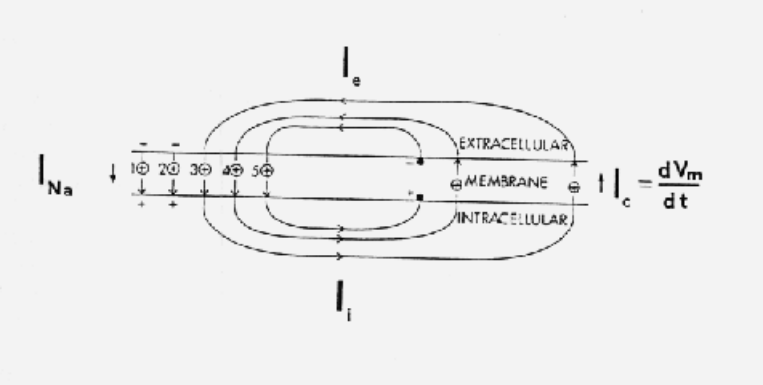

Fig 1.3 Schematic diagram of the events taking place during transmission of excitation by means of local circuit currents. Components of local circuit current are: I_{Na}=inward sodium current; I_c=capacitative current; I_i =intracellular current; I_e =extracellular current.

Simultaneous to these events, a transmembrane capacitative current (which appears due to the time varying transmembrane voltage) permits that the pathway of the intracellular current is completed by a return extracellular current in the opposite direction. The intracellular and extracellular currents which result from the initial rush of Na^+ ions going down their gradient are named electrotonic currents. Concurrent with propagation of excitation to other portions of membrane, the Na channels of the initial patch of membrane begin to inactivate. Subsequently, the rest of the ionic channels of the initial patch of membrane are then activated according to equations 1.6b and 1.6c. Therefore, at the same time that the excitation is transmitted to other portions of membrane, the action potential takes place at the initial patch of membrane. Since the refractory period lasts about 90% of the whole action potential, reexcitation of the initial patch of membrane cannot occur.

In summary, during action potential, the total transmembrane current (i_t) is composed by the sum of the individual ionic currents (i_{ionic}), by the pumping currents (i_{pumps}), and by the capacitative current which appears due to the cell membrane capacitance:

$$i_t = c_m \frac{\partial V_m}{\partial t} + i_{ion} + i_{pumps} \tag{1.7}$$

The experimental technique which made possible the study of the different ionic currents is the voltage clamp technique which consists in maintaining the intracellular potential at fixed values different from the resting potential by means of electronic feedback mechanisms (this action effectively converts the capacitative component of the current to zero). Manoeuvres with the ionic concentration of the extracellular medium permit to study the individual timecourse of each ionic current. There are many types of ionic currents which may or may not be shared among the various specialised cardiac cells. In a final instance, the ionic currents determine the characteristic morphology of the action potential, which in turn determines the electrical function of each cell type in the excitation sequence of the heart.

The currents can be grossly classified in two types: inward currents that depolarise and outward currents that repolarise the cell membrane [38,39]. Inward currents are carried mainly by sodium ions (in ventricular cells) and calcium ions (in sino-atrial cells), whereas outward currents are composed primarily of potassium and chloride ions. The main ionic currents in cardiac cells are the

following:

I_{Na} is the inward excitatory current carried by Na^+ through voltage-activated Na^+ channels [16]. The current is activated at threshold to produce rapid depolarisation and to provide the current to drive action potential or impulse propagation in atrial, His-Purkinje, and ventricular cells [40]. These Na^+ channels are sparse or absent in SA and AV nodal cells.

The cardiac sarcolemma of most animal species contains two Ca^{2+} channel types that have been named L-type and T-type [41]. These two channels share a high selectivity for Ca^{2+} over other ions but differ in the voltage range of their activation and inactivation, as well as their microscopic (single cell) and macroscopic (whole cell) gating kinetics.

$I_{Ca\text{-}L}$ is the calcium current that is activated regeneratively from a relatively depolarised potential to produce depolarisation and propagation in SA and AV nodal cells. It is also present in atrial, His-Purkinje, and ventricular cells, where it contributes to the plateau and triggers calcium release from the sarcoplasmatic reticulum. It is inactivated by both depolarisation and $[Ca^{2+}]_i$ [42].

$I_{Ca\text{-}T}$ is a calcium current through a different voltage dependent channel that is activated at potentials intermediate between thresholds for I_{Na} and $I_{Ca\text{-}L}$. This current probably contributes to the inward current at the later stages of phase 4 depolarisation in SA and His-Purkinje cells [43].

I_f is an inward current carried by Na^+ through a relatively non-specific cationic channel that is activated by polarisation to high membrane potentials in SA and AV nodal cells and His-Purkinje cells. This current is responsible for generating phase 4 depolarisation and contributes to pacemaker function. Its kinetics are fairly slow, and it is strongly modulated by neurotransmitters [44].

There are many types of potassium channels which are related to the repolarisation phase of the action potential [45]. The potassium currents include the delayed rectifier K^+ -current (I_k), the background inwardly rectifying K^+ -current (I_{k1}), the I_{to} current, the acetylcholine (Ach)-activated inwardly rectifying K^+ -current (I_{KACh}), the K^+ -current that is inhibited by intracellular adenosine triphosphate (I_{KATP}), the K^+ -current that is activated by elevated levels of intracellular Na^+ (I_{KNa}), and the Ca^{2+} -activated K^+ -current (I_{KCa}).

I_{k1} is the K^+ current responsible for maintaining the resting potential near the equilibrium potential in atrial, AV nodal, His-Purkinje, and ventricular cells. This current shuts off during depolarisation (inward rectification)

I_k is a K^+ current carried through voltage-gated channels with slow activation kinetics. It turns on slowly during the action potential plateau and is the major current causing repolarisation.

I_{to} is a K^+ current that turns on rapidly after depolarisation and then inactivates. One type of I_{to} is activated by $[Ca^{2+}]_i$, and the other is voltage-activated and modulated by neurotransmitters. I_{to} can play an important role in modifying action potential duration and in contributing to the heterogeneity of repolarisation because of its non-uniform distribution.

The pumps and carriers also generate ionic currents [46]. The $I_{Na/k\ pump}$ is the current generated by the Na/K pump. Because each cycle transports 3 Na^+ out and 2 K^+ into the cell, it generates a small outward current that is relatively constant during cardiac cycle. $I_{Na/Ca}$ is the current generated by the Na/Ca countertransport system, which exchanges 1 Ca^{2+} ion for 3 Na^+ ions, and is the chief means of Ca^{2+} efflux through the sarcolemma.

Electrical activity of the heart

Normal cardiac rhythm: The regular rhythmic contraction of the ventricles which is the basis for the optimal pumping function of the heart is maintained by the co-ordinated action of the various specialised tissues which form the heart. The basis of this synchronised action is the electrical interaction, by the conduction of the action potential, between the various specialised myocardial cells (Fig 1.4). Each specialised tissue has particular anatomical and electrophysiological characteristics that determine its specific function.

The genesis of the electrical impulse takes place in the sinoatrial (SA) node which is situated in the upper part of the right atrium. During the normal function of the heart, the SA nodes generate an electrical impulse at a rate of 60 to 100 beats per minute. The competing effects of parasympathetic and sympathetic nerves modify this rate. The process of spontaneous depolarisation of the SA node is known as pacemaker activity. The electrical signal generated in the SA node extends through the atrial muscle to the atrio-ventricular (AV) node in 120 to 210 ms.. The AV node is the only functional link between the atria and the ventricles and is characterised by being a slow conducting tissue (in the order of 0.2 m/s). This slow AV node conduction ensures an adequate delay between the atrial and ventricular contraction that is essential for the proper filling and pumping of the ventricles. Conduction of the excitation wavefront from the AV node to the ventricles is mediated by excitation of the bundle of His. Each ventricle is respectively excited by the right and left branches which constitute the bundle of His. These branches then ramify into the specialised Purkinje system which directly initiates excitation of the ventricular cells at specific points of the

ventricles ensuring a uniform pumping action of the ventricular chambers. Both specialised tissues are characterised by allowing a rapid propagation (about 5 m/s) of the excitation wavefront.

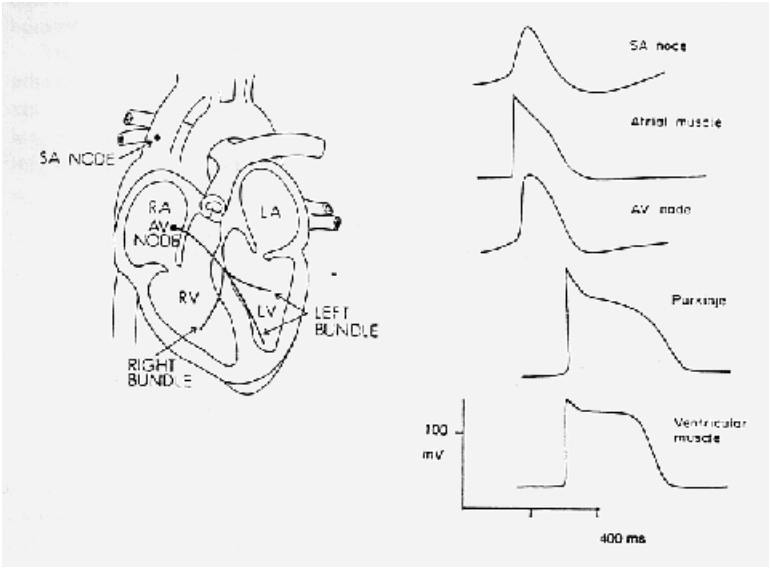

Fig 1.4 Characteristic action potentials of the various specialised tissues.

The electrocardiogram: The electrocardiogram (ECG) is the graph obtained when the electrical potentials of the electrical field originated in the heart are recorded from the body surface [47,48]. A normal ECG is characterised by a series of deflections (P, Q, R, S, T, U) and intervals between these deflections (PR and ST) which are related to the progress of the excitation wavefront across the various specialised tissues of the heart (Fig 1.5). The P wave is considered to reflect the passage of the excitation wavefront through the atria, whereas the QRS complex reflects the excitation of the ventricles. The PR interval, of about 80 ms in duration, is related to the passage of the excitation through the AV node and is almost devoid of electrical signal since excitation includes a small number of

fibres far from the surface. The ST segment is a quiescent period between the QRS complex and the T deflection which is concurrent with the depolarisation of the ventricular myocytes.

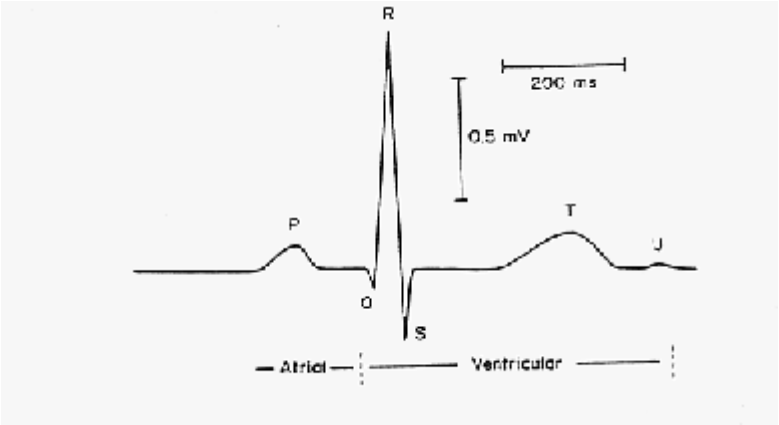

Fig 1.5 A typical ECG form of one of the standard electrocardiographic leads.

The ECG provides a useful clinical tool and has various uses such as: an independent marker of myocardial disease; it may reflect anatomic, hemodynamical, molecular, ionic, or drug induced abnormalities of the heart; and it might provide information that is essential for the proper diagnosis and therapy of many cardiac problems.

PASSIVE ELECTRICAL PROPERTIES OF THE MYOCARDIUM

The cell passive electrical properties are the electrical characteristics of the intracellular, extracellular, and transmembrane pathways that subthreshold ionic currents generated by the active membrane properties find when going in, out, or across the cell membrane. Therefore, the key role of the passive electrical properties in the normal function of the heart is that they modulate the magnitude of the circulating electrotonic currents generated during the excitation process, and

therefore play a crucial role in determining propagation of excitation across the normal and pathological myocardium. To understand quantitatively how the passive electrical properties determine propagation of excitation, the core conductor equivalent model of the cell and its solutions, the cable equations, must be considered [49].

The core conductor model (Fig. 1.6) considers that the cell is cylindrical and that intracellular (V_i) and extracellular (V_e) potentials vary only along the longitudinal axis. Cytoplasm is approximated as an ideal ohmic conductor of resistance per unit length r_i, and extracellular space as an ideal ohmic conductor of resistance per unit length r_e. The cell membrane behaves as resistance r_m in parallel with a capacitance c_m.

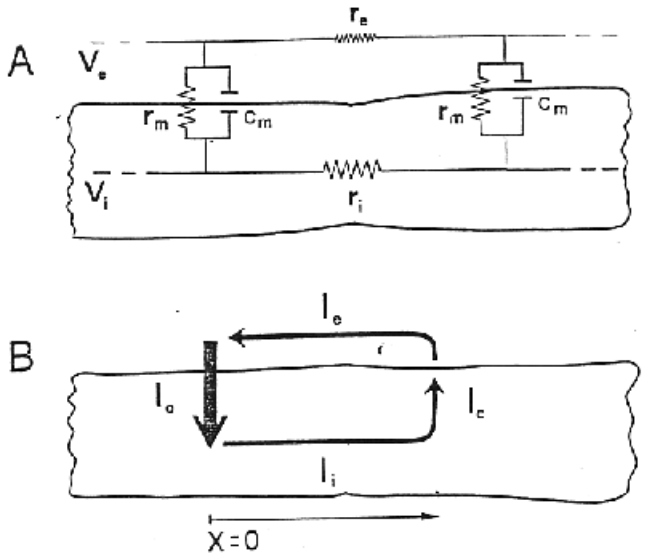

Fig 1.6 This figure depicts the core conductor model (panel A) equivalent to a segment of a cylindrical myocardial fibre (panel B). Also shown are the local currents that circulate when an intracellular current I_0 is applied at X=0.

Application of Kirchoff's laws to the core-conductor network of Fig. 1.6 leads to the cable equations (equations 1.8). These differential equations describe the time course and spatial distribution of the transmembrane voltage of cylindrical fibres submitted to subthreshold stimuli.

$$\lambda^2 \frac{\partial^2 V_m}{\partial x^2} - V_m = \tau \frac{\partial V_m}{\partial t} \tag{1.8}$$

Where the transmembrane potential is defined as $V_m=V_i-V_e$, and τ and λ are the time and length constant respectively which are defined as:

$$\tau = c_m r_m \tag{1.9a}$$

and

$$\lambda = \sqrt{\frac{r_m}{r_e + r_i}} \tag{1.9b}$$

If time (t) and distance (x) are transformed by $X=x/\lambda$, and $T=t/\tau_m$, the solution for a subthreshold electric current step I_0 applied intracellularly at point X=0, and at time T=0, in a cable extending to infinity in both directions, is given by equation 1.10.

$$V_m(X,T) = \frac{r_i I_0 \lambda}{4}\left\{e^{-X}\left[1-\mathrm{erf}\left(\frac{X}{2\sqrt{T}}\right)-\sqrt{T}\right]-e^{X}\left[1-\mathrm{erf}\left(\frac{X}{2\sqrt{T}}\right)+\sqrt{T}\right]\right\} \tag{1.10}$$

Where erf(X,T) is the error function. The solutions of the cable equation are represented in Fig 1.7**.**

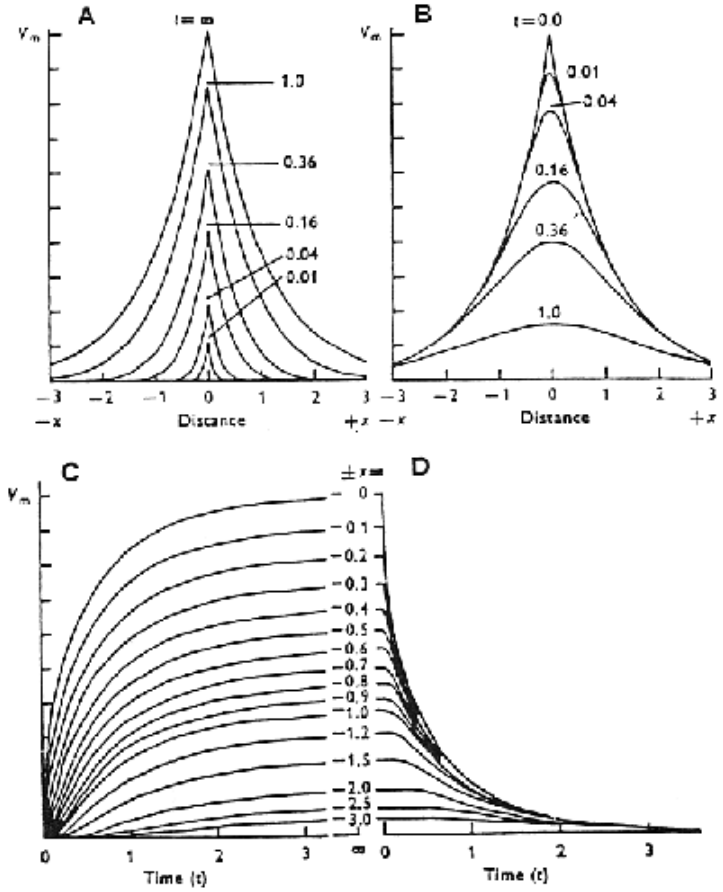

Fig 1.7 Solutions of the cable equation for the application (A and C) and withdrawal (B and D) of constant intracellular current pulse applied at X=0. (A) and (B) depict the spatial distribution of potential at different times, and (C) and (D) show the timecourse at different points in the cell segment. Distance is normalised to the length constant λ, and time is normalised with respect to the time constant τ.

Special solutions of equation 1.10 are the voltage distribution along the cable at t=∞ (i.e. when the pulse has reached steady state).

$$V_{x\,(t=\infty)} = V_{\left(\begin{smallmatrix}x=0\\t=\infty\end{smallmatrix}\right)} e^{\lambda/x} \tag{1.11}$$

where $V_{x,\ t=\infty}$ is the voltage along the cable at point x, and $V_{x=0,t=\infty} = r_i I_0 \lambda/2$. The voltage declines from the point of current application exponentially. The constant λ represents the distance required for the voltage change to fall $1/e$ (i.e. 63%) of its value at the input point. Typical values of λ for Purkinje fibres are 0.2 cm.

Another special solution of equation 1.10 is the timecourse of voltage change at x=0.

$$V_{t\,(x=0)} = V_{\left(\begin{smallmatrix}x=0\\t=\infty\end{smallmatrix}\right)} \mathrm{erf}\sqrt{t/\tau} \tag{1.12}$$

Since erf(1) = 0.84, it can be deduced that the voltage rises to 84% of its final value (at t=∞) in one time constant. A typical time constant for Purkinje fibres is 18 ms.

From these equations it is deduced that the magnitude and the time course of the electrotonic currents that play a key role in transmission of cell excitation are determined by the length and time constants. In addition, both constants are determined by the intrinsic passive electrical properties of the cell (r_i, r_e, r_m, c_m) according to equations 1.9a, and 1.9b.

To gain further insight into the role of the passive properties in determining the propagation of excitation, the cable equations should be expressed in terms of the propagation velocity. If an action potential is conducted along a uniform fibre at a constant velocity (Θ (m/s)) then the distribution of voltage in space is the same to its distribution in time. This equivalence is expressed as: $\partial^2 V/\partial x^2 = (1/\Theta^2)\,\partial^2 V/\partial t^2$. Therefore, the cable equation can be transformed to:

$$\frac{\lambda^2}{\Theta^2}\frac{\partial^2 V_m}{\partial x^2} - V_m = \tau\frac{\partial V_m}{\partial t} \tag{1.13}$$

Solving the cable equation in this form the following expression can be found

for the conduction velocity:

$$\Theta^2 = \frac{1}{2\tau_{foot} r_i c_m} \tag{1.14}$$

Where τ_{foot} is the time constant of the exponentially rising membrane voltage that precedes action potential.

This expression shows that changes in the upstroke velocity of the action potential, or an increase in the passive electrical properties, mainly intracellular resistance and membrane capacitance, directly alter the velocity of propagation of the action potential along a cell that behaves like a 1-dimensional uniform cable.

The anatomical conditions required to apply the core conductor model to a tissue are very restrictive and are only partially accomplished by the Purkinje fibres and by the papillary muscle. In general, cardiac tissue forms a 3-dimensional structure in which the myocytes are electrically connected both longitudinally and transversally. To describe the electrical behaviour of normal cardiac muscle, the bidomain model, which is an extension to 3-dimensions of the core conductor model is used [50-53]. This model represents 3-dimensional cardiac tissue as two interpenetrating domains, one representing the volume-averaged passive properties of the intracellular region and one representing the volume-averaged passive properties of the interstitial region. These domains coexist spatially and the flow of current from one domain to the other occurs via the cell membrane which is continuously spread throughout the whole space. As with the cable model, the bidomain model assumes uniform tissue properties, permitting the currents and potentials to be described by continuous partial differential equations. These assumptions can be made because despite the fact myocardial tissue is composed by many discrete cells it acts in many respects as an electrical syncytium due to the interconnection between cells by means of low resistance gap junctions. Further equations can be obtained fom this model that confirm the role of the passive properties in determining the velocity of propagation of the excitation wavefront in 3-dimensional tissue.

Measurement of myocardial passive electrical properties

The first measurements of the passive electrical properties of cardiac tissue were performed using the *in vitro* cable analysis technique with Purkinje fibres of dog [16]. This technique consists in injecting current into the excised cardiac fibre by

means of an intracellular electrode, and then determining the time course of the transmembrane voltage change measured with other microelectrodes at different consecutive points along the axis of the fibre. These set of measures permit values of the length and time constants to be obtained by adjusting the data to the appropriate functions obtained from the cable equations. Following this procedure values for intracellular resistance r_i (470 Ωcm), extracellular resistance r_e (47 Ωcm) and membrane capacitance c_m (12 μF/cm^2) were obtained. In addition to obtaining values for the passive properties of Purkinje fibres, these measurements also provided the first evidence that myocardial cells were electrically connected by means of low resistance junctions since the space constant of the voltage decay (1.9 mm) was greater than various cell lengths (≅100 μm).

A number of studies have used the cable analysis technique to study the passive properties of various specialised cardiac tissues. Fozzard studied the membrane capacitance of sheep Purkinje fibres and obtained similar values to those obtained by Wiedmann in dogs [21]. These measurements raised the question on the validity of the core conductor model for Purkinje fibres since the predicted theoretical membrane capacitance was 1 μF/cm^2. Fozzard also studied the effect of stretch on the passive properties of Purkinje fibres [54], and Wiedmann studied the effect of temperature obtaining that intracellular resistance increased when the temperature of the preparation was decreased [55]. Studies were also performed to see the effect of action potential generation on the passive properties. Pacing up to 3 Hz produced no significant effect on the passive properties [56], but higher frequency stimulation increased intracellular resistance slightly [57]. Studies in other animal models such as rabbit Purkinje fibre showed a slightly lower membrane capacitance (6.5 μF/cm^2) and a higher intracellular resistance (453 Ωcm) [58]. These differences were attributed to the different anatomy of the species. Bonke studied the passive properties rabbit atrial trabeculae [60] and of the rabbit SA node [61]. Measures performed by Clerc [59] using the ventricular trabeculae of sheep obtained a higher transversal than longitudinal intracellular resistance. A concomitant difference in longitudinal and transversal propagation velocity was also found. These differences were attributed to the anatomical anisotropy that characterises this tissue. Kléber and Weidmann also studied the effects of sucrose solutions on trabeculae muscle of mammalian hearts [62,63]. Wojtczak [64] and Ikeda [65] studied the effect of hypoxia on cow ventricular muscle and obtained that intracellular resistance increased 77%.

A modified cable analysis technique using arterially perfused rabbit papillary muscle was employed by Kléber et al to measure intracellular and extracellular resistances independently during arrest of coronary flow [66]. To perform the

measures, a current pulse is a applied at one end of the muscle, and the consequent extracellular voltage drop is recorded with two extracellular electrodes along the fibre axis. Assuming intracellular and extracellular pathways to form a parallel circuit, an equation is obtained in terms of the total resistance measured (r_t) and the intracellular (r_i) and extracellular (r_e) resistances. Independent measurement of both the intracellular and bipolar extracellular potentials as well as r_t, permit to resolve the intracellular and extracellular resistances. Following this technique, baseline values of 115 Ωcm and 70 Ωcm were found for intracellular and extracellular resistance, respectively. Furthermore, both intra-extracellular resistances increased during ischemia and this was correlated to a slowing of excitation velocity across the papillary muscle fibre.

A great deal of attention has been given to the mechanisms which produce alterations in the electrical passive properties. The injection of Ca^{2+} ions into the cytosol of intact cardiac Purkinje cells indicated that the elevation of free $[Ca]_i$ above certain levels causes a gradual decline of electrical coupling that culminates in total cell decoupling [67,68]. The physiological role of calcium ions in the physiological modulation of junctional conductance has been later supported by studies in isolated heart cell pairs in which a Ca^{2+} concentration of 0.2 μm suppresses junctional communication [69]. Other factors are also involved in the regulation of junctional conductance in the heart. When hydrogen ions are injected into normal Purkinje cells the electrical coupling is quickly abolished, whereas alkalisation of the cytosol causes an increase in gap junction conductance [70,71]. Recent studies have found that cAMP is an important regulator of junctional conductance [72]. Hermsmeyer reported that angiotensin II increased conduction velocity above normal (in tyrode solution) [73]. Furthermore, he found a concomitant fall of internal resistance with trabeculae of mammalian hearts.

Another approach to the study of the cardiac tissue passive properties is the measurement of tissue electrical impedance. This technique permits the study of the passive properties of the heart in vivo models which has the advantage that other clinically and physiologically important parameters such as arrhythmias, epicardial injury currents, and hemodynamic and contractile function can be measured simultaneously. The first in vivo measurements of myocardial tissue impedance in the 10 Hz to 10 kHz frequency range were performed by Schwan and Kay in dogs [74,75]. The results were 800 Ωcm for cardiac tissue resistivity and 100000 for the dielectric constant at 1 kHz. In this study no anisotropic ratio was found between the transverse and the longitudinal set of measurements. In addition, the behaviour of tissue electrical impedance was found to be linear with the voltage applied up to the threshold point were excitation occurred. Further

measurements of tissue impedance were performed by Rush and by Sperelakis [76,77]. Rush obtained values for the cardiac tissue electrical impedance of 563 Ωcm and 252 Ωcm in the transversal and longitudinal fibre axis directions, respectively.

More recent measures of the myocardial passive properties using the electrical impedance technique concern measurements performed in diverse pathophysiological situations such as chronic infarction [78,79], acute ischemia [80-82], ischemia of preconditioned hearts [83], and hearts with hypertrophic cardiopathy [84]. The resistivity of the six week old transmural healing aneurysm of an infarcted sheep heart has been reported to be 75 Ωcm, whereas the resistivity of the surrounding normal tissue is 145 Ωcm [78]. Resistance of ischemic tissue has been reported to increase during coronary occlusion. This increase in tissue resistance has been correlated to the occurrence of ventricular arrhythmias taking place during ischemia as well as to the changes in the epicardial potentials caused by the appearance of injury currents [80]. Measurements performed with hypertrophic guinea pigs reported a 140% increase of intracellular resistance at 37 ºC whilst sarcoplasmatic resistance remained unaltered.

The most recent advance in the measure of the myocardial cell passive properties is the direct measurement of gap junction conductance. The development of the double voltage clamp technique applied to coupled pairs of myocytes has made this advance possible [85-89]. Briefly, each cell of the myocyte pair, enzimatically dissociated from the whole heart tissue, is voltage clamped independently at the same holding potential, resulting in zero junctional current. When the clamp potential of one of the two cells is changed, a constant voltage drop across the junctional resistance is established; by measuring the current delivered to the non-stepped cell and dividing by the voltage, junctional conductance is obtained directly. Measurements performed with this technique have obtained a value of 41 MΩ for the nexal resistance (r_n) in cell pairs across which action potential was transmitted [89]. Maurer and Weingart studied the relationship between intracellular resistance and impulse transfer. Uncoupling was induced in cell pairs by exposing them to cardiac glycosides or low $[Na^+]_o$. Successful impulse transmission was found in cell pairs with values of r_n ranging from 5 to 265 MΩ. In these preparations action potential occurred almost simultaneously in both cells. Occasional failures in action potential transfer were observed in cell pairs whose r_n ranged from 155 to 375 MΩ. In this case impulse was delayed up to 24 ms. Impulse transfer was completely blocked when r_n was larger than 780 MΩ.

Gap junction conductance can be modulated by a variety of factors. Several

studies have proved that moderate elevations of $[Ca^{2+}]_i$ do [69] or do not [85,87] decrease junctional conductance. Elevation of $[H^+]_i$ also decreases gap junction conductance [90,91]. Gap junction conductance can be blocked by lipophilic agents such as heptanol, octanol, halothane, and enflurane [92,93]. All these agents reduce junctional conductance in a dose dependant manner. Physiologically important acids like long-chain acylcarnitines and artachidonic acid, which increase in intracellular concentration during ischemia, also induce an irreversible decrease in junctional conductance [94,95]. Gap junction conductance has also been found to be voltage sensitive [96]. Finally, cyclic nucleotides affect the cell to cell coupling in cardiac tissues [97]. More specifically, an elevation of cAMP in cell pairs of neonatal rat hearts is accompanied by an increase in r_n (75%) whereas a rise in cyclic guanosine monophosphate cGMP is associated with a decrease in r_n (30%) [98].

Equivalent electrical models of myocardial tissue

Since cardiac tissue is highly heterogeneous both at a cellular level (intracellular vs. extracellular spaces) and at a tissular level (fibre anisotropy, cellular variability), measurement of the whole tissue electrical impedance is an overall estimation of the passive electrical properties of the myocardium [99].

The monodomain model of cardiac tissue is the simplest equivalent electrical model. According to this model, cardiac muscle is assumed to be uniform and continuous and characterised by a resistance (R) and a capacitance (C). With this assumption any information of the cell structure and therefore of the impedance values of the various cell components (i.e. intra-extracellular spaces, gap-junction, cell membrane etc.) is lost. The monodomain model can assume the tissue to be isotropic [74,75,78,83] or anisotropic [76,82]. The anisotropic monodomain model still contains no information on the cellular structure, but admits directional differences in the passive electrical properties due to the arrangement of the cardiac fibres.

To more accurately describe the frequency behaviour of myocardial tissue electrical impedance, the myocardium has been modelled as a combination of a resistance (R_e) in parallel with a series combination of a resistance (R_i) and a capacitance C_m (Fig 1.8) [100]. According to this model, each element represents average macroscopic values of the following microscopic passive properties: extracellular resistance (r_e), intracellular resistance (r_i), cell membrane capacitance (c_m), respectively. In contrast to the monodomain model, this model gives a good approximation to the high and low frequency values of myocardial tissue impedance.

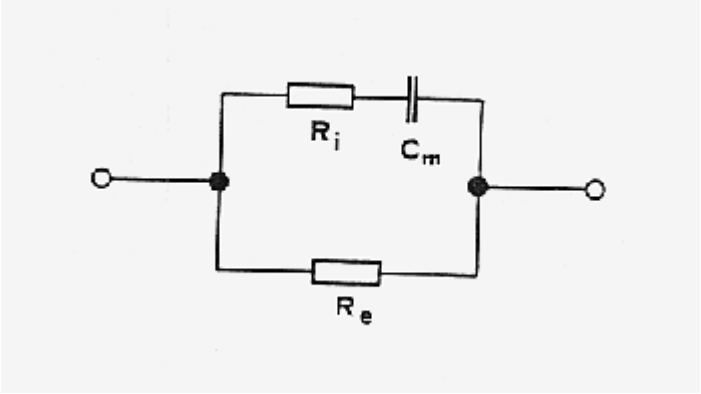

Fig 1.8 Equivalent electric circuit of the myocardium for description of high and low frequency tissue impedance values

However, the electric circuit models of the myocardium which contain frequency independent elements just described do not accurately describe the frequency behaviour of electrical impedance. In the complex plane, the locus of the impedance of biological tissues is an arc of a circle with its centre below the real axis. To describe this behaviour, models based on the Cole-Cole empirical formula (equation 1.15) have to be used.

$$\varepsilon^*(\omega) - \varepsilon_\infty = \frac{\varepsilon_s - \varepsilon_\infty}{1 - (j\omega\tau)^{1-\alpha}} \tag{1.15}$$

Where α is a constant with values between 0 and 1. This equation is based on the Debye equation (equation 1.16), which is obtained theoretically when the interaction between the alternating electrical field (E(ω)) with the dipoles in a dielectric is solved [101].

$$\varepsilon^*(\omega) - \varepsilon_\infty = \frac{\varepsilon_s - \varepsilon_\infty}{1 - j\omega\tau} \tag{1.16}$$

where ε^* is the complex permittivity, τ is the time constant (called the relaxation time) of the of the exponential decay function which describes the dynamics of the dipoles submitted to the electric field; and ε_s and ε_∞ are the permittivity before and after the relaxation, respectively.

When either the Cole-Cole or the Debye equations are plotted in the complex plane, they depict a semicircle stretching from ε_s to ε_∞. The parameter alfa of the Cole-Cole equation causes the centre of the semicircle to be below the real axis. In the limit of α towards zero, the Cole Cole equation is the same as the Debye equation. In contrast to the Debye equation, the Cole-Cole empirical formula is not based on a microscopic description of the interaction between the tissue and the applied electric field. The parameter α has no real physical significance, but it describes the distribution of time constants and activation energies caused by cell variability, orientation differences, intracellular heterogeneity among others.

The following equation is an equivalent form of the Cole-Cole equation in terms of the complex impedance (Z^*):

$$Z^*(w) - R_\infty = \frac{R_0 - R_\infty}{1 + (j\frac{f}{f_c})^{1-\alpha}} \tag{1.17}$$

R_0 is the resistance at 0 Hz, R_∞ is the resistance at a frequency approximating ∞, f_c is the central frequency of the relaxation. If the myocardium is modelled by the equivalent circuit of Fig 1.8, values for R_e, R_i, C_m can be obtained by adjusting the impedance spectrum to equation 1.17, and applying the following equalities:

$$R_e = R_0 \tag{1.18a}$$

$$R_i = \frac{R_0 R_\infty}{R_0 - R_\infty} \tag{1.18b}$$

$$C_m = \frac{R_0^{\,2}}{R_0 - R_\infty}(\frac{f}{f_c})^{1-\alpha} \tag{1.18c}$$

The models just reviewed do not explicitly relate the macroscopic elements of the equivalent model (R_e, R_i, C_m) and the real microscopic passive elements of the

myocardium (r_e, r_i, c_m, r_m). The problem of finding an overall macroscopic effective conductivity in terms of the microscopic intracellular and extracellular conductivity tensors which describe the passive electrical behaviour of the intracellular and extracellular spaces in the bidomain model has been approached by various authors [102-105]. The following equations (1.19a-1.19d) relate the effective longitudinal and transversal effective conductivities (g_l, g_t, respectively) to the microscopic conductivity tensors (σ_e, σ_i) according to the bidomain model.

$$g_{el} = (1-k)\sigma_e \tag{1.19a}$$

$$g_{et} = \frac{1-k}{1+k}\sigma_e \tag{1.19b}$$

$$g_{il} = \frac{1}{1+\frac{\pi a^2 \sigma_i}{bG_e}}\, k\sigma_i \tag{1.19c}$$

$$g_{it} = \frac{1}{1+\frac{b\sigma_i}{G}}\, k\sigma_i \tag{1.19d}$$

where $g_{i\text{-}e,l\text{-}t}$ is the effective conductivity in the extracellular (e) and intracellular (i) spaces and in the longitudinal (l) and transverse (t) directions, respectively; G is the gap junction conductance (S/m^2); k is the fraction of the cross sectional area of the intracellular space respect to the extracellular space; and b and a are the cell length and radius, respectively.

MYOCARDIAL ISCHEMIA AND INFARCTION

Under normal conditions the heart derives over 90% of its energy from aerobic metabolism. Anaerobic glycolisis accounts for less than 10% of total cardiac adenosine triphosphate (ATP) production when adequate oxygen is present. During ischemia, the aerobic pathway is shut down and the only pathway for ATP generation is glycolisis. However, glycolisis alone cannot fulfil the myocardial energy requirements.

The lack of energy to maintain ionic transport across the cell membrane induced by ischemia causes an ionic imbalance in both intracellular and extracellular spaces which is worsened due to the lack of washout in case of no-flow ischemia. This process acts in a feedback manner and directly affects the different membrane channels and pumps (which are in many instances voltage or pH dependant) as well as the gap junctions and the sarcolemmal integrity.

Effect of ischemia on electrolyte balance

Potassium: After arrest of coronary flow, K^+ begins to accumulate in the extracellular space in both animal and human hearts [106,107]. The increase in K^+ occurs in three phases. The initial phase begins 15 seconds after coronary occlusion and lasts 5 to 10 minutes. In this phase K^+_e increases rapidly and achieves values of 15 mmol/L. The first phase is followed by a 10 to 15 minute plateau phase during which K^+ does not change or might even decline. The third final phase begins as a secondary increase in K^+_e.

Acidosis: During ischemia, H^+ ions are generated by a variety of metabolic processes [108]. Proton production leads to rapid acidification of the intracellular space. Transsarcolemmal diffusion or transport of H^+ acidifies the extracellular space. Studies in vivo pig hearts and in isolated blood perfused rabbit hearts using H^+-sensitive electrodes have shown that pH_e falls continuously for 30 to 40 minutes, reaching levels of 6.0 and remains constant at that level [109,110]. Measurements of pH_i, determined both by ion-sensitive microelectrodes and by nuclear magnetic resonance (NMR) techniques, have shown that pH_i initially changes less than pH_e [111]

Intracellular Sodium: During ischemia Na^+_i increases. The cause of this may be an increase in the Na^+ influx, or a decrease in the Na^+ efflux. Experiments studying

the timecourse of the changes in Na concentration have yielded conflicting results. In guinea pig heart, Na^+_i remains unchanged or increases slightly during a variable time after the onset of ischemia and then increases rapidly [112]. However, in ischemic rat hearts or the rabbit papillary muscle, Na^+_i rises rapidly [113].

Intracellular Calcium: There are a variety of methods for measuring Ca^{2+}_i, and the results on the timecourse of the changes of intracellular calcium during ischemia are inconsistent depending on the animal species and on the experimental model used. Nuclear magnetic resonance spectroscopy has shown that the mean Ca^{2+}_i does not increase until 5 to 10 minutes after no-flow ischemia in rat and in ferret hearts [114-116]. In contrast, epifluorescense studies using indo-1, show that following the onset of no-flow ischemia in rabbit heart, Ca^{2+}_i increases substantially within the first minute after coronary arrest.

Intracellular Magnesium: Much of the Mg^{2+}_i is bound to ATP, and therefore the rapid consumption of ATP during ischemia results in an increase in Mg^{2+}_i . The time course of the Mg^{2+}_i concentration measured by NMR in isolated ischemic rat hearts shows that Mg^{2+}_i increased from 0.85 to 2.15 mmol/L after 10 to 15 minutes of ischemia [117].

Effect of ischemia on cardiac electrophysiology

The ischemia induced changes in both intracellular and extracellular ion concentrations and the accumulation of the by-products of ischemic metabolism, ultimately combine to cause alterations in excitability, refractoriness, automaticity, electrical passive properties, and conduction.

Alterations in action potential: A few seconds after coronary occlusion a progressive loss in transmembrane resting potential can be observed which after 10 minutes of ischemia can reach values of up to -60 mV in pig hearts [118-120]. Concurrently, a decrease in upstroke velocity, in action potential amplitude, and in action potential duration are observed [119,120]. At further stages of ischemia, membrane depolarisation renders the cell inexcitable. These changes have been found to be qualitatively similar in human, canine and rabbit hearts [66,121].

Of the factors influencing resting membrane potential, the increase in K^+_e is the most important. However, there are additional factors which cause K-independent changes in resting membrane potential such as the decrease in pO_2, the fall in pH_i

and pH_e, and the accumulation lysophosphoglycerides.

The loss in resting membrane potential and in action potential amplitude of the ischemic cells produces intracellular electric gradients between the ischemic and normal myocardial cells. Since myocardial cells are electrically connected by low resistance gap junctions, the potential gradient causes injury currents to flow intracellularly from ischemic to normal cells during systole and in the reverse direction during diastole. In both cases, the pathway of the intracellular injury currents is completed by extracellular currents which flow in the opposite direction.

Alterations in excitability and refractoriness: The time interval that defines the refractory period depends on both the time necessary for potential to reach the threshold potential at which the sodium current is reactivated (usually -60 mV) and on the time at that given V_m required for activation to occur [122]. Ischemia induced shortening of the action potential decreases the time for the membrane to return to its reactivation voltage level, but at the same time the change in resting membrane potential increased by hypoxia and acidosis lengthens the time required for activation to occur at that voltage level. As a combined result of these changes induced by ischemia, the refractory period is first shortened [123] and then lengthened [124] during coronary occlusion.

Alterations in cellular passive properties: Various studies show that tissue resistance increases during acute ischemia [80-82]. A more specific study by Kleber et al. performed with the papillary muscle of rabbits, reports that during the first two to four minutes of coronary occlusion extracellular resistance increases 30% from the baseline value (70 Ωcm), and then progressively increases thereafter to attain levels of +80% after 20 minutes [66]. The initial changes of extracellular resistance are attributed to the collapse of the extracellular space upon cessation of blood flow, and the posterior slower changes to the cell swelling which occurs due to altered osmotic equilibrium. During the initial stages of ischemia intracellular resistance remains unaltered at baseline values (115 Ωcm), but rapidly increases after about 15 to 17 minutes of coronary occlusion leading to cell to cell electrical uncoupling as assessed by intracellular recordings of action potential.

There are multiple ionic and metabolic changes induced by ischemia which could be responsible for electric cell-to-cell uncoupling. The rise in Ca^{2+}_i and the fall in pH_i probably contribute significantly to cellular uncoupling [85,87,90,91]

Alterations in conduction velocity: In the normal Langendorff-perfused pig heart

conduction velocity is in the order of 50 cm/sec in the longitudinal fibber direction and 20 cm/sec in the transverse direction [125]. During the first two minutes of coronary occlusion conduction velocity remains unchanged and then decreases to about 30 cm/sec in the longitudinal direction and to 13 cm/sec in the transverse direction. Between 4 and 6 minutes of ischemia total conduction block (i.e. lack of propagation of the myocardial excitation) is observed.

Alterations of the normal conduction of the action potential can be induced by a number of situations that alter the membrane excitability [126,127] or the electrical communication between cells which permits the transmission of the electrotonic currents [8,128,92].

Since the inward currents responsible for excitation are generated by the Na^+ and Ca^{2+} voltage-gated ion channels, they are sensitive to resting membrane potential. Therefore pathological alterations of V_m such as abnormal extracellular K^+ levels, ischemia or drugs, theoretically alter normal conduction [129,130]. The changes in the membrane ionic mechanisms that mainly affect velocity of conduction are those altering the sodium current since this directly determines the inward flux of ions into intracellular space. In fact the action of many antiarrhythmic drugs whose effect is the decrease of propagation velocity is upon the Na^+ channels [129]. Changes in extracellular or intracellular Na^+ have an impact on the magnitude of the Na^+ inward current, and by this mechanism influence the upstroke of the action potential and the speed of impulse propagation. Measurements performed on Purkinje fibres [131] and in guinea pig papillary muscle [129] showed that a decrease in extracellular Na^+ concentration will, if large enough, decrease the magnitude of the Na^+ inward current, and thus V_{max} and conduction velocity which is in accordance to the results predicted by cable theory. An increase of intracellular Na^+ occurs when the stimulation frequency is increased [132], when the Na^+/ K^+ pump is depressed or when the Na/H exchange or the Na/Ca exchange are altered. Increases in intracellular Na^+ lessen the Na^+ concentration gradient, and thus the driving force when the Na^+-channel opens.

There are less studies exploring the variations in propagation velocity related to the electric coupling of the cells, or the passive properties in general [133-134]. In any case this is a difficult question to resolve since many factors may alter both the active and the passive properties, and to determine which of both and to what extent they are affecting the speed of excitation propagation is a complex task. Weingart (1977) [135] showed that ouabain increases the internal longitudinal resistance of ventricular muscle and that the increase in resistance contributes to the associated decrease in conduction velocity. Additional information relating propagation velocity and cell-to-cell coupling comes from experiments on

anisotropic cardiac muscle where directional differences in velocity of propagation are best accounted for by differences in effective axial resistivity with direction due largely to the spatial distribution of cell-to-cell connections [11,59,136]. Furthermore, studies performed by Gettes [137] and Kleber [66] in vitro guinea pig papillary muscle show that conduction block is concurrent with a steep rise in intracellular resistance.

Alteration in extracellular cardiac potentials: The flow of extracellular injury currents during ischemia are reflected as alterations in the local epicardial potentials. Specifically, after coronary occlusion there is an ST segment elevation and a TQ segment depletion respectively. It has been shown that the loss of resting potential is the cause of TQ depression, and the alterations in membrane action potential amplitude and duration the cause of epicardial potential ST segment elevation [118,119,138,139].

Heterogeneity of ischemia induced alterations in cardiac electrophysiology: The metabolic and ionic derangements induced by acute ischemia are inhomogeneously distributed [140-142]. The consequence is that the electrophysiologic properties of the ischemic tissue are also altered in a heterogeneous manner. It is widely recognised that an inhomogeneous distribution of electrophysiologic parameters is a favourable substrate for the initiation of arrhythmias, since areas of conduction block coexist with excitable tissue and conduction velocity is not homogeneous which favours the occurrence of re-entrant pathways of the excitation wavefront. Furthermore, inhomogeneities contribute to the increase in dispersion of the recovery of excitability which occurs during acute ischemia [143]. However, no study has explicitly studied the heterogeneity of the cardiac passive properties during ischemia.

Myocardial infarction

Timecourse and spatial distribution of cellular necrosis: After coronary occlusion ischemic myocytes do not die instantaneously. Mildly ischemic myocytes may survive indefinitely, and within the region that undergoes infarction not all the cells die simultaneously [144]. The time course of ischemic cell death has been studied by performing various periods of temporary occlusion followed by reperfusion. In anaesthetised open chest pigs, even the most severely ischemic myocytes remain viable at least 15 minutes [145]. If reperfusion is established during

this time interval, infarction can be prevented, and cellular metabolism, ultrastructure, and contractile function all eventually recover. Beyond 15 minutes of coronary occlusion in this experimental model, increasing numbers of ischemic myocytes become irreversibly injured, as defined by the fact that reperfusion does not prevent subsequent infarction. By 40 minutes, much of the subendocardial zone (28% of the region at risk) has been irreversibly injured in dogs [145,146]. After three hours the percentage of irreversibly damaged tissue has increased to 70%. By six hours infarcts have reached their full size. If ischemia is uninterrupted infarcts eventually involve an average of 80% of the ischemic region.

The geometrical progression of necrosis has been studied experimentally and theoretically [147]. Necrosis appears 20 to 30 minutes after coronary occlusion in the subendocardial myocardial layers and thereafter extends laterally and towards the epicardium. This pattern of infarct enlargement is found in all animal species independently of the presence or absence of well developed native collaterals.

Infarct healing: After the initial stages of acute ischemia, the area at risk which has become necrotic begins to suffer a remodelation which forms part of the healing process of the infarcted tissue. In this process the dead myocytes must be removed and eventually replaced by the infarct scar. In humans the speed of healing of the myocardial infarct takes place over 6 weeks to 6 months, but depends foremost on the size of the infarct and on the extent of microvascular damage.

In an extensive study performed with biopsies of human infarct scars Fishbein et al. studied the histopathological evolution of the healing infarction [148]. In 90% of the patients dying the first day of infarction, necrotic fibres were clearly evident. These fibres exhibited increased eosinophilia, loss of cross-striations, granularity of the cytoplasm and nuclear pyknosis or karyolysis. By the second day, 100% of the infarcts showed severe necrotic changes, with increased loss of recognisable cellular organelles. As infarcts increased in age, necrosis was observed less frequently. However, 50% of the infarcts that were 22 to 28 days old still had areas of necrosis in the centre of the infarct. Finally, none of the patients studied with infarcts between 36 and 90 days old had areas of necrosis in the heart. In this study the infiltration by inflammatory cells was also analysed. Seventy six percent of the infarcts that were 24 hours old or less showed necrotic fibres surrounded by polymorphonuclear leukocytes. At 48 hours, 100% of the infarcts were surrounded by a distinct zone of polymorphonuclear leukocytes which extended into the peripheral portions of the zone of necrotic muscle. By the third day the neutrophilic infiltrate was most dense, and did not begin declining in

prominence until the sixth or seventh day, and disappeared completely by the 28th day. Lymphocytes did not appear at the edge of the infarcts until the second day (in 9% of the infarcts). Not until the 6th day were lymphocytes present in 100% of the infarcts. On the 4th day phagocytes and the removal of necrotic fibres first became evident along the margins of the infarct. Hemosiderin-laden macrophages did not appear until the seventh day and persisted until the 90th day. As far vascular changes are concerned, vascular congestion, interstitial oedema, and focal areas of haemorrhage were present in infarcts within 24 hours, and actual proliferation of small blood vessels was observed at the edge of the infarcts by the fourth day. Such proliferation was present in 100% of the infarcts that were 6 days or more old, and dilated vessels persisted in healed scars. Finally, proliferation of fibroblasts (responsible for the production of collagen) was not evident until the fourth day, when spindle-shaped cells with plump to elongated nuclei appeared at the edge of the necrotic muscle, usually beneath the epicardium and in perivascular areas. All infarcts had fibroblastic proliferation, along with deposition of collagen, from the seventh day until the formation of the scar was complete.

Other studies of the of the histopathological evolution of infarction have been performed in animal models. In a series of experiments performed with dogs submitted to progressively longer periods of infarction the content of hydroxyproline (a marker of collagen content) during healing was studied [149]. A progressive increase of infarct hydroxyproline content during six weeks was observed. A twofold increase was attained by 7 days, and a further fivefold increase by six weeks were hydroxyproline values reached a plateau. Furthermore, there were regional differences within the infarcted area, with higher contents of hydroxyproline in the central zone of the scar than in the margins and the border.

Electrophysiology of myocardial infarction: Various studies have proved that infarcted tissue has specific electrophysiological properties. In isolated superfused tissues, transmembrane action potential duration at 90% depolarisation (APD90) recorded from surviving endocardial muscle cells overlying healed myocardial infarctions are prolonged, with proportional prolongations in local refractory periods. At the margins between the healed scar and the normal tissues APD90 are markedly shortened in some cell clusters, while others remain normal or slightly prolonged. Ursell et al., also studied the transmembrane potentials of surviving myocytes in subacute infarcts (1 and 5 days old) and chronic infarcts (2 weeks and 2 months old) [150]. In preparations from subacute infarcts resting potential, action potential amplitude, upstroke velocity and duration were significantly reduced. Furthermore, there were well defined directional differences (anisotropy) in

propagation. After two week healing of the infarction, resting potential, action potential amplitude, and upstroke velocity returned to normal values, but action potential duration was further increased. By two months, action potentials were normal, but the muscle fibres were widely separated and disorientated by connective tissue. The effect of chronic infarction on the space constant of in vitro preparations of canine myocardium has been studied by Spear et al by means of microelectrode techniques [151]. A reduced space constant of 0.720±0.130 mm compared to the normal (0.939±0.172 mm) was obtained. More recently the passive properties of Purkinje fibres surviving in infarcted regions of canine ventricles 24 hours after coronary ligation were measured [152]. The results depicted significant increases for input resistance (40.5%), membrane resistance (43.9%), and axial resistance (47.5%), whereas membrane capacitance was found to be significantly decreased (-24.3%).

Electrocardiography: Myocardial infarction is characterised by specific electrocardiographic changes which are the main tool for infarct diagnosis within the clinical setting. According to conventional ECG theory, injury of the myocytes is manifested as abnormal ST segment shifts [153]. In the clinical setting an ST segment elevation observed in the diverse standard leads is one of the most powerful diagnostic tools for the detection of myocardial infarction [138,139,153,154]. In addition, abnormal Q waves appear several hours after total occlusion of the coronary artery as a result of the necrosis of the myocytes. The number of affected cells must be large enough to produce changes reflected at the body surface. In general, the depth of the Q wave is proportional to the wall thickness involved [155,156].

Arrhythmias during myocardial ischemia and infarction

Myocardial infarction is associated with a high incidence of malignant arrhythmias [157]. Furthermore, severe ventricular arrhythmias and sudden cardiac death (fibrillation) are the main causes of mortality in acute myocardial infarction and postinfarct patients [158]. In experimental animals, the stability of the heartbeat is disturbed within a few minutes after occlusion of a main coronary artery and ventricular tachycardia or ventricular fibrillation occur in 50% or more of the infarctions. In a study performed by Stephenson et al. in dogs submitted to coronary occlusion, fibrillation occurred in 28% of the animals during the first 30 minutes [159]. Kaplinsky et al. found that during the initial stages of acute ischemia

in dogs, premature ventricular beats, ventricular tachycardia, and ventricular fibrillation are grouped in two distinct phases which peak at 5 and 20 minutes, respectively [160]. These phases were named phase Ia and phase Ib. This bimodal distribution of arrhythmias during ischemia has been found in other animals [161-162], although so far there is no information on the distribution of arrhythmias in humans during the first 30 minutes of infarction. In a study performed by Janse et al. with isolated porcine hearts submitted to regional ischemia by proximal occlusion of the left anterior descending coronary artery a high incidence of arrhythmias was obtained between 2 to 8 minutes. More specifically, ventricular premature beats occurred in 78% of the cases, ventricular tachycardia in 45%, and ventricular fibrillation in 28% of the animals [164]. The mechanism of the arrhythmias occurring during the early stages of ischemia has been subject to much controversy. Different studies prove that not a single mechanism is responsible for these arrhythmias. In the latter study performed in isolated dog and pig hearts, there is evidence that re-entry occurred in the ventricular myocardium during ventricular tachycardia and that fragmentation of the circus movement into multiple re-entrant wavelets induced ventricular fibrillation. However, single premature beats, and the ectopic beats initiating the run of tachycardia are thought to be due to some focal mechanism localised in the ischemic border zone [165]. Further studies showed that the focal mechanism were the normal Purkinje fibres close to the border, and that the mechanism was probably induced by injury currents.

Arrhythmias continue to occur during the later stages of infarction. In dogs, there is a second distinct phase which begins four to eight hours after coronary occlusion and which can last for 24 to 48 hours [157]. The mechanism of these arrhythmias has been related to the surviving Purkinje fibres in the infarcted areas [166].

In man, further phases of arrhythmias in infarcted hearts have been described. About 3% of the patients who survived the acute phase of myocardial infarction developed ventricular tachycardias between 48 hours and six weeks [167]. The mechanism of these tachycardias has been studied experimentally by high resolution mapping and clinically using programmed stimulation [168]. Most of the evidence supports that the arrhythmia is caused by macro-re-entry [169-171]. The re-entrant circuit is usually around the scar tissue as well as the subendocardial border zone between healthy and damaged tissue. However, a study by de Bakker et al. pointed out a possible microreentrant circuit as the origin of the great majority of tachycardias which appeared to originate from small circumscript areas [172].

REFERENCES

1 Maxwell JC. Treatise on Electricity and Magnetism. Oxford University Press. London 1873

2 Cole KS. Membranes, ions and impulses. University of California Press. Los Angeles. 1968, pp 6-113.

3 Littwitz C, Ragheb T, Geddes LA. Cell constant of the tetrapolar conductivity cell. Med Biol Eng Comput 1990;28:587-590

4 Hoyt RH, Cohen ML, Saffitz JE. Distribution and three-dimensional structure of intercellular junctions in canine myocardium. Circ Res 1989;64:563

5 Nielsen PMF, Le Grice IJ, Smaill BH, Hunter PJ. Mathematical model of geometry and fibrous structure of the hear. Am J Physiol 1991;260 (Heart Circ Physiol),29:H1365

6 Streeter D. Gross morphology and fiber geometry of the heart. *In* Geiger SR (Ed). Handbook of physiol, sect 2, The Cardiovascular System. American Physiology Society, Betheseda, 1979

7 Johnson EA, Sommer JR. A strand of cardiac muscle: its ultrastructure and the electrophysiologic implications of its geometry. J Cell Biol 1967;33:103-129

8 Delmar M, Michaels DC, Johnson T, Jalife J. Effects of increasing intercellular resistance on transversal and longitudinal propagation in sheep epicardial muscle. Circ Res 1987;60:780-785

9 Spach MS, Heidlage JF. Models of discontinuous anisotropic propagation in cardiac muscle: A question of size scale. Comments Theoret Biol 1990;1:359-386

10 Spach MS, Miller WT III, Geselowitz DB. The discontinuous nature of propagation in normal canine cardiac muscle: Evidence for recurrent discontinuities of intracellular resistance that affect the membrane currents. Circ Res 1981;48:39-45

11 Spach MS, Kootsey JM, Sloan JD. Active modulation of electrical coupling betweeen cardiac cells of the dog. Circ Res 1982;51:347-362

12 Heidenheim M. Über die structure des menslischen herzmuskels. Anat Anz 1901;20:3-79

13 Sjostrand FS, Andersson E. Electron microscopy of the intercalated disks of cardiac muscle tissue. Experientia 1954; 10:369-370

14 Sjostrand FS, Andersson-Cedergen E, Dewey MM. The ultrastructure of the intercalated disks of frog, mouse, and guinea pig cardiac muscle. J Ultrastr Res 1958;1:271-287

15 De Mello WC. Intercellular communication in cardiac muscle. Circ Res 1982;51:1-9

16 Weidmann S. The electrical constants of Purkinje fibres. FJ. Physiol 1952;118:348-360

17 Weidmann S. The diffusion of radiopotassium across intercalated discs of mammalian cardiac muscle. J Physiol 1966;187:323-342

18 Severs NJ. The cardiac gap junction and intercalated disc. Int J Cardiol 1990;26:137-173

19 Sperelakis N. Origin of the cardiac resting potential. *In* Geiger SR (Ed). Handbook of physiol, sect 2, The Cardiovascular System. American Physiology Society, Betheseda, 1979

20 Fricke H. The electric capacity of suspensions with special reference to blood. J Gen Physiol 1925;19:19-

21 Fozzard HA. Membrane capacity of the cardiac Purkinje fibre. J Physiol (Lond) 1966;182:255-267

22 Singer SJ, Nicolson GL. The fluid mosaic model of the structure of the cell membrane. Science 1972;175:720-731

23 Ling G, Gerard RW. The normal membrane potential of frog sartorius fibers. J Cellular Comp Physiol 1949;34:383-396

24 Sperelakis N. Electrogenesis of biopotentials in the cardiovascular system. Kluwer Academic

Publishers. Boston. 1995
25 Skou JC. The influence of some cations on an adenosine triphosphatase from peripheral nerves. Biochim Biophys Acta 1957;23:394-401
26 Vaughn-Jones RD. Intracellular chloride activity of quiescent cardiac Purkinje fibres. J Physiol (Lond) 1977;272:32P-33P
27 DiPolo R. Ca pump driven by ATP in squid axons. Nature 1978;274:390-392
28 Baker PF, Blaustein MP, Hodgkin AL, Steinhardt RA. The effect of sodium concentration on calcium movements in giant axons of Loligo forbesi. J Physiol 1967;192:43P-44P
29 Mullins LJ, Noda K. The influence of sodium free solutions on the membrane potential of frog muscle fibers. J Gen Physiol 1963;47:117-132
30 Hoffman BF, Cranefield PF. Electrophysiology of the heart. McGraw Hill. New York. 1960
31 Hoffman BF, Cranefield PF. The physiological basis of cardiac arrhythmias. Amer J Med 1964;37:670-689
32 DiFrancesco D. A new interpretation of the pacemaker current in calf Purkinje fibers. J Physiol (Lond) 1981;314:359-376
33 Moe GK, Mendez C, Han J. Aberrant AV impulse propagation in the dog heart: a study of functional bundle branch block. Circ Res 1965;16:261-286
34 Beeler GW, Reuter H. Reconstruction of the action potential of ventricular myocardial fibers. J Physiol (Lond) 1977;286:177-210
35 Ebihara L, Johnson EA. Fast sodium current in cardiac muscle: a quantitative description. Biophys J 1980;32:779-790
36 Rudy Y, Quan W. A dynamic model of the cardiac ventricular action potential, I: simulation of ionc currents and concentration changes. Circ res 1994;74:1071-1096
37 Hodgkin AL, Huxley AF. A quantitative description of membrane current and its application to conduction and excitation in nerve. J Physiol (Lond) 1952;117:500-544
38 Boyett MR, Harrison SM, Janvier NC, McMorn SO, Owen JM, Shui Z. A list of vertebrate cardiac ionic currents: nomenclature, properties, function, and cloned equivalents. Cardiovasc Res 1996;32:455-481
39 The task force of the working group on arrhythmias of the European society of cardiology. The sicilian gambit: A new approach ti the classification of antiarrhythmic drugs based on their actions on arrhythmogenic mechanisms. European Heart Journal 1991;12:1112-1131
40 Coraboeuf E, Deroabaix E, Coulombe A. Effect of tetrodoxin on action potentials of the conduction system in dog heart. Am J Physiol 1979;236:H561-H567
41 Nilius B, Hess P, Lansman JB, et al. A novel type of cardiac calcium channel in ventricular cells. Nature 1985;316:443-446
42 Pelzer D, Pelzer S, MacDonald TF. Properties and regulation of calcium channels in muscle cells. Rev Physiol Biochem Pharmacol 1990;114:107-207
43 Hagiwara N, Irisawa H, Kassanuki H, Hosoda S. Background current in sino-atrial node cells of the rabbit heart. J Physiol (Lond) 1992;448:53-72
44 DiFrancesco D, Ferroni A, Mazzanti M, Tromba C. Properties of the hyperpolarizing-activated current (i_f) in cells isolated from the rabbit sinoatrial node. J Physiol (Lond) 1988;405:123-145
45 Pennefather P, Cohen IS. Molecular mechanisms of cardiac k^+-channel regulation. *In* Zipes DP, Jalife J (Ed). Cardiac electrophysiology: from cell to bedside. Saunders. Philadelphia. 1990
46 Gadsby DC. The Na/K pump of cardiac cells. Ann Rev Biophys Bioeng 1984;13:373-378
47 Macfarlane PW, Lawrie TDV (Ed). Comprehensive electrocardiology: theory and practice in

health and disease. Pergamon. New York. 1989

48 Einthoven W, Fahr G, de Waart A. Über die richtung und die manifeste grosse der potentialschwankungen in menschlichen herzen und über den einfluss der herzlage auf die form des elektrokardiograms. Arch Physiol 1913;150:275-315

49 Plonsey R. Bioelectric phenomena. McGraw-Hill. New York. 1969

50 Tung L. A bidomain model for describing ischemic myocardial DC potentials. Ph D dissertation. Cambridge, Massachusetts Institute of Technology. 1978

51 Henriquez CS. Simulating the electrical behaviour of cardiac tissue using the bidomain model. Crit Rev Biomed Eng 1993;21(1):1-77

52 Geselowitz D, Miller WT. A bidomain model for anisotropic cardiac muscle. Ann Biomed Eng 1983;11:191-

53 Sepulveda NG, Roth BJ, Wikswo JP Jr. Current injection into two-dimensional anisotropic bidomain. Biophys J 1989;55:987-999

54 Dominguez G, Fozzard HA. Effect of strech on conduction velocity and cable properties of cardiac Purkinje fibres. Am J Physiol 1979;237:C119-C124

55 Coraboeuf E, Weidmann S. Temperature effects on the electrical activity of Purkinje fibres. Helv Physiol Pharmacol Acta. 1954;12:32-41

56 Pressler ML. Cable analysis in quiescent and active sheep Purkinje fibres. J Physiol 1984;352:739-757

57 Bredikis J, Bukauskas F, Veteikis R. Decreased intercellular coupling after prolonged rapid stimulation in rabbit atrial muscle. Circ Res 1981;49:815-820

58 ColatskyTJ, Tsien RW. Electrical properties associated with wide intercellular clefts in rabbit Purkinje fibres. J Physiol (Lond) 1979;290:227-252

59 Clerc L. Directional differences of impulse spread in trabecular muscle from mammalian heart. J Physiol (London) 1976;255:335-346

60 Bonke FIM. Passive electrical properties of atrial fibres of the rabbit heart. Pflügers Arch 1973;339:1-15

61 Bonke FIM. Electrotonic spread in the sinoatrial node of the rabbit heart. Pflügers Arch 1973;339:17-23

62 Weidmann S. Electrical constants of trabecular muscle from mammalian heart. J Physiol (Lond) 1970;210:1041-1054

63 Kléber AG. Effects of sucrose solution on longitudinal tissue resistivity of trabecular muscle from mammlian heart. Pflugers Arch 1973;345:195-205

64 Wojtczak J. Contractures and increase in internal longitudinal resistance of cow ventricular muscle induced by hypoxia. Circ Res 1979; 44:88-95

65 Ikeda K, Hiraoka M. Effects of hypoxia on passive electrical properties of canine ventricular muscle. Pflugers Arch 1982;393:45-50

66 Kleber AG, Riegger CB, Janse MJ. Electrical uncoupling and increase in extracellular resistance after induction of ischemia in isolated, arterially perfused rabbit papillary muscle. Circ Res 1987;61:271-279

67 De Mello WC. The healing-over process in cardiac and other muscle fibers. *In* WC deMello (Ed). Electrical Phenomena in the Heart. Academic Press. New York. 1972, pp 323-351

68 De Mello WC. Effect of intracellular injection of calcium and stronium on cell communication in heart. J Physiol 1972;250:231-245

69 Noma A, Tsuboi N. Dependence of junctional conductance on proton, calcium and magnesium ions incardiac paired cells of guinea pig. J Physiol 1987;382:193-211

70 De Mello WC. Influence of intracellular injection of H^+ on the electrical coupling in cardiac Purkinje fibres. Cell Biol Int Rep 1980;4:51-57

71 De Mello WC. The influence of pH on the healing-over of mammalian cardiac muscle. J Physiol 1983;339:299-307

72 De Mello WC, van Loon P. Further studies on the influence of cyclic nucleotides on junctional permeability in heart. J Moll Cell Cardiol 1987;19:763-771

73 Hermsmeyer K. Angiotensin II increases electrical coupling in mammalian ventricular myocardium. Circ Res 1980;47:524-529

74 Schwan H.P., Kay C.F. Specific resistance of body tissues. Circ Res 1956; 4:664-670

75 Schwan H.P., Kay C.F. Capacitative properties of body tissues. Circ. Res. 1957; 5: 439-443

76 Rush S, Abildskov JA, McFee R. Resistivity of body tissues at low frequencies. Circ. Res. 1963; 12: 40-50

77 Sperelakis N, Hoshiko T. Electrical impedance of cardiac muscle. Circ Res 1961;9:1280-1283

78 Fallert MA, Mirotznik MS, Downing SW, Savage EB, Foster KR, Josephson ME, Bogen DK. Myocardial electrical impedance mapping of ischemic sheep hearts and healing aneurysms. Circulation 1993; 87: 199-207

79 Cinca J, Warren M, Rodríguez-Sinovas A, Tresànchez M, Carreño A, Bragós R, Casas O, Domingo A, Soler-Soler J. Passive transmission of ischemic ST segment changes in low electrical resistance myocardial infarct scar in the pig. Cardiovasc Res 1998;40:103-112

80 Smith WT, Fleet WF, Johnson TA, Engle CL, Cascio WE. The Ib phase of ventricular arrhythmias in ischemic in situ porcine heart is related to changes in cell-to-cell electrical coupling. Circulation. 1995;92:3051-3060.

81 Ellenby MI, Small KW, Wells RM, Hoyt DJ, Lowe JE. On-line detection of reversible myocardial ischemic injury by measurement of myocardial electrical impedance. Ann Thorac Surg.1987;44:587-597.

82 van Oosterom A, de Boer RW, van Dam RTh. Intramural resistivity of cardiac tissue. Med Biol Eng Comput. 1979; 17: 337-343

83 Cinca, J., Warren, M., Carreño, A., Tresànchez, M., Armadans, L., Gómez, P., Soler-Soler, J. Changes in miocardial electrical impedance induced by coronary artery occlusion in pigs with and without preconditioning. Correlation with local ST segment potential and ventricular arrhythmias.Circulation. 1997; 96:3079-3086

84 Changes in cell-to-cell electrical coupling associated with left ventricular hypertrophy. Cooklin M, Wallis WRJ, Sheridan DJ, Fry CH. Circ Res 1997;80:765-771

85 Maurer P, Weingart R. Cell pairs isolated from adult guinea pig and rat hearts: effects of $[Ca^{2+}]_i$ on nexal membrane resistance. Pfluegers Arch. 1987;409:394-402

86 Kameyama M. Electrical coupling between ventricular paired cells isolated from guinea-pig heart. J Physiol. 1983;336:345-357

87 White RL, Spray DC, Campos de Carvhalo AC, et al . Some electrical and pharmacological properties of gap junctions between adult ventricular myocytes. Am J Physiol 1985;249:C447-C455

88 Metzger P, Weingart R. Electric current flow in cell pairs isolated from adult rat hearts. J Physiol 1985;366:177-195

89 Weingart R, Maurer P. Action potential transfer in cell pairs isolated from adult rat and guinea pig ventricles. Circ Res 1988;63:72-80

90 Spray DC, Burt JM. Structure-activity relations of the cardiac gap junction channel. Am J Physiol 1990;258:C195-C205

91 Reber WR, Weingart R. Ungulate cardiac Purkinje fibres: the influence of intracellular pH on the electrical cell-to-cell coupling. J Physiol (Lond) 1982;328:87-104

92 Takens-kwak BR, Jongsma HJ, Rook MB, van Ginneken CG. Mechanism of heptanol-induced uncoupling of cardiac gap junctions: a perforated patch-clamp study. Am J Physiol 1992;262:C1531-C1538

93 Rüdisüli A, Weingart R. Electrical properties of gap junction channels in guinea-pig ventricular cell pairs as revealed by exposure to heptanol. Pfluegers Arch 1989;415:12-21

94 Wu J, McHowat J, Saffitz JE, et al. Inhibition of gap junctional conductance by lomg-chain acylcarnitines and their preferential accumulation in junctional sarcolemma during hypoxia. Circ Res 1993;72:879-889

95 Fluri GS, Rudisuli A, Willi M, et al. Effects of arachidonic acid on the gap junctions of neonatal rat heart cells. Pflugers Arch 1990;417:149-156

96 Rook MB, Jongsma HJ, van Ginneken AC. Properties of single gap junction channels between isolated neonatal rat heart cells. Am J Physiol 1988;255:H770-H782

97 Estapé E, De Mello WC. Cyclic nucleotides and calcium. Their role in the control of cell to cell communication in the heart. Cell Biol Int Rep 1983;7:91-97

98 Burt JM, Spray DC. Inotropic agents modulate gap junctional conductance between cardiac myocytes. Am J Physiol 1988;254:H1206-H1210

99 Plonsey R., Barr R. A critique of impedance measurements in cardiac tissue. Ann Biomed Eng 1986;14:307-322

100 Gebhard MM, Gersing E, Brockhoff CJ, Schnabel A, Bretschneider HJ. Impedance spectroscopy: a method for surveillance of ischemia tolerance of the heart. Thorac cardiovasc Surgeon 1987;35:26-32

101 Frölich FH. Theory of dielectrics: dielectric constant and dielectric loss. Oxford University Press. London 1958

102 Plonsey R, Barr R. The four electrode technique as applied to cardiac muscle. IEEE Trans Biomed Eng 1982;29(7):541-546

103 Roth BJ. The electrical potential produced by a strand of cardiac muscle: a bidomain analysis. Ann Biomed Eng 1988;16:609

104 Henriquez CS Simulating the electrical behaviour of cardiac tissue using a bidomain model. Crit Rev Biomed Eng 1993;21:1

105 Neu JC, Krassowska W. Homogenization of syncytial tissues. Crit Rev Biomed Eng 1993;21:137

106 Hill JL, Gettes LS. Effect of acute coronary artery occlusion on local myocardial extracellular K^+ activity in swine. Circulation 1980;61:768-778

107 Webb SC, Canepa-Anason R, RickardsAF et al. Myocardial potassium loss after acute coronary occlusion in humans. J An Coll Cardiol 1987;9:1230-1234

108 Dennis SC, Gevers W, Opie LH. Protons in ischemia: Where do they come from where do they go? J Mol Cell Cardiol 1991;23:1077-1086

109 Gettes LS, Cascio WE. Effect of acute ischemia on cardiac electrophysiology. *In* Fozzard HA, Haber E, Jennings RB, et al (Ed). The Heart and Cardiovascular System. Scientific Foundation. 2nd De. Raven Press, New York, 1991, pp. 2021-2054

110 Owens L, Murphy E, Fralix TA, et al. Relationship of cellular electrical uncoupling to changes in Ca_i, pH_i, ATP, and contracture in ischemic rabbit myocardium. (Abstract) Circulation 1993;88:I-373

111 Yan GX. Changes in extracellular and intracellular pH in ischemic rabbit papillary muscle.

Circ Res 1992;71:460-470

112 Kleber AG. Resting membrane potential, extracellular potassium activity, and intracellular sodium acitvity during acute global ischemia in isolated perfused guinea pig hearts. Circ Res 1983;52:442-450

113 Pike MM, Luo CS, Clark MD, et al. NMR measurement of Na+ and cellular energy in ischemic rat heart: Role of Na^+-H^+ exchange. Am J Physiol 1993;265:H2017-H2026

114 Steenbergen C, Murphy E, Watts JA, et al. Correlation between cytosolic free calcium, contracture, ATP, and irreversible ischemic injury in perfused rat heart. Circ Res 1990;66:135-146

115 Koretsune Y, Marban E. Mechanism of ischemic contracture in ferret heart: Relative roles of $[Ca^{2+}]_i$ elevation and ATP depletion. Am J Physiol 1990;258:H9-H16

116 Lee JA, Allen DG. Changes in intracellular free calcium concentration during long exposures to simulated ischemia in isolated mammalian ventricular muscle. Circ Res 1992;71:58-69

117 Murphy E, Steenbergen C, Levy LA, et al. Cytosolic free magnesium levels in ischemic rat heart. J Biolo Chem 1989;264:5622-5627

118 Kleber AG, Janse MJ, Van Capelle FJL, Durrer D. Mechanism and timecourse of ST and TQ segment changes during acute regional myocardial ischemia in the pig's heart determined by extracellular and intracellular ecordings. Circ Res 1978;42:603-613

119 Cinca J, Janse MJ, Morena H, Candell J, Valle V, Durrer D. Mechanism and timecourse of early electrical changes during acute coronary artery occlusion. An attempt to correlate the early ECG changes in man to the cellular electrophysiology in the pig. Chest 1980;77:499-505

120 Downar E, Janse MJ, Durrer D. The effect of acute coronary artery occlusion on subepicardial transmembrane potentials in the intact porcine heart. Circulation 1977;56:217-224

121 Janse MJ, Kleber AG. Electrophysiological changes and ventricular arrhythmias in the early phase of regional myocardial ischemia. Circ Res 1981;49:1069-1081

122 Gettes LS, Reuter H. Slow recovery from inactivation of inward currents in mammalian myocardial fibres. J Physiol (Lond) 1974;240:703-724

123 Brooks CM, Gilbert JL, Greenspan ME, Lange G, Mazzella HM. Excitability and electrical response of ischemic heart muscle. Am J Physiol 1960;198:1143-1147

124 Elharr V, Zipes DP. Cardiac electrophysiological alterations during myocardial ischemia. Am J Physiol 1977;233:H329-HH345

125 Kleber AG, Janse MJ, Wilms-Schopman FJG, et al. Changes in conduction velocity during acute ischemia in ventricular myocardium of the isolated porcine heart. Circulation 1986;73:189-198

126 Peon J, Ferrier GR, Moe GK. The relationship of excitability to conduction velocity in canine Purkinje tissue. Circ Res 1978;43:125-135

127 Buchanan JW, Gettes LS. Ionic environment and propagation. *In* Zipes DP, Jalife J (Ed). Cardiac electrophysiology: from cell to bedside. Saunders. Philadelphia. 1990, pp 149-156

128 Jalife J, Sicouri S, Delmar M, Michaels DC. Electrical uncoupling and impulse propagation in isolated sheep Purkinje fibres. Am J Physiol 1989;257:H179-H189

129 Buchanan JW Jr, Saito T, Gettes LS. The effects of antiarrhythmic drugs, stimulation frequency, and potassium-induced resting membrane potential changes on conduction velocity and dV/dt_{max} in guinea pig myocardium. Circ Res 1985;56:696-703

130 Spear JF, Mopore EN. Supernormal excitability and conduction in the His-Purkinje system of the dog. Circ Res 1974;35:782-792

131 Walton MK, Fozzard HA. Experimental study of the conducted action potential in cardiac

Purkinje strands. Biophysics J 1983;44:1-8

132 Cohen CJ, Fozzard HA, Shey-Shing S. Increase in intracellular sodium ion activity during stimulation in mammalian cardiac muscle. Circ Res 1982;50:651-662

133 Lieberman M, Kootsey JM, Johnson EA, Sawanobori T. Slow conduction in cardiac muscle. A biophysical model. Biophys J 1973;13:37-55

134 Pressler ML. Passive electrical properties of cardiac tissue. *In* Zipes DP, Jalife J (Ed). Cardiac electrophysiology: from cell to bedside. Saunders. Philadelphia. 1990, pp 108-122

135 Weingart R. The actions of ouabain on intercellular coupling and conduction velocity in mammalian ventricular muscle. J Physiol (Lond) 1977;264:341-365

136 Sano T, Takayama N, Shimamoto T. Directional differences of conduction velocity in the cardiac ventricular syncytium studied by microlelectrodes. Circ Res 1959;7:262-26

137 Gettes LS, Buchanan JW Jr, Saito T, Kagiyama Y, Oshita S, Fujino T. Studies concerned with slow conduction. *In* Zipes DP, Jalife J (Ed). Cardiac electrophysiology and arrhythmias. Grune and Straton. Orlando. 1985

138 Samson WE, Scher AM. Mechanism of ST segment alteration during acute myocardial injury. Circ Res 1960;8:780-787

139 Prinzmetal M, Toyoshima H, Ekmeki A, Mizuno Y, Nagaya T. Nature of ischemic electrocardiographic patterns in mammalian ventricles as determined by intracellular electrocardiographic and metabolic changes. Am J Cardiol 1961;8:493-503

140 Wilensky RL, Tranum-Jensen J, Coronel , et al. The subendocardial border zone during acute ischemia of the rabbit heart: an electrophysiologic, metabolic and morphologic correlative study. Circulation 1986;74:1137-1146

141 Fiolet JWT, Baartscheer A, Schumacher CA, et al. Transmural inhomogeneity of energy metabolism during acute global ischemia in the isolated rat heart: Dependence of enviromental conditions. J Moll Cardiol 1985;17:87-92

142 Coronel R, Fiolet JWT, Wilms-Schopman FJG, et al. Distribution of extracellular potassium and its relation to electrophysiologic changes during acute myocardial ischemia in the isolated perfused porcine heart. Circulation 1988;77:1125-1138

143 Han J, Moe GK. Nonuniform recovery of excitability of ventricular muscle. Circ Res 1964;14:44-60

144 Reimer KA, Lowe JE, Rasmussen MM, Jennings RB. The wavefront phenomenon os ischemic cell death. I. Myocardial infarct size vs duration of coronary occlusion in dogs. Circulation 1977;56:786-794

145 Jennings RB, Schaper J, Hill ML, Steenbergen C, Reimer KA. Effect of reperfusion late in the phase of reversible ischemic cell injury. Changes in cell volume, electrolytes, metabolites and ultrastructure. Circ Res 1985;56:262-278

146 Reimer KA, Jennings RB. The “wave front phenomenon” of myocardial ischemic cell death. II. Transmural progression of necrosis within the framework of ischemic bed size (myocardium at risk) and collateral flow. Lab Invest 1979;40:633-644

147 Garcia-Dorado D, Theroux P, Desco M, Solares J, Elizaga J, Fernandez-Aviles F, Alonso J, Soriano J. Cell-to-cell interaction: a mechanism to explain wave-front progression of myocardial necrosis. Am J Physiol 1989;256:H1266-H1273

148 Fishbein MC, Maclean D, Maroko PR. The histopathologic evolution of myocardial infarction. Chest 1978;73:843-849

149 Jugdutt BI, Amy RWM. Healing after myocardial infarction in the dog: changes in infarct hydroxyproline and topograhy. J Am Coll Cardiol 1986;7:91-102

150 Ursell PC, Gardner PI, Albala A, Fenoglio JJ, Wit AL. Structural and electrophysiological changes in the epicardial border zone of canine myocardial infarcts during infarct healing. Circ Res 1985;56:436-451

151 Spear JS, Michelson EL, Moore EN. Reduced space constant in slowly conducting regions of chronically infarcted canine myocardium. Circ Res 1983;53:176-185

152 Argentieri TM, Frame LH, Colatsky TJ. Electrical properties of canine subendocardial Purkinje fibres surviving in a 1.day old experimental myocardial infarction. Circ Res 1990;66:123-134

153 Holland RP, Brooks H. Precordial and epicardial surface potentials during myocardial ischemia in the pig. Circ Res 1975;37:471-480

154 Pardee HEB. Electrocardiographic sign of coronary artery obstruction. Arch Intern Med 1920;26:244-249

155 Castellanos A, Kessler MK, Meyburg RJ. The resting electrocardiogram. *In* Alexander RW, Schlant RC, Fuster V (Ed). The heart. McGraw-Hill. New York. 1998

156 Sodi-Pallares D, Medrano GA, Bisteni A, Ponce de Leon JJ. Deductive and polyparametric electrocardiography. Mexico: Instituto nacional de cardiologia Mexico. 1970;36:136

157 Harris AS. Delayed developement of ventricular ectopic rhythm following experimental coronary occlusion. Circulation 1950;1:1318-1328

158 Bigger JT, Fleiss JL, Kleiger R, Miller JP, Rolnitzky LM, and the Multicenter Post-Infarction Research Group. The relationship among ventricular arrhythmias, left ventricular dysfunction, and mortality in the 2 years after myocardial infarction. Circulation 1984;69:250-258

159 Stephenson SE, Cole RK, Parrish TF, Bauer FM, Jhonson IT, Kochtitzky M, Anderson JS, Hibbitt LL, McCarthy JE, Young ER, Wilson JR, Meiers NH, Neador CK, Ball OT, Neneely GR. Ventricular fibrillation during and after coronary artery occlusion. Incidence and protection afforded by various drugs. Am J Cardiol 1960;5:77-87

160 Kaplinsky E, Ogawa S, Balke CW, Dreifus LS. Two periods of early ventricular arrhythmia in the canine acute myocardial infarction model. Circulation 1979;60:397-403

161 Euler DE, Spear JF, Moore EN. Effects of coronary occlusion on arrhythmias and conduction in the ovine heart. Am J Physiol 1983;245:H82-H89

162 Hirche HJ, Franz C, Bos L, Bissig R, Lang R, Schramm M. Myocardial extracellular K^+ and H^+ increase and noradrenaline release as possible cause of early arrhythmias following acute coronary artery occlusion in pigs. J Mol Cell Cardiol 1980;12;579-593

163 Kabell G, Scherlag BJ, Hope RR, Lazzara R. Regional myocardial blood flow and ventricular arrhythmias following one-stage and two-stage coronary artery occlusion in anesthetized dogs. Am Heart J 1982;104:537-545

164 Janse MJ, van Capelle FJL, Morsink H, Kleber AG, Wilms-Schopman F, Cardinal R, Nauman d'Alnoncourt C, Durrer D. Flow of "injury" current and patterns of excitation during early ventricular arrhythmias in acute regional myocardial ischemia in isolated porcine and canine hearts: Evidence for two different arrhythmogenic mechanisms. Circ Res 1980;47:751-759

165 Janse MJ, van Capelle FJL. Electrotonic interaction across an inexcitable region as a cause of ectopic activity in acute regional myocardial ischemia. A study in intact porcine and canine hearts and computer model. Circ Res 1982;50:527-537

166 Horowitz LN, Spear JF, Moore EN. Subendocardial origin of ventricular arrhythmias in 24-hour-old experimental myocardial infarction. Circulation 1976;53:56-

167 Wellens HJJ, Bar FWHM, vanagt EJ, Brugada P. Medical treatment of ventricular tachycardia: considerations in the selection of patients for surgical treatment. Am J Cardiol 1982;49:186

168 Wit AL, Allessie MA, Bonke FIM, Lammers W, Smeets J, Fenoglio JJ. Electrophysiologic mapping to determine the mechanism of experimental ventricular tachycardia initiated by premature impulse: experimental approach and initial results demonstrating reentrant excitation. Am J Cardiol 1982;49:166-

169 Josephson ME, Horowitz LN, Farshidi A, Spear JF, Kastor JA, Moore EN. Recurrent sustained ventricular tachycardia. 1 Mechanisms. Circulation 1978;57:431-

170 Josephson ME, Horowitz LN, Farshidi A, Spear JF, Kastor JA, Moore EN. Recurrent sustained ventricular tachycardia. 1 Endocardial mapping. Circulation 1978;57:431-

171 Allessie MA, Bonke FIM, Schopman FJG. Circus movement in rabbit atrial muscle as a mechanism of tachycardia. III The “leading circle” concept: a new model of circus movement in cardiac tissue without the involvement of an anatomical obstacle. Circ Res 1977;41:9

172 de Bakker JMT, van Capelle FJL, Janse MJ, Wilde AAM, Coronel R, Becker AE, Dingemans KP, van Hemel NM, Hauer RNW. Reentry as a cause of ventricular tachycardia in patients with chronic ischemic heart disease: electrophysiologic and anatomic correlation. Circulation 1988;77:589-606

Chapter 2

Methods

Contents

Experimental preparation

Acute ischemia experimental model: Pigs weighing 25 to 30 kg were anesthetized with alpha-chloralose (100 mg/kg, IV) followed by a continuous perfusion of this drug (25 mg/kg/ min). Pulmonary ventilation was maintained with a pressure respirator (TransPAC 5K257) at 41% oxygen concentration. The thorax was opened through a midsternotomy and the pericardium was incised and its free margins were sutured to cradle the heart. The left anterior descending (LAD) coronary artery was dissected above the first diagonal branch and was looped with a Prolene 5/0 snare. The two ends of the suture were threaded through a smooth plastic tube. The artery was acutely occluded by sliding the tubing over the suture and clamping it with a small hemostat. Coronary reperfusion was accomplished by releasing the ligature. Systemic blood pressure was sampled with a pig-tail 7F catheter introduced percutaneously through the right femoral artery. Arterial blood gases were measured at regular intervals and were kept within normal limits. Isotonic saline perfusion was administered to compensate blood losses. The appropriate position of the various electrodes with respect to the ischemic area was verified at the end of the study by injecting 10 ml of 25% fluorescein into the left atrium [1]. The ischemic area appears unstained whereas the normal myocardium is stained by the dye.

Chronic infarct experimental model: Three month old pigs (25-30 kg) of either sex premedicated with azaperone (4 mg/kg, IM) underwent general anesthesia with sodium thiopental (30 mg/kg, IV). Pulmonary ventilation was maintained with a pressure respirator (Trans-PAC 5K257) at 41% oxygen concentration. The thorax was opened through a sterile left lateral thoracotomy at the level of the 5th intercostal space and the corresponding rib was removed. The pericardium was incised and the left anterior descending (LAD) coronary artery was dissected and was permanently ligated below the first diagonal branch using a Prolene 5/0 snare. The chest was immediately closed in layers and pleural air was aspirated. Cardiac rhythm was monitored with standard ECG leads I, II, and III during the ensuing two hours to allow reversion of ischemic malignant ventricular arrhythmias by external electric DC countershock of 200 Joules. Immediately after LAD occlusion a prophylactic dose of lidocaine (100 mg, IM) was administered. The animals were allowed to recover and received analgesics (magnesium metamizol, 2g IM), and antibiotics (sodium benzylpenicillin 5.000.000 IU, IM).

One to two months after the first coronary ligature the surviving pigs (73%) received a dose of azaperone (4 mg/kg, IM) and were anesthetized with

metomidate (4 mg/kg, IV) followed by alpha-chloralose (100 mg/kg, IV). Aortic blood pressure was measured with an intraarterial femoral cannula. At regular intervals blood gases were analyzed and were kept within normal limits.

In protocols requiring the open chest model, the thorax was opened through a midsternotomy under mechanical ventilation and the pericardium was gently detached. When induction of acute peri-ischemia was necessary, the LAD was dissected 2 to 3 cm above the primary ligature and a Prolene 5/0 snare was placed around the vessel for further coronary reocclusion. The appropriate location of the impedance probes and of the extracellular electrodes was verified at the end of each study. The acute ischemic peri-infarction region was identified as a nonstained region after a left intra-atrial injection of 10 ml of 25% fluorescein [1], whereas the infarcted region was recognized by its thinning and fibrotic consistency.

Pigs used in all the studies were handled in accordance with the position of the American Heart Association and the European Community Rules on Research Animal Use. This study was approved by the ethics committee of our institution.

Postmortem model: After sacrifice of the pigs, the heart was explanted and samples of the left ventricle were cut and put in a 0.9% saline solution bath.

Myocardial impedance

Impedance probes: Transmural measurements of tissue impedance were performed using a four-electrode configuration because with this electrode arrangement the measures are not distorted by the presence of the electrode-tissue interface impedance [3,4]. However, catheter measures of myocardial impedance were performed using a three-electrode configuration because this disposition increased the specificity to myocardial tissue of the catheter impedance probe. The impedance probes used were the following:

a) Impedance of acute ischemic myocardium was measured with a probe which consisted of four platinum electrodes (5 mm long, 0.4 mm diameter) mounted as a linear array on an insulating substrate separated by an interelectrode distance of 2.5 mm. This electrode arrangement allows the current electrodes to be considered as point sources [5].

b) The impedance probes used for the measurement of the impedance of

chronic infarction were similar to the ones used in measuring ischemic myocardium, but had shorter platinum electrodes (length= 3.5 mm, diameter= 0.2 mm). Furthermore, they were isolated to the tip with a teflon layer to reduce the possible interference of the thin layer of epicardial inflammatory reaction [4]. However, the reduced electrode-tissue contact area of the isolated electrodes increased electrode capacitance and this caused a phase angle shift that hampers an accurate measurement of absolute phase angle values.

c) The catheter probe used for the detection of infarcted tissue was a purposely designed 8F BARD bipolar electrocatheter (2 mm interelectrode distance).

d) The silicon impedance sensor consists of four square platinum electrodes (300x300 μm) placed upon a specifically designed silicon needle of the following dimensions: 7 mm in length, 1,2 mm in width and 525 μm thick. The process of fabrication of the sensors is as follows. The starting silicon is a p-type substrate of 525 μm thick on which a thermal field oxide of 800 nm is grown. To fabricate the platinum electrodes with their corresponding connections to the pads, a titanium/platinum (30 nm/150 nm) metalisation is performed with a lift off technique. According to this technique, a photoresist layer (PR) is initially deposited on the front side wafer oxide layer. The following step consists in etching the PR layer with a photolitographic mask, after which the two metal layers are deposited. The electrodes and the connections are obtained by removing away the photoresist. The role of the inner titanium layer is to to obtain a good adherence of the platinum to the substrate. After this process a passivation layer consisting of $SiO_2/Si_3N_4/SiO_2$ (400 nm/700 nm/300 nm) sandwich is deposited and etched with its corresponding photolitographic mask, opening windows only at the site of the platinum electrodes. The last step in the process is to cut the silicon wafer into the shape of the needle. For this, an aluminum mask of 1 μm thick is deposited. Finally, the reactive ion etching (RIE) process is carried out on both sides of the wafer to obtain 68 needles from each 100 mm diameter wafer.

Recording systems: The two recording systems used for the measurement of myocardial impedance were the following:

a) Myocardial impedance at a single frequency was measured using a high input impedance lock-in amplifier (Princeton Applied Research model 5110). Measures were performed by applying an alternating current (10 μA, 1110 Hz) to

the tissue through the outer pair of electrodes, and by determining both the in phase and in quadrature components of the resulting voltage across the inner pair of electrodes. Before performing each myocardial impedance measurement, the exact current flowing through the tissue was determined by measuring the voltage across a 56 kΩ resistance placed in series with the tissue. This procedure was undertaken to account for the possible electrical current variations caused by the changes in tissue impedance in the ischemic area.

b) In protocols requiring a more complete characterization of the myocardial passive electrical properties, tissue impedance spectrum was measured in the 1 kHz to 1000 Mhz frequency range with both a Hewlett-Packard 4192A impedance analyzer and a front-end amplifier [2] adapted to obtain a common-mode rejection ratio of 72 dB at 1 MHz. This frequency range was chosen because measurement errors may occur both below 1 kHz due to electrode impedance and above 1000 kHz due to cable effects. The front end was placed close to the heart and was connected to the impedance probes with 15 cm length cables. Data acquisition and management obtained with both measuring systems was done with a customized software.

Correction of errors and cell constant: To exclude the effects of the electrode geometry on tissue resistance (R) measurements performed with the 4-point electrodes and with the silicon needle, we calculated tissue resistivity (r) from the relation R=kr, where k is the electrode constant obtained by measuring the electrical resistance of a 0.9% saline solution at 25 °C of known resistivity (70 Ωcm) with each electrode probe.

To correct the loading dependent errors of the Hewlett-Packard impedance analyzer and front end measuring system, we did a three-reference calibration procedure [6] by measuring the impedance spectrum (1 to 1000 kHz) of three NaCl solutions of different concentrations. The three NaCl concentrations were adjusted to bring a resistivity similar to the maximum, minimum, and intermediate values found in each explored myocardial tissue. Calibration measurements were made with the same electrode probe used in the in vivo study in order to reduce errors caused by electrodes, cables and by the amplifier response.

Measuring errors due to catheter capacitance and amplifier response in the open chest group of pigs, were corrected by measuring the resistance and phase angle of a 0.9% NaCl solution (R_{NaCl} and Φ_{NaCl}) of a known resistivity. Then, the measured resistance (R(f)) was corrected by the quotient $R(f)\cdot R_{NaCl}(1\ kHz)/ R_{NaCl}(f)$, and the phase angle value ($\Phi(f)$) by the subtraction $\Phi(f)- \Phi_{NaCl}(f)$.

In the closed chest group, measuring errors due to electrode placement, impedance of the skin-reference electrode, stray capacitance of the electrocatheter wires, and amplifier response were corrected by the quotient $R(f) \cdot R_{Ao}(1\ kHz)/R_{Ao}(f)$ for the resistance, and by the subtraction $\Phi(f)-\Phi_{Ao}(f)$ for the phase angle, where R_{Ao} and Φ_{Ao} are respectively the resistance and phase angle measured at the aortic root. The aortic root is an easily accessible myocardium-free tissue that keeps a spatial catheter-reference electrode relationship similar to that existing during myocardial impedance measurements.

Epicardial ST segment potential

Extracellular direct-current epicardial electrograms were recorded with a multi-channel differential amplifier system. Electrodes were made with polyethylene tubes of 0.5 mm diameter containing a cotton thread imbibed with isotonic saline solution and were connected to the amplifiers through a chloride silver interface. A 0 mV potential reference was given by a cotton wick electrode placed at the mediastinal fat.

Epicardial electrograms were recorded at samples of 2-second duration, digitized at a frequency of 500 Hz, and stored in a computer. In addition, selected analog signals were continuously recorded with a 7-channel Elema ink jet polygraph. ST segment was expressed as total TQ+ST segment displacement because this corresponds to the ST segment recorded by conventional ECG [7].

Arrhythmia analysis

Ventricular premature beats (VPB), ventricular tachycardia (VT), and ventricular fibrillation (VF) occurring during acute LAD coronary occlusion or during periinfarction were monitored by continuous recording of conventional ECG with an Elema Mingograf 82 ink jet polygraph. VT was defined as the succession of more than 3 VPB's at a rate higher than 100 beats/min. Sustained VT was considered as a VT lasting more than 30 seconds. Sustained VT and VF were terminated by direct DC electrical countershock of 10 J. During application of the DC current the tissue impedance recording systems were transiently disconnected.

Electrical transmission in healed infarction

Electrical transmission through the necrotic scar was estimated in vivo and in vitro by measuring the voltage decay of current pulses applied in the infarction area.

Current pulses of 30 mA amplitude and 25 ms duration were delivered at a frequency of 10 Hz using a GRASS S88 stimulator (Grass Medical Instruments, Quincy, Mass, USA) modified to act as a current generator with a 1 MW source resistance. The recorded potential pulses were amplified with an AC-coupled instrumentation amplifier [8] and were visualized on a digital oscilloscope (Kenwood CS 8010). The signals were digitized at 10 ksamples per second and were stored in a computer. Pulse amplitude was plotted against distance and the slope of the regression line that best fits the data was considered to represent the magnitude of voltage attenuation.

Histological examination

Samples of the infarct tissue were included in paraffin and stained with Masson's trichrome [9] and hematoxylin-eosin. Histologic examination was performed under conventional light microscopy.

REFERENCES

1 Garcia-Dorado D, Théroux P, Duran JM, Solares J, Alonso J, Sanz E, Munoz R, Elizaga J, Botas J, Fernandez-Avilés F, Soriano J, Esteban E. Selective inhibition of the contractile apparatus. A new approach to modification of infarct size, infarct composition, and infarct geometry during coronary artery occlusion and reperfusion. Circulation 1992;85:1160-1174.

2 Gersing E. Measurements of electrical impedance in organs - measuring equipment for research and clinical application. Biomedizinische Technik. 1991;36:6-11.

3 Ackmann JJ. Complex bioelectric impedance measurement system for the frequency range from 5 Hz to 1 MHz. Ann Biomed Eng. 1993;21:135-146.

4 Steendijk P, Mur G, Van der Velde ET, Baan J. The four-electrode resistivity technique in anisotropic media: theoretical analysis and application on myocardial tissue in vivo. IEEE Trans Biomed Eng. 1993;40: 1138-1147.

5 Suesserman MF, Spelman FA. Quantitative in vivo measurements of inner ear tissue resistivities: I.In vitro characterization. IEEE Trans Biomed Eng. 1993;40:1032-1047.

6 Bao JZ, Davis CC, Schmukler RE. Impedance spectroscopy of human erythrocytes: System calibration and nonlinear modeling. IEEE Trans Biomed Eng. 1993;40:364-378.

7 Cinca J, Bardají A, Carreño A, Mont Ll, Bosch R, Soldevilla A, Tapias A, Soler-Soler J. ST segment elevation at the surface of a healed transmural myocardial infarction in pigs. Conditions for passive transmission from the ischemic peri-infarction zone. Circulation. 1995;91:1552-1559.
8 Pallas-Areny R, Colominas J, Rosell J. An improved buffer for bioelectric signals. IEEE Trans Biomed Eng. 1989;36:490-493.
9 Masson P. Some histological methods: Trichrome stainings and their preliminary technique. J Techn Meth 1929;12:75-90

Chapter 3

Changes in Myocardial Electrical Impedance Induced by Coronary Artery Occlusion in Pigs With and Without Preconditioning.

Correlation With Local ST Segment Potential and Ventricular Arrhythmias

Contents

INTRODUCTION

Acute myocardial ischemia increases intra- and extracellular electrical resistance and causes cell-to-cell electrical uncoupling [1]. Cellular uncoupling occurs as a result of an increase in gap junctional resistance elicited by ischemia-induced accumulation of intracellular Ca^{2+} [2], reduction of adenosine triphosphate content [3], and accumulation of amphipathic lipid metabolites [4], among others. Changes in intracellular resistance can be estimated in the in situ heart by measuring the whole tissue myocardial impedance [5,6] which reflects, in addition to intracellular and extracellular resistance, gap junction conductance and membrane capacitance [7].

Increases in intracellular resistance caused by ongoing ischemia may reduce the magnitude of intra- and extracellular currents that are driven by membrane potential differences created between normal and ischemic cells [8,9]. In these circumstances, the extracellular potential gradients that are responsible for the TQ and ST segment shift in local electrograms may decrease and, hence, account for the spontaneous reversion of TQ segment changes in experimental models [8] and for the reduction of ST segment elevation in patients with acute myocardial infarction [10,11]. However, studies correlating myocardial impedance and ST segment changes in ischemic conditions are lacking.

The rise in intracellular resistance impairs electrical conduction in the ischemic myocardium and this may favor the genesis of ventricular arrhythmias [12]. Recent studies performed in swine [13,14] reported a temporal relationship between early phases of acute ischemic arrhythmias (termed phase Ia and Ib [15]) and the steep rise in tissue resistivity which is thought to reflect the onset of cellular electrical uncoupling [1,13]. On the other hand, studies in perfused rabbit heart [16] have shown that the onset of the steep rise in myocardial resistivity can be postponed by preconditioning the myocardium with short lasting ischemia [16]. Therefore, preconditioning could allow to assess whether an artificially induced adjournment of changes in resistivity is associated with a parallel delay in phase Ib arrhythmias. Such an investigation has not been performed in vivo and could contribute to gain insight into the hypothesis that unlike phase Ia, phase Ib arrhythmias are associated with alterations in tissue electrical impedance.

This study was designed to analyze the effects of coronary artery occlusion on myocardial impedance in open chest pigs with and without ischemic preconditioning and to correlate these changes with local epicardial ST segment potential and ventricular arrhythmias.

STUDY PROTOCOL AND DATA ANALYSIS

Data were obtained from from 26 pigs. In 13 pigs (Group I) the LAD was occluded during 4 hours whereas in the remaining 13 pigs (Group II) a similar LAD ligature was preceded by preconditioning the myocardium with three LAD occlusion-reperfusion sequences lasting respectively 5 and 20 minutes (Fig 3.1).

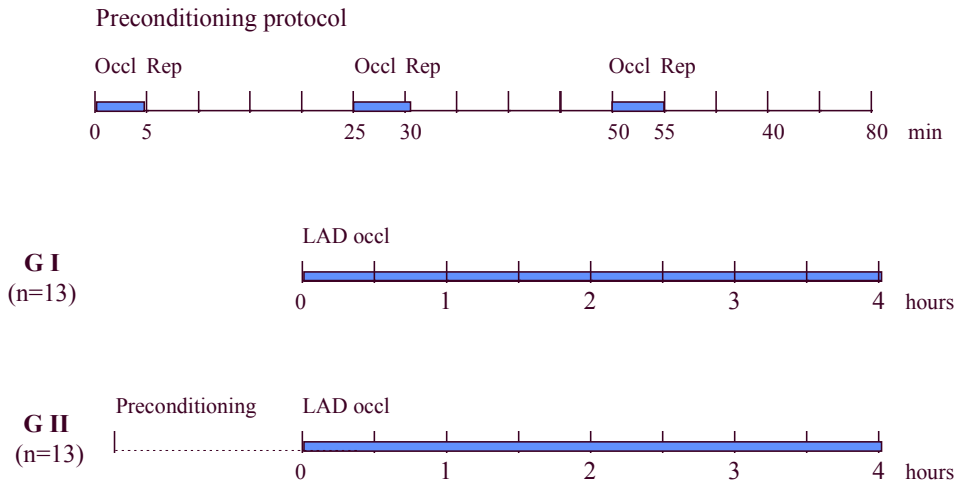

Fig 3.1 Schematic diagram depicting the protocols followed in group I (GI) and group II (GII) pigs.

Myocardial impedance, epicardial electrograms, conventional ECG, and blood pressure were recorded at baseline and during 4 hours of LAD occlusion. ECG and blood pressure were recorded continuously, impedance measurements were taken every two minutes, and samples of epicardial electrograms of 2-second duration were acquired every minute during the first 60 minutes of ischemic and every 15 minutes thereafter.

Myocardial impedance was measured at the center of the ischemic area and at remote normal myocardial zones using two probes which were sutured to the epicardium and were connected to the lock-in amplifier via an automatic multiplexor system (Fig 3.2). Extracellular electrograms were recorded with thirty-

two cotton electrodes sutured to a rubber membrane at interelectrode distances of 5 mm forming three parallel rows. This membrane was sutured to the left ventricular epicardium in a direction parallel to the LAD covering an area extending from the acute ischemic region to the normal myocardial zone. The two impedance probes were inserted parallel to the rows of epicardial cotton electrodes (Fig 3.2) and impedance measurements were correlated to the mean ST segment potential values measured in the six cotton electrodes surrounding the impedance probe.

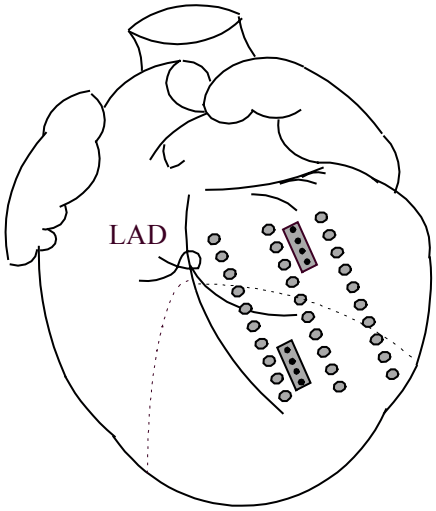

Fig 3.2 Schematic diagram of the experimental preparation showing spatial relationship between impedance probe (Ω) and surrounding epicardial electrodes (electrogram)

Data analysis: Differences between normal and ischemic myocardial resistivity, phase angle, and ST segment potential during 4 hours of coronary occlusion were assessed by repeated measures analysis of variance (ANOVA) using a commercially available software (SYSTAT Inc.). Samples were taken at baseline and every hour. Since preconditioning affects primarily the onset of the rapid changes in myocardial resistivity and phase angle, we assessed the differences between groups by applying the ANOVA test to the samples taken at 30, 40, 50, 60 and 70 minutes after coronary occlusion. For this analysis we normalized the

individual curves to their baseline value by subtracting it from each measurement. To assess group differences in early ST segment changes the ANOVA test was performed at baseline, 10, 20, 30, 40, 50 and 60 minutes. Results are expressed as mean±1 standard deviation, and as significance test for lineal, quadratic, and cubic contrasts the level was set to $p<0.05$. The assumption of normality for ANOVA residuals was graphically verified using normal probability plots. Correlation between myocardial impedance and ST segment potential was assessed by linear regression and results are presented as subject-adjusted regression coefficient [17]. Group differences in the onset and in maximal changes of myocardial resistivity and phase angle, in the time to peak of phase Ia and Ib arrhythmias, and in the total number of ventricular premature beats were evaluated by the Student's t test.

Impedance data analysis: Previous studies on isolated myocardial preparations [1,18] have shown a relationship between the sharp increase in tissue resistance and the onset of cellular electrical uncoupling assessed by intracellular potential recordings. Since in the present intact heart model we do not have a direct estimation of cellular uncoupling, the onset of this condition can be only indirectly inferred from the steep impedance changes. On the other hand, uncoupling may not start simultaneously in all ischemic cells because electrical and metabolic derangements are heterogeneously distributed across the ischemic region. The onset of the steep resistivity rise was determined as the moment at which the first derivative of resistivity versus time was maximal. Phase angle changes are more sharply demarcated and in these curves we measured both the maximal rate of change and the earliest time at which a value exceeds 10% of baseline.

RESULTS

Myocardial impedance

Coronary artery occlusion induced a significant ($p<0.01$) rise in myocardial resistivity and a decrease in phase angle in the ischemic area but did not elicit appreciable changes in the normal myocardium (Fig 3.3). Two pigs of group I died prematurely because of a nonreversible ventricular fibrillation and were excluded from the analysis.

Changes in tissue resistivity: As illustrated in Fig 3.3, two to four minutes after coronary occlusion the nonpreconditioned pigs showed an initial slight increase in myocardial resistivity (from 237±41 to 259±41 Ωcm) which was followed by a progressive rise up to 359±59 Ωcm at 34±7 minutes. A second phase began thereafter and was characterized by a rapid increase in resistivity leading to values of 488±100 Ωcm at 60 minutes of coronary occlusion. This second phase was followed by a slow rise until maximal plateau values (718±266 Ωcm) were reached 150±69 minutes after coronary occlusion. Ischemic preconditioning induced significant ($p=0.004$) differences in the time course of myocardial resistivity during the first 30 to 70 minutes of ischemia (Fig 3.4). As shown in Fig 3.5, preconditioning postponed the steep rise in myocardial resistivity (from 34±7 to 52±25 minutes, $p=0.04$), although this treatment did not affect significantly the baseline (209±47 Ωcm) nor the maximal resistivity values (569±178 Ωcm).

Changes in phase angle: In contrast to the prompt onset of resistivity changes, phase angle shift was less than 10% of baseline until 17 minutes of ischemia had elapsed (Fig 3.3 and Fig 3.6). After this interval phase angle slowly decreased from -3.0±1.6 to -4.2±1.2° at 29±8 minutes of occlusion. These initial changes were followed by a sharp shift to -12.5±5.3° at 144±56 minutes leading to a maximal plateau phase that lasted until the end of the study. The slope of the phase angle shift after 30 minutes of coronary occlusion was greater than the slope of the concurrent resistivity rise (% change from baseline per minute, 4.9±3.1%, $P=0.01$) Ischemic preconditioning induced significant ($P=0.004$) differences in the time course

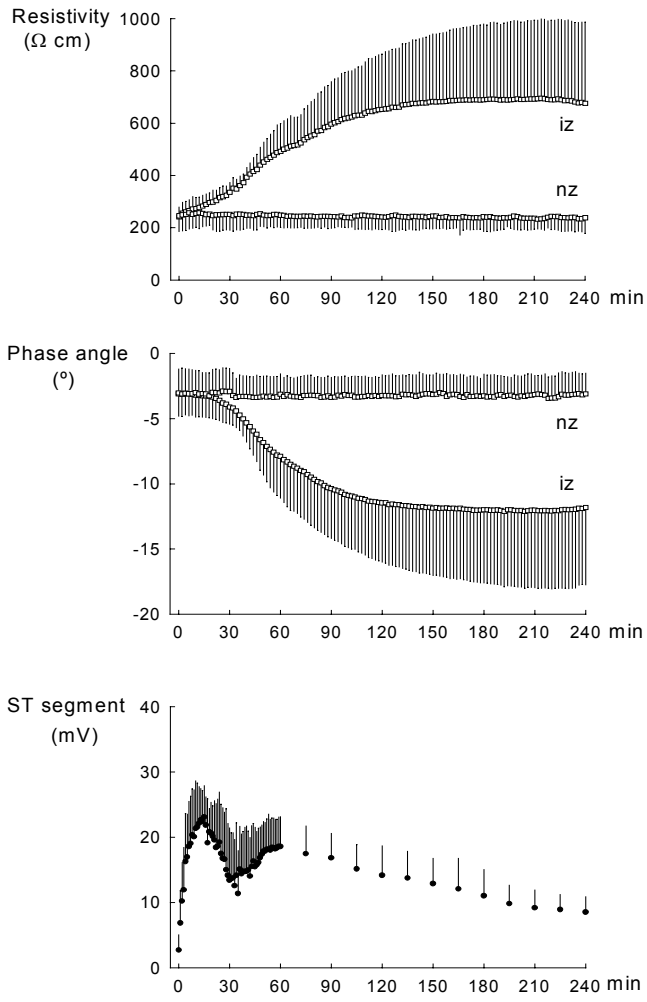

Fig 3.3 Sequential changes in myocardial resistivity, tissue phase angle, and epicardial ST segment potential during 4 hours of acute coronary artery occlusion in 11nonpreconditioned pigs. Dots represent mean value and bars 1 SD of samples from ischemic (iz) and normal (nz) myocardial zones.

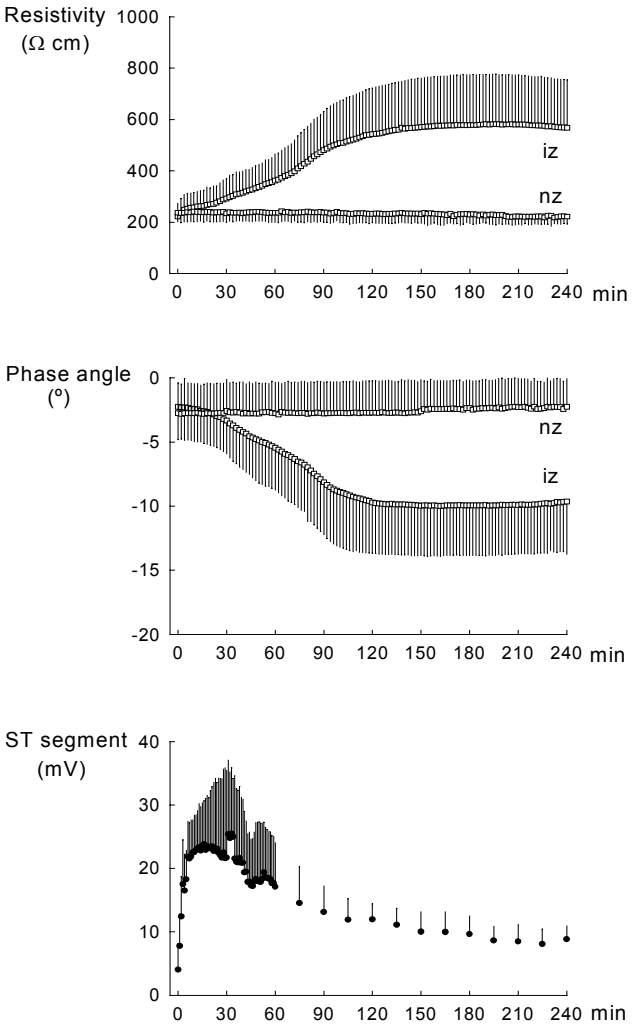

Fig 3.4 Sequential changes in myocardial resistivity, tissue phase angle, and epicardial ST-segment potential during 4 hours of acute coronary artery occlusion in 13 preconditioned pigs. Abbreviations as in Fig 3.3.

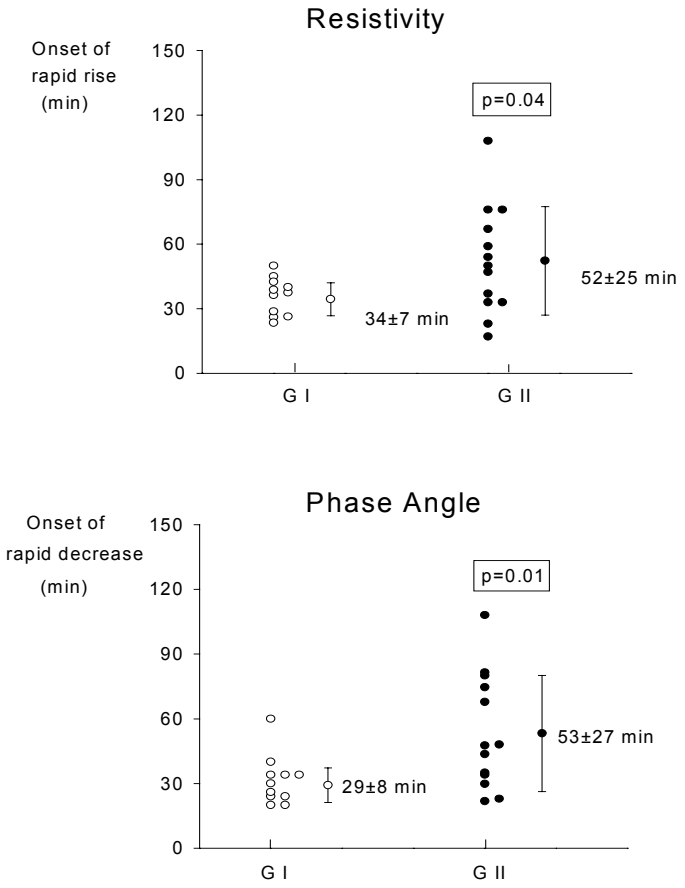

Fig 3.5 Time to onset of fast change in myocardial resistivity and phase angle in 11 nonpreconditioned pigs (GI) and in 13 preconditioned pigs (GII).

of tissue phase angle shift during the first 30 to 70 minutes of ischemia (Fig 2.2). This treatment postponed (Fig 3.5) the onset of the sharp phase angle deviation (29±8 vs 53±27 minutes, p = 0.01) but did not exert a significant influence on baseline (-2.3±2.3°) nor on maximal phase angle values (-11.3±4.3°).

Preconditioned pigs showed slight phase angle changes during the first 17 minutes of ischemia, but these were not significantly different to those in the nonpreconditioned series.

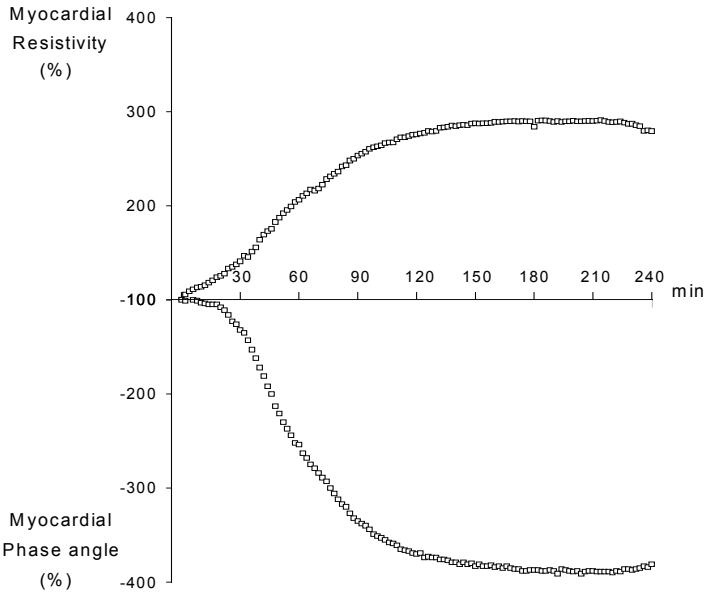

Fig 3.6 Graphs showing mean percent change from baseline in myocardial resistivity and phase angle during 4 hours of coronary artery occlusion in the same 11 pigs as Fig 3.3. To allow comparison with Fig 3.3, percent decrease in phase angle is represented as a negative trend.

ST segment changes

Epicardial electrodes located in the ischemic area showed significant ($p<0.01$) ST segment elevation during the four hours of coronary occlusion in both series of pigs. In the nonpreconditioned group (Fig 3.3), ST segment potential depicted an early sharp rise up to 22.1±4.8 mV at 15 minutes. This was followed by a transient

reversion of ST segment to 11.4±6.3 mV at 35 minutes and by a subsequent reelevation up to 18.0±4.8 mV at 60 minutes of ischemia. From 1 hour onwards, ST segment elevation declined progressively to 9.2±2.8 mV. Peconditioned pigs attained a similar ST segment peak at 15 minutes of ischemia (23.5±6.8 mV) and a comparable ST segment decline (8.8±2.1 mV) at 4 hours of occlusion (Fig 3.4). By contrast, during the first 30-35 minutes of ischemia the preconditioned series showed a less marked ST segment recovery (21.5±13.1 mV, $p=0.01$) than nonpreconditioned pigs, although the ST segment dispersion was larger because four preconditioned pigs still showed transient ST segment recovery (Fig 3.4).

Ventricular arrhythmias

Ventricular premature beats (VPB) depicted a three phase pattern (Fig 3.7). The first phase began two minutes after occlusion, peaked at 6±2 min, and ended approximately 20 min later. After a brief arrhythmia free period there was a second arrhythmia phase peaking at 30±5 minutes which vanished one hour after occlusion. The third arrhythmia period began approximately 75±3 minutes after occlusion and lasted until the third hour of coronary occlusion. Ischemic preconditioning (Fig 3.7, lower panel) attenuated the incidence of ventricular premature beats (total events: 2110 vs 2905, $p<0.05$) especially during the third phase. In addition, preconditioning delayed the time to the peak of the second phase of ventricular ectopic activity (53±25 vs 30±5 minutes, $p=0.02$) but had no significant effect on the time to peak of the first arrhythmia phase.

The incidence and temporal distribution of more severe forms of ventricular arrhythmias is graphically illustrated in Fig 3.8. Two out of the 13 nonpreconditioned pigs (Fig 3.8A) died prematurely because of nonreversible ventricular fibrillation. Episodes of nonsustained VT occurred in 8 of these remaining 11 pigs and tended to group in two phases like those of ventricular ectopic activity. Sustained VT developed in 5 cases, whereas VF occurred in 9 out of the 13 nonpreconditioned pigs. Preconditioning (Fig 3.8B) did not modify significantly the incidence of malignant ventricular arrhythmias.

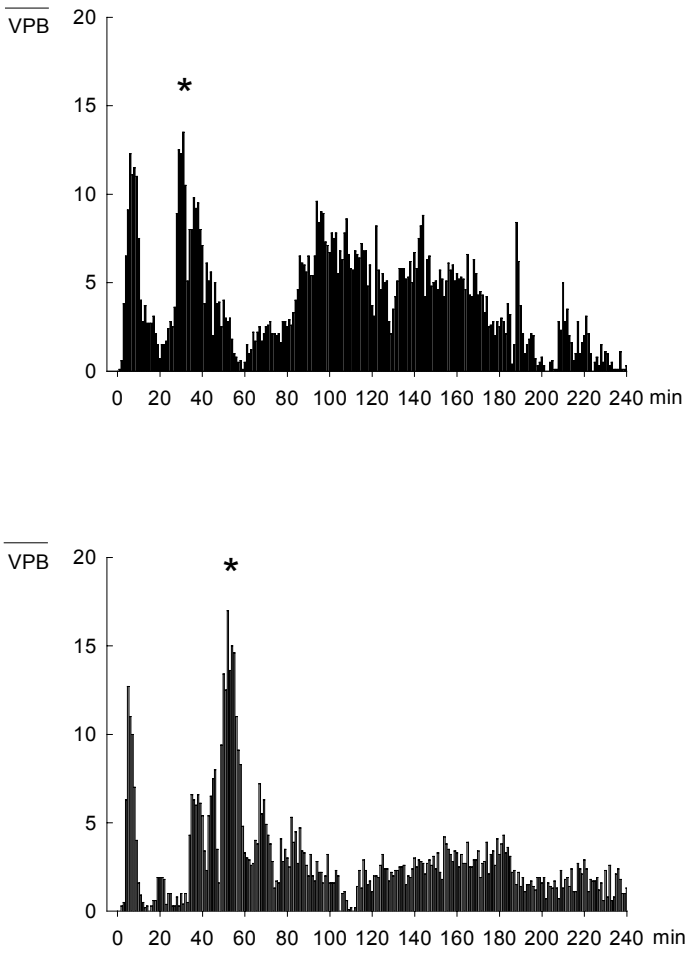

Fig 3.7 Ventricular ectopic activity elicited during 4 hours of coronary artery occlusion in 11 nonpreconditioned (A) and 13 preconditioned (B) pigs. Bars represent mean number of VPBs recorded every minute. Ischemic preconditioning delays second arrhythmia activity peak (*).

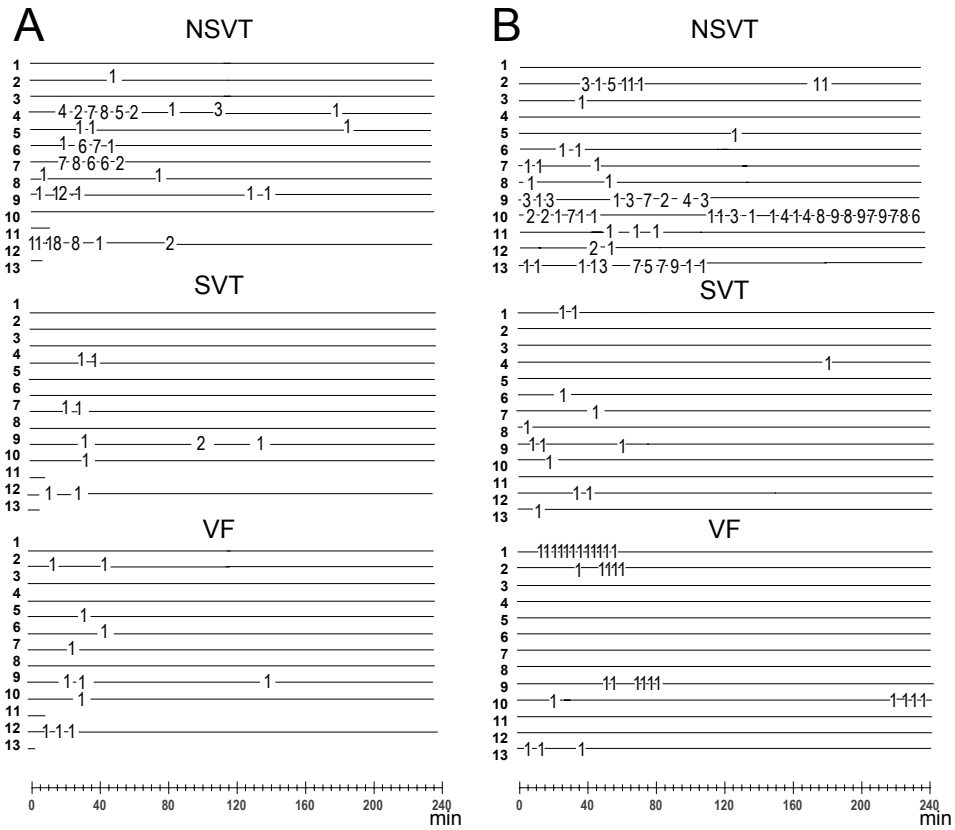

Fig 3.8 Individual distribution of ventricular arrhythmias during 4 hours of coronary artery occlusion in 13 nonpreconditioned (A) and 13 preconditioned (B) pigs. Numbers on lines indicate arrhythmia episodes in each case. NSVT indicates nonsustained VT; SVT, sustained VT. Interruption of lines in pigs 11 and 13 indicates premature death caused by nonreversible VF.

Correlative analysis

The relationship between ST segment and myocardial impedance is complex (Fig 3.3). ST segment elevation peaking at 15 minutes of ischemia was not

accompanied by phase angle shift and only a slight resistivity rise was observed. Between 15 to 60 minutes of ischemia resistivity and phase angle shifted monotonically whilst ST segment elevation depicted a reversion followed by a transitory reelevation. From 1 hour of coronary occlusion onwards, ST segment elevation decreased progressively and tissue resistivity and phase angle attained maximal plateau values in both nonpreconditioned (Fig 3.3) and preconditioned series (Fig 3.4). However, during this late period of time the correlation between ST segment potential and tissue resistivity ($r = -0.26$ for nonpreconditioned and $r = -0.17$ for preconditioned series) and between ST segment and phase angle ($r = 0.31$ and $r = 0.16$, for each group respectively) did not reach statistical significance.

Ventricular ectopic activity peaking at 6-10 minutes of coronary occlusion was associated with a slight tissue resistivity rise but was not accompanied by phase angle changes. By contrast, the second arrhythmia period occurring at about 30 minutes of ischemia was accompanied by a sharp change in resistivity and phase angle and all these variables were delayed by ischemic preconditioning. The third arrhythmia phase was associated with maximal resistivity and phase angle values.

DISCUSSION

Tissue impedance of ischemic myocardium

This study shows that coronary artery occlusion causes alterations in myocardial electrical impedance which are characterized by a tissue resistivity rise begining immediately after occlusion and by a negative phase angle shift that starts after 17 minutes of ischemia.

The mechanism underlying the changes in myocardial impedance in the in situ ischemic heart is not well known. The sharp rise in tissue resistivity has been related to cell-to-cell electrical uncoupling in ischemic heart preparations [1,2,19], but data on phase angle changes elicited by coronary occlusion are scanty [20]. The major determinants of myocardial impedance are the extracellular and intracellular resistance, the gap junction conductance, and the cell membrane capacitance [5-7]. Extracellular resistance increases during the first 10-15 minutes of ischemia in the perfused papillary muscle [1] as a result of the collapse of the extracellular compartment caused by cessation of coronary perfusion and by osmotic cell swelling [21]. By contrast, intracellular resistance increases after 10-15 minutes of ischemia [1] and leads to cellular electrical uncoupling as a result of a drop in gap

junctional conductance induced, among others, by the intracellular accumulation of both free Ca^{2+} [2] and amphipathic lipid metabolites [4] and by the reduction of adenosine triphosphate content [3] in the ischemic myocardium. Intracellular acidosis affects gap junction conductance [22] but it does not appear to be a major trigger for cellular uncoupling during ischemia [2].

Assuming that the time course of extra- and intracellular resistance changes in the ischemic papillary muscle [1] could be extrapolated to the in situ heart, there would be a temporal relationship between the initial increase in extracellular resistance and the immediate slow tissue resistivity rise. Likewise, the subsequent increase in intracellular resistance would correlate with the sharp phase angle and resistivity changes. To further interpret the alterations in myocardial impedance, an equivalent circuit composed by two parallel branches modelling the passive electrical elements of the myocardium [7] may be considered: one branch modelling the extracellular resistance and a second branch composed by a series of three elements modelling respectively the membrane capacitance, the intracellular resistance, and gap junctional resistance. Since phase angle shift is caused by membrane capacitance [23] then the initial changes in extracellular resistance, which in the equivalent circuit is in parallel with this capacitance, will affect tissue resistivity more than phase angle as seen during the first 17 minutes of coronary occlusion in our study. By contrast, the ensuing rise in intracellular resistance [1], which in the equivalent circuit is in series with the capacitance, may account for both the phase angle shift that begins after 17 minutes of ischemia and the further resistivity rise seen in this study as well. Thus, the alterations in intracellular resistance which lead to cell-to-cell electrical uncoupling, may be better defined by the changes in phase angle than by the changes in tissue resistivity. However, since no direct assessment of the uncoupling process is made in this study, we can not precisely ascertain which moment of the phase angle changes indicates the onset of uncoupling. Moreover, uncoupling is not expected to begin simultaneously in all ischemic cells provided that electrical and metabolic derangements are not uniformly distributed in the ischemic area.

This study reveals that ischemic preconditioning postpones the steep changes in both tissue resistivity and phase angle and this is in agreement with the delayed resistivity rise seen in preconditioned papillary muscle [16]. The mechanism by which preconditioning postpones the impairment of passive myocardial properties has been linked to activation of $I_{K\text{-}ATP}$ channel because this delay can be abolished by the channel blocker glibenclamide or, at the contrary, reproduced by the $I_{K\text{-}ATP}$ opener cromakalim [16]. On the other hand, preconditioning postpones the onset of intracellular Ca^{2+} accumulation [2], circumstance that impairs gap junctional

conductance [22]. As compared with nonpreconditioned series, preconditioned pigs depict slight phase angle changes during the first 17 minutes of ischemia suggesting that the three episodes of ischemia and reperfusion performed prior to the sustained coronary occlusion might have yielded residual abnormalities in intracellular resistance, but this needs to be confirmed.

Myocardial impedance and ST segment changes

Myocardial ischemia impairs active electrical cell properties [8,9] and this creates membrane potential differences between the ischemic and normal zones that are responsible for TQ and ST segment shifts in extracellular recordings [8,9]. The current flowing as a result of the regional membrane voltage differences is expected to decrease when tissue resistivity increases in the ischemic region [24,25], thus leading to TQ and ST segment potential attenuation. This circumstance might explain the spontaneous decline in the magnitude of the ST segment elevation seen in patients with acute myocardial infarction [10,11], but correlative studies between ST segment and myocardial impedance in ischemic intact heart are lacking. Our study reveals that there is a transient ST segment recovery at 15-30 minutes of ischemia associated with minor impedance changes, whereas 1 hour after occlusion ST segment elevation declined progressively and impedance changes attained their maximal values. The early ST segment potential decline has been previously described in the porcine model [26] and bears a temporal relationship with the well recognized transitory improvement of action potential characteristics of the ischemic cells [8,9] which coincide with the plateau phase of extracellular K^+ accumulation. It might be therefore anticipated that the recovery of active cell properties will reduce the regional membrane potential differences responsible for ST segment shift and hence play a major role on early ST segment recovery. We observed that ischemic preconditioning tends to lessen the magnitude of transient ST segment recovery, but the mechanism of this action is uncertain. In accordance with the early ST segment recovery other studies in pigs [13] have reported reversion of TQ segment displacement 20-30 minutes after coronary occlusion, although correlative ST segment data were not available. Reversion of ST segment elevation after 1 hour of occlusion is associated with marked myocardial impedance changes suggesting a relationship between these two phenomena. However, other factors like the loss of membrane potential caused by irreversible cell membrane damage may further reduce the regional membrane potential differences between normal and ischemic myocardium and therefore attenuate the ST segment shift.

Myocardial impedance and ventricular arrhythmias

Recent studies by Smith et al [13] and by our group [14] in anesthetized pigs show that phase Ia arrhythmias coincide with the initial slow rise in myocardial resistivity and that phase Ib arrhythmias concur with the steep resistivity rise. Present data further evidence that these arrhythmias can be better defined by the changes in tissue phase angle because phase Ia arrhythmias are not associated with significant changes in tissue phase angle, whereas phase Ib arrhythmias coincide with the fast phase angle shift. The third arrhythmia phase began 1 hour after coronary ligature and coincided with maximal values of tissue resistivity and phase angle. In addition to the relationship with tissue impedance changes, phase Ia arrhythmias coincide with the first rise in extracellular K^+ accumulation and with progressive acidosis in the ischemic area, whereas phase Ib arrhythmias concur with the second K^+ rise [13]. Changes in extracellular K^+ concentration are heterogeneously distributed in the ischemic myocardium [27] and they can be used as a surrogate for the ionic and metabolic derangements induced by ischemia since K^+ changes correlate with the alterations in intracellular Ca^{2+}, intra- and extracellular pH, tissue resistance, and phosphocreatine and adenosine triphosphate (ATP) elicited in the ischemic myocardium [19].

Alterations in tissue impedance may depress conduction of the excitation wavefront [12] and favor the maintenance or the initiation of reentrant arrhythmias. The mechanism underlying the distinct phases of early ischemic arrhythmias is not entirely known. Multisite recordings of local electrograms [24,28] suggest a reentrant mechanism for phase Ia arrhythmias. By contrast, attenuation of phase Ib arrhythmias after β-blockade [29] or after myocardial denervation [30] may indicate that these arrhythmias might be caused by abnormal automaticity provided that this arrhythmogenic mechanism is linked to the action of catecholamines. Present data suggest that alterations in intracellular resistance may play a role on the genesis of phase Ib and late (2 to 4 hours) ischemic arrhythmias but not those of phase Ia. This assumption is further strengthened by the fact that preconditioning postpones in a parallel fashion both the steep changes in myocardial impedance and the peak of the phase Ib arrhythmias.

The beneficial effect of preconditioning on reperfusion arrhythmias has been largely recognized [31-33] but its influence on arrhythmias during acute coronary occlusion is less known. In our series preconditioning attenuated the incidence of ventricular premature beats during coronary occlusion but not the incidence of

more severe ventricular arrhythmias. Other studies report reduction in the number of severe ventricular arrhythmias during coronary occlusion in preconditioned hearts [31,34,35].

REFERENCES

1 Kléber AG, Riegger CB, Janse MJ. Electrical uncoupling and increase of extracellular resistance after induction of ischemia in isolated, arterially perfused rabbit papillary muscle. Circ Res. 1987;61:271-279.

2 Dekker LRC, Fiolet JWT, VanBavel E, Coronel R, Opthof T, Spaan JAE, Janse MJ. Intracellular Ca^{2+}, intracellular electrical coupling, and mechanical activity in ischemic rabbit papillary muscle. Effects of preconditioning and metabolic blockade. Circ Res. 1996;79:237-246.

3 Sugiura H, Toyama J, Tsuboi N, Kamiya K, Kodama I. ATP directly affects junctional conductance between paired ventricular myocytes isolated from guinea pig heart. Circ Res. 1990;66:1095-1102.

4 Wu J, McHowat J, Saffitz JE, Yamada KA, Corr PB. Inhibition of gap juctional conductance by long-chain acylcarnitines and their preferential accumulation in junctional sarcolemma during hypoxia. Circ Res. 1993;72:879-889.

5 van Oosterom A, de Boer RW, van Dam RT. Intramural resistivity of cardiac tissue. Med Biol Eng Comput. 1979;17:337-343.

6 Ellenby MI, Small KW, Wells RM, Hoyt DJ, Lowe JE. On-line detection of reversible myocardial ischemic injury by measurement of myocardial electrical impedance. Ann Thorac Surg.1987;44:587-597.

7 Gebhard MM, Gersing E, Brockhoff CJ, Schnabel A, Bretschneider HJ. Impedance spectroscopy: A method for surveillance of ischemic tolerance of the heart.Thorac Cardiovasc Surg. 1987;35:26-32.

8 Kléber AG, Janse MJ, van Capelle FJL, Durrer D. Mechanism and time course of ST and TQ segment changes during acute regional ischemia in the pig heart determined by extracellular and intracellular recordings. Circ Res. 1978;42:603-613.

9 Cinca J, Janse MJ, Mórena H, Candell J, Valle V, Durrer D. Mechanism and time course of the early electrical changes during acute coronary artery occlusion. An attempt to correlate the early ECG changes in man to the cellular electrophysiology in the pig. Chest. 1980;77:499-505.

10 Zmyslinski RW, Akiyama T, Biddle TL, Shah PM. Natural course of ST segment and QRS complex in patients with acute anterior myocardial infarction. Am J Cardiol. 1979;43:29-34.

11 Madias JE. Electrocardiography in myocardial infarction. J Electrocardiol.1979;12:411-423.

12 Janse MJ, Kléber AG.Propagation of electrical activity in ischemic and infarcted myocardium as the basis of ventricular arrhythmias.J Cardiovasc Electrophysiol.1992;3:77-87.

13 Smith WT, Fleet WF, Johnson TA, Engle CL, Cascio WE. The Ib phase of ventricular arrhythmias in ischemic in situ porcine heart is related to changes in cell-to-cell electrical coupling. Circulation. 1995;92:3051-3060.

14 Warren M, Cinca J, Mont L, Soldevilla A, Carreño A, Romero B, J Soler-Soler. Impedancia eléctrica y arritmias ventriculares durante la oclusión aguda de la arteria coronaria en cerdos. Rev Esp Cardiol. 1995;48(suppl 6 Abstract):75.

15 Kaplinsky E, Ogawa S, Balke CW, Dreifus LS. Two periods of early ventricular arrhythmia in the canine acute myocardial infarction model. Circulation. 1979;60:397-403.
16 Tan HL, Mazón P, Verberne HJ, Sleeswijk ME, Coronel R, Opthof T, Janse MJ. Ischaemic preconditioning delays ischaemia induced cellular electrical uncoupling in rabbit myocardium by activation of ATP sensitive potassium channels. Cardiovas Res. 1993;27:644-651.
17 Kleimbaum DG, Kupper LL, Muller KE. Dummy variables in regression. In: Applied regression analysis and other multivariable methods. Kleimbaum DG, Kupper LL, Muller KE ed. PWS-KENT Publishing Co. Boston 1988 pp 260-296.
18 Cascio WE, Yan GX, Kleber AG. Passive electrical properties, mechanical activity, and extracellular potassium in arterially perfused and ischemic rabbit ventricular muscle. Circ Res. 1990;66:1461-1473.
19 Owens LM, Fralix TA, Murphy E, Cascio WE, Gettes LS. Correlation of ischemia-induced extracellular and intracellular ion changes to cell-to-cell electrical uncoupling in isolated blood-perfused rabbit hearts. Circulation. 1996;94:10-13.
20 Fallert MA, Mirotznik MS, Downing SW, Savage EB, Foster KR, Josephson ME, Bogen DK. Myocardial electrical impedance mapping of ischemic sheep hearts and healing aneurysms. Circulation. 1993;87:199-207.
21 Tranum-Jensen J, Janse MJ, Fiolet JWT, Krieger WJG, d'Alnoncourt CN, Durrer D. Tissue osmolality, cell swelling, and reperfusion in acute regional myocardial ischemia in the isolated porcine heart. Circ Res. 1981;49:364-381.
22 Noma A, Tsuboi N. Dependence of junctional conductance on proton, calcium and magnesium ions in cardiac paired cells of guinea pig. J Physiol (Lond). 1987;382:193-211.
23 Cole KS. Linear and passive cell properties. In: Membranes, ions and impulses. Cole KS ed. University of California Press. Berkeley, Los Angeles. 1968, pp 6-113.
24 Janse MJ, van Capelle FJL, Morsink H, Kléber AG, Wilms-Schopman F, Cardinal R, D'Alancourt CN, Durrer D. Flow of "injury" current and patterns of excitation during early ventricular arrhythmias in acute regional myocardial ischemia in isolated porcine and canine hearts: Evidence for two different arrhythmogenic mechanisms. Circ Res. 1980;47:151-165.
25 Plonsey R, Fleming DG. Bioelectric phenomena. McGraw-Hill. New York 1969, p 210.
26 Bardají A, Cinca J, Worner F, Schoenenberger A. Effects of anaesthesia on acute ischaemic arrhythmias and epicardial electrograms in the pig heart in situ. Cardiovasc Res. 1990;24:227-231.
27 Coronel R, Wilms-Schopman FJG, Opthof T, Cinca J, Fiolet JWT, Janse MJ. Reperfusion arrhythmias in isolated perfused pig hearts. Inhomogeneities in extracellular potassium, ST and TQ potentials, and transmembrane action potentials. Cir Res. 1992;71:1131-1142.
28 Scherlag BJ, El-Sherif N, Hope R, Lazarra R. Characterization and localization of ventricular arrhythmias resulting from myocardial ischemia and infarction. Circ Res. 1974;35:372-383.
29 Penny WJ. The deleterious effects of myocardial catecholamines on cellular electrophysiology and arrhythmias during ischaemia and reperfusion. Eur Heart J. 1984;5:960-973.
30 Cinca J, Bardají A, Salas-Caudevilla A. Ventricular arrhythmias and local electrograms after chronic regional denervation of the ischemic area in the pig heart. J Am Coll Cardiol. 1989;14:225-232.
31 Hagar JM, Hale SL, Kloner RA. Effect of preconditioning ischemia on reperfusion arrhythmias after coronary artery occlusion and reperfusion in the rat. Circ Res. 1991;68:61-68.
32 Shiki K, Hearse DJ. Preconditioning of ischemic myocardium: reperfusion-induced arrhythmias. Am J Physiol 1987;253:H1470-H1476.

33 Osada M, Sato T, Komori S, Tamura K. Protective effect of preconditioning on reperfusion induced ventricular arrhythmias of isolated rat hearts. Cardiovasc Res. 1991;25:441-444.
34 Cohen MV, Yang XM, Downey JM. Conscious rabbits become tolerant to multiple episodes of ischemic preconditioning. Circ Res 1994;74:998-1004.
35 Li Y, Kloner RA. Cardioprotective effects of ischaemic preconditioning are not mediated by prostanoids. Cardiovasc Res. 1992;26:226-231.

Chapter 4

Passive Transmission of Ischemic ST Segment Changes in Low Electrical Resistance Myocardial Infarct Scar in the Pig

Contents

INTRODUCTION

Myocardial ischemia depresses active electrical cell membrane properties and this generates regional potential differences between normal and ischemic compartments [1,2]. As a result of these potential gradients, intra- and extracellular injury currents flow between normal and ischemic myocardial areas during the cardiac cycle [1,2]. During the early repolarization period an extracellular current flowing from ischemic to normal areas is responsible for the ST segment elevation in electrodes overlying the acute ischemic region [1-3] whereas, at the same time, electrodes brought in contact with normal bordering myocardium show isoelectric ST segment potential or reciprocal downward ST segment deviation. Although ST segment elevation is a characteristic feature of ischemia, a similar electrocardiographic pattern can be observed when the exploring electrode is brought in contact with a contiguous region of healed myocardial infarction. Indeed, in a model of ischemia superimposed at the borders of a healed myocardial infarction we [4] have recorded ST segment elevation in electrodes overlying the contiguous necrotic scar despite that no ischemia of viable tissue was present in this particular region. We hypothesized that ST segment potential changes were passively transmitted from the peri-infarction zone towards the necrotic scar, but the passive electrical properties of the infarct scar were not investigated in this model. Theoretically, to allow propagation of injury currents the infarcted tissue should possess low resistance properties. Data on tissue electrical resistance in areas of chronic infarction have been only reported in sheep [5] and showed values lower than in normal myocardium. However, the electrical properties of the scar during superimposed peri-infarction ischemia are not known and have not been correlated with ST segment potential transmission in the infarct scar.

Therefore, this study aimed to delineate the passive electrical properties of a healed myocardial infarction devoid of viable tissue and to correlate these properties with the ST segment potential changes transmitted into the infarct scar during acute peri-infarction ischemia.

STUDY PROTOCOL AND DATA ANALYSIS

Data were obtained from 19 pigs that survived a 1 month coronary occlusion. In 12 open chest pigs (group I), we recorded tissue electrical resistivity at 1 kHz, ST segment potential, conventional ECG, and blood pressure at baseline and every minute during one hour of LAD reocclusion (Fig 4.1). In the remaining 7 open chest pigs (group II) baseline impedance spectrum and pulse voltage decay was measured in normal and necrotic myocardium in vivo. In 5 of these 7 hearts the same variables were measured in explanted infarcted tissue and anatomical analysis was undertaken at the end of the protocol.

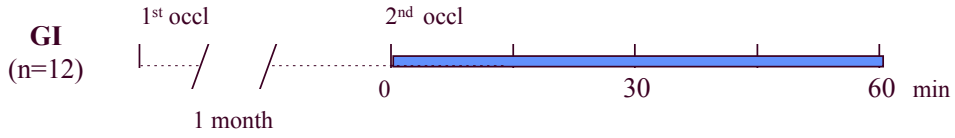

Fig 4.1 Schematic figure of the protocol in 12 open chest infarcted pigs of group I (GI) submitted to a reocclusion of the LAD.

Changes in tissue resistivity were measured simultaneously by inserting one probe electrode at the center of the infarction zone and a second electrode in the bordering noninfarcted myocardium that became ischemic after the second LAD ligature. The latter electrode was always sutured perpendicular to the LAD to avoid the influence of tissue anisotropy on the impedance measurements [6]. However, the interelectrode distance is larger than myocardial fiber dimensions and is expected to average the effects of fiber orientation [5]. Extracellular electrograms were recorded with twelve cotton electrodes sutured to a rubber membrane at interelectrode distances of 5 mm, forming a linear array. The electrode membrane was sutured parallel to the LAD and covered an area extending from the center of the necrotic scar towards the acute ischemic peri-infarction zone and normal myocardium (Fig 4.2).

To study electrical transmission through the necrotic scar, current pulses were applied between a pair of platinum electrodes (length= 3.5 mm, diameter= 0.4 mm) inserted transmurally in the infarcted tissue. As illustrated in Fig 4.2, these two current electrodes (I^+ and I^-) were inserted at two opposite sites within the

infarcted region separated by 32.5 mm. The resulting potential difference was measured between a fixed reference electrode (V^-) located next to the current reference electrode (I^-) and an exploring electrode (V^+) that was moved at 2.5 mm intervals from the active current electrode (I^+) towards the reference potential electrode using a millimetric scale. In each case eleven sites were sampled.

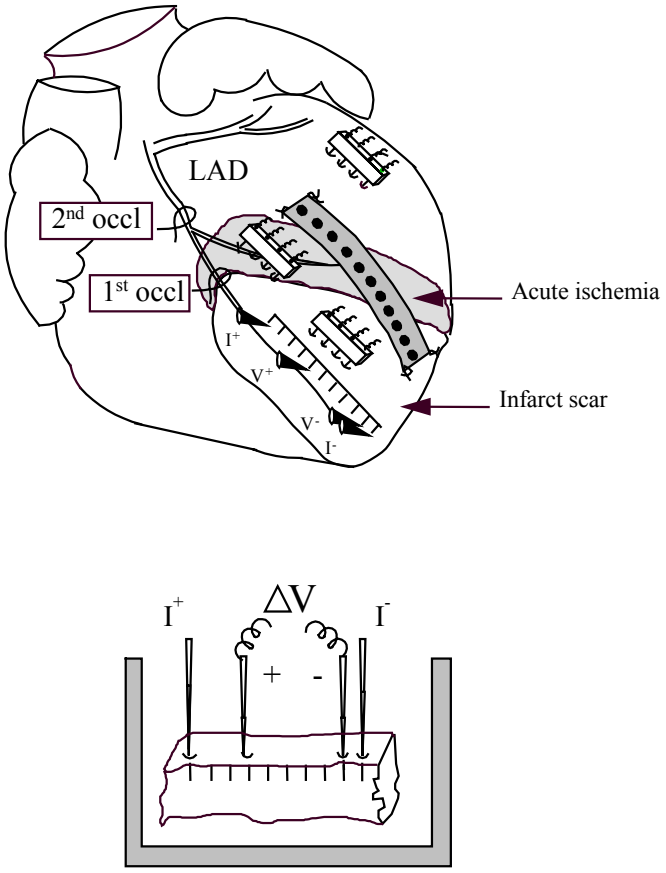

Fig 4.2 Schematic representation of the experimental preparation. Upper: Relative position of impedance probes (P) and the epicardial row of electrodes with respect to the chronic infarction area, acute ischemic peri-infarction region (shaded area), and proximal normal myocardium. Lower: Measurements of current pulse propagation in explanted tissue samples. See text for details.

In vitro measurements: After completion of the in vivo study the heart was removed and a transmural strip of the necrotic scar of approximately 35 mm long and 17 mm wide was placed into a bath chamber (40x35x15 mm). The thickness of the necrotic scar varied between 3 and 4 mm. Current pulses like those used in the in vivo preparation were applied between two intramural platinum electrodes (length= 3.5 mm, diameter= 0.4 mm) inserted at the opposite ends of the preparation (Fig 1). Like in the in vivo study, the potential generated by the stimulating electrodes was measured by moving the exploring electrode at 2.5 mm intervals using a micromanipulator. Voltage attenuation was also calculated as the slope of the regression line that best fits pulse amplitude data plotted against distance. Seven sites were explored on each tissue sample. The aim of the in vitro studies was to validate the measurements obtained in vivo. Specifically, we focused on the possibility that electrodes inserted in the thinner infarcted region might be in close proximity with the intracardiac blood and that this influenced measurements of both resistivity and electrical pulse transmission. Therefore, we measured: a) the resistivity of the scar and blood separately using the four-electrode probe and b) the voltage attenuation in explanted infarct scar covered with nonoxygenated blood at 37°C, in explanted infarct scar alone kept at room temperature, and in nonoxygenated blood alone at 37°C. The amount of blood used for the measurements was equivalent to that needed to fill the bath chamber.

To have comparative reference data we also measured voltage decay in low resistance 0.9% NaCl solution and in high resistance 300 mmol/L sucrose solution at 37°C.

Since explantation of the infarct scar may alter its passive electrical properties, we assessed the biophysical stability of the in vitro preparation in two cases by continuously measuring tissue resistivity with the same implanted electrodes at room temperature during 80 minutes beginning immediately after explantation. Likewise, the in vitro resistivity measurements were done using the same four-electrode probe employed in vivo and its cell constant was calculated by measuring the resistance of 0.9% NaCl solution at 37°C in a volume equivalent to that of the bath chamber.

Data analysis: Changes in tissue resistivity and ST segment potential induced by 1 hour of LAD reocclusion in the acute ischemic peri-infarction area and in the infarct scar were compared and differences between these two regions were assessed by repeated measures analysis of variance (ANOVA) using a commercially available software (SYSTAT Inc.). Results are expressed as mean±1 standard deviation, and as significance test for linear, quadratic, and cubic

contrasts the level was set to $p<0.05$. The assumption of normality for ANOVA residuals was graphically verified using normal probability plots. The regression line of pulse amplitude against distance was accepted if the correlation coefficient $r >0.90$. Differences between in vivo ST segment and pulse current slopes were assessed by paired Student's t test, whereas the slopes measured in vitro were evaluated by ANOVA and Tukey tests.

RESULTS

Pigs submitted to one hour of coronary reocclusion showed a significant decrease of aortic blood pressure (from 111±14 mmHg to 98±14 mmHg, p=0.002) and a tendency to increase the heart rate, but the latter was not statistically significant (124±33 bpm vs 132±26 bpm).

Myocardial impedance

Tissue resistivity: Resistivity of 1-month-old myocardial infarction at 1 kHz was significantly lower than that of normal myocardium (110±30 Ωcm vs 235±60 Ωcm, $p<0.0001$) in the 19 pigs included in this study. Fig 4.3 shows that one hour after proximal reocclusion of the LAD the 12 pigs of group 1 depicted a marked increase of tissue resistivity in the acute ischemic region (from 265±74 Ωcm to 510±135 Ωcm, $p<0.01$) whereas this variable remained virtually unchanged in the center of the necrotic scar (113±40 Ωcm vs 116±42 Ωcm). Individual analysis of the resistivity changes revealed an initial slow rise of 49% from baseline during the first 25 to 30 minutes followed by a faster rise leading to a 121% increase after 60 minutes of coronary occlusion.

Application of DC countershocks to treat episodes of ventricular fibrillation did not shift significantly the values of tissue resistivity.

In vitro measurements of the resistivity of the infarct scar and blood at room temperature showed lower values in the scar than in blood (166±26 Ωcm vs 218±38 Ωcm, $p<0.01$). The stability of the electrical properties of the explanted strips of infarct scar was assessed in two cases during a period of 80 minutes. In these two pigs, resistivity values of the explanted scar remained unchanged during the study period (233 Ωcm and 226 Ωcm, respectively). By contrast, strips of explanted nonperfused normal myocardium from the same two animals showed a progressive resistivity rise leading to maximal values of 926 Ωcm and 850 Ωcm respectively.

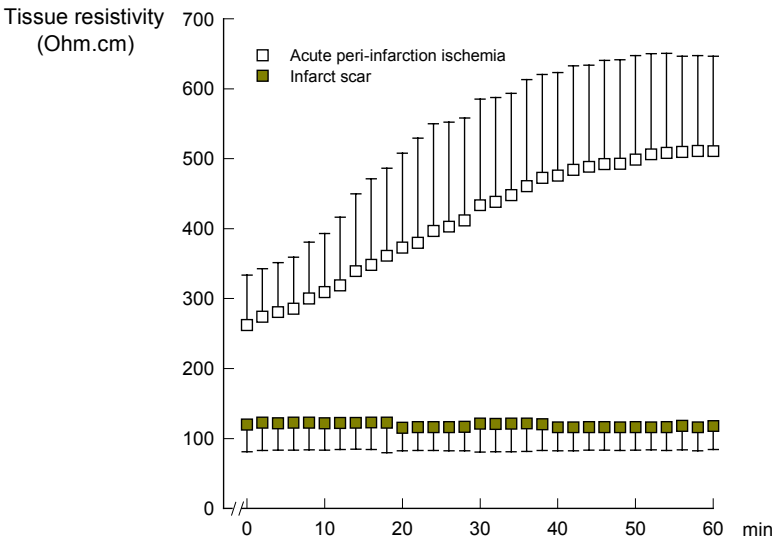

Fig 4.3 Sequential changes in tissue resistivity elicited during 60 min of proximal coronary reocclusion in 12 pigs with a one. month old infarction. Symbols represent the mean value, bars represent one standard deviation. Note a marked rise in the ischemic peri-infarction zone with no changes in the contiguous infarcted region.

Tissue impedance spectroscopy: Data from the 7 pigs of group 2 indicate that normal myocardium and healed infarcted tissue can be differentiated by their distinct impedance spectrum. Fig 4.4 shows that as current frequency increases, the resistivity of the normal myocardium decreases progressively (from 254±86 Ωcm to 176±25 Ωcm at 1000 kHz, $p<0.01$), whereas resistivity of the infarct scar remained unchanged throughout the frequency spectrum (122±21 Ωcm vs 123±22 Ωcm). Likewise, phase angle of normal myocardium decreased progressively from -1.0±1.4° at 1 kHz to a transient minimum value of -11.5±5.6° at 250 kHz, whereas phase angle of the infarcted tissue did not change significantly (-3.45±5.6° vs -2.15±1.7°). The slight negative phase angle shift seen at low frequencies is due to electrode impedance effects.

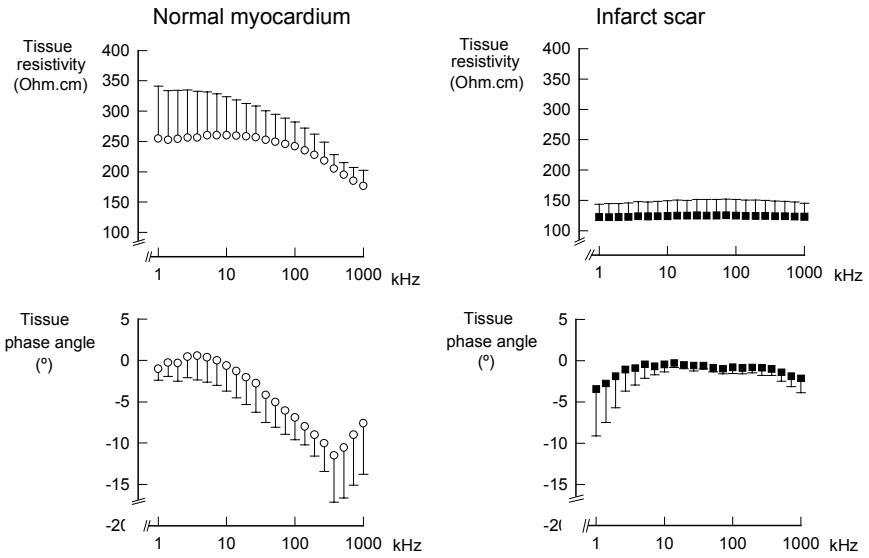

Fig 4.4 Impedance spectrum of normal myocardium and healed infarction at baseline conditions in 7 pigs of group 2. While tissue resistivity and phase angle of normal myocardium decrease at increasing current frequencies, these variables remained constant in the infarcted tissue. Current frequencies are depicted in a logarithmic scale.

Epicardial ST segment potential

Coronary occlusion above the primary LAD ligature induced significant ST segment elevation in electrodes located in the peri-infarction area (from 0.6±0.7 mV to 9.5±5.1 mV at 5 min of ischemia, p=0.002) and also significant ST segment elevation in the center of the necrotic scar (from 0.5±0.5 mV to 3.8±2.6 mV, p=0.03). The remote normal myocardium showed normal ST segment potential or specular ST segment depression. As illustrated in Fig 4.5, the time course of the ST segment changes in the ischemic peri-infarction area paralleled those recorded in the necrotic scar, although the magnitude was higher in the acute ischemic peri-infarction region than at the center of the scar (ANOVA: p=0.03). ST segment potential decreased as the epicardial electrode moved from the periphery towards the center of the necrotic region (Fig 4.6A). The decay of ST segment potential shift in the infarction region was -0.12±0.08 mV/mm (Fig 4.6B).

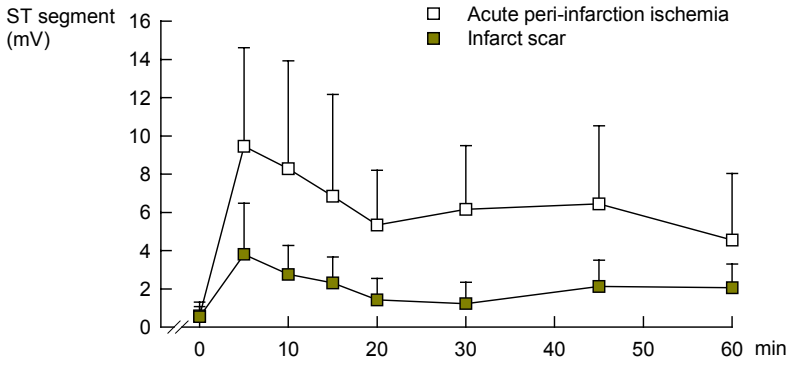

Fig 4.5 Time course of the mean ST segment changes induced by proximal reocclusion of the left anterior descending coronary artery in seven pigs of group 1. ST segment elevation in the ischemic peri-infarction zone was associated with parallel, although less marked, ST segment changes in the center of healed infarction.

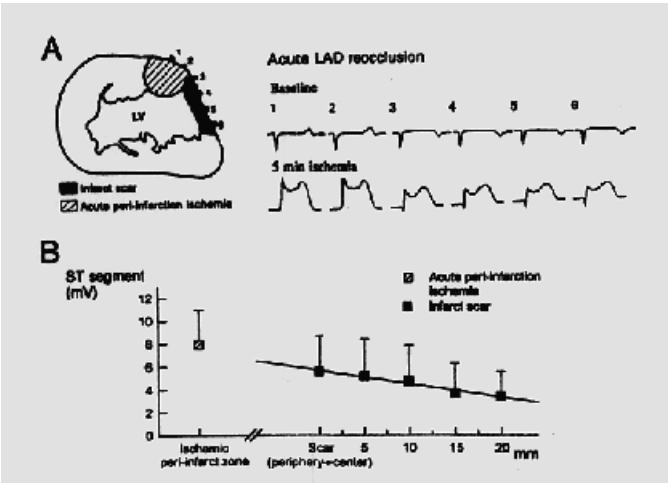

Fig 4.6 A) Computer-generated digital reconstruction of epicardial electrograms showing ST segments changes elicited by 5 min of proximal coronary reocclusdion in an acute ischemic peri-infarction zone and over the adjacent one-month-old infarction. B) Plot of ST segment potential attenuation vs. distance from the ischemic peri-infarction zone in seven pigs of group 1. The slope of the regression line connecting the data was –0.12±0.08 mV/mm.

Electrical transmission in healed infarction

In vivo measurements of pulse amplitude attenuation in the infarcted myocardium performed in 5 pigs of group 2 indicated a decay of -0.07±0.05 mV/mm. This voltage decay was comparable to the ST segment potential attenuation measured in the same anatomical region (illustrated in Fig 4.6B).

In vitro measurement of the voltage decay in the necrotic scar, blood, and 0.9% NaCl solution was performed in 5 pigs of group 2 (Fig 4.7). A voltage attenuation of -0.55±1.1 mV/min was observed in the scar exposed to the air; a decay of -0.37±0.09 mV/mm in the scar covered by nonoxygenated blood; an attenuation of -0.18±0.04 mV/mm in 0.9% NaCl solution; and a decay of -0.58±0.09 mV/mm in nonoxygenated blood alone. By contrast, voltage attenuation in a high resistive solution containing 300 mmol/L of sucrose was markedly higher (-111±74 mV/mm, $p < 0.001$).

Arrhythmia analysis

During the two hours following the first coronary occlusion, 7 out of 26 pigs presented ventricular fibrillation. In four cases the arrhythmia was successfully terminated by external DC shocks, whereas in the three other cases the electrical defibrillation was followed by irreversible atrio-ventricular conduction block.

During the second intervention, 7 out of the 12 pigs of group 1 developed ventricular fibrillation during 1 hour of LAD coronary reocclusion. These animals presented a total number of 17 episodes of fibrillation which were successfully terminated by a single internal DC countershock in 9 instances. The remaining eight episodes required two to three DC shocks. In no instances, animals had to be excluded for irreversible ventricular fibrillation. The hemodynamic conditions remained stable after electrical defibrillation. During the reocclusion period all pigs developed episodes of ventricular tachycardia. This arrhythmia occurred in 184 instances grouped into two phases with a peak activity at about 4 and 30 minutes respectively. Twelve out of the 17 episodes of ventricular fibrillation occurred during the second arrhythmic phase whereas the remaining 5 episodes appeared during the first arrhythmia phase.

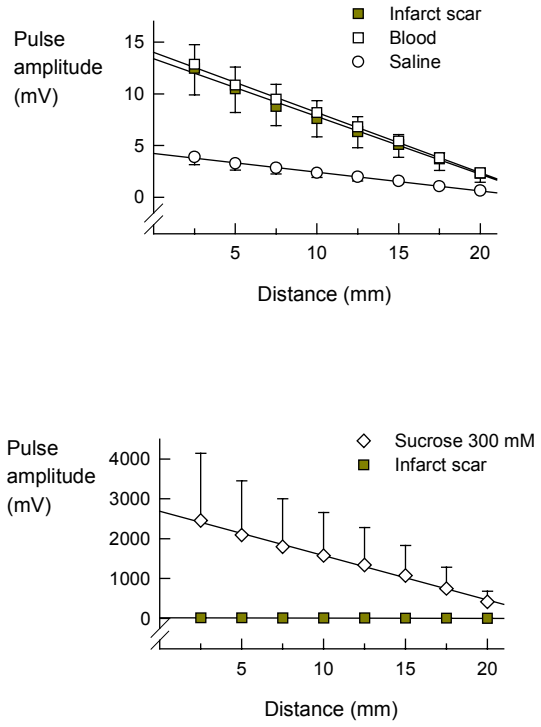

Fig 4.7 Plot of subthreshold current pulse (30 mA) attenuation vs. distance from the current source measured in vitro in explanted healed infarction and test solutions. Electrical conduction across a healed infarction approximates that of blood and saline solution, but is markedly better than that of sucrose. Notice that the pulse voltage developed across the sucrose solution is higher than that generated in the other in vitro solutions due to the high resistivity of sucrose. See text for slope values of the regression lines.

Post mortem examination

One month after permanent coronary occlusion all pigs developed a transmural healed myocardial infarction with sharply demarcated margins. The infarcted

tissue was composed by fibroblasts, collagen fibers, and few capillary vessels. In the center of the scar we observed necrotic myocardial cells heterogeneously distributed. A thin layer of surviving fibers were observed in the subendocardium forming a rather homogeneous band of approximately 0.20 to 0.30 mm width. Surviving bands of about 0.03 mm were also present in the epicardium but in this region they were irregularly distributed. Surviving myocardial cells at the edges of the infarction depicted slight to moderate signs of hypertrophy, but degenerative changes such as pyknosis or steatosis were not observed.

DISCUSSION

Electrical impedance of healed myocardial infarction

This study shows that areas of healed myocardial infarction can be differentiated from normal myocardium by their low electrical resistivity and negligible capacitative response. In accordance with the study by Fallert et al [5] in sheep, the present study in swine shows an approximately 50% lower impedance in healed infarcted tissue than in normal myocardial regions. Our analysis of impedance spectroscopy from 1 to 1000 kHz further revealed that the normal myocardium and the infarct have a different impedance spectrum: the normal myocardium shows a negative shift in resistivity and phase angle at increasing frequencies, whereas the infarcted tissue depicts negligible frequency related changes. The absence of a frequency dependent response suggests that the infarct scar is a noncapacitative medium. This is based on the fact that a frequency response in biological media occurs if cell membranes with preserved capacitative properties are present [7]. Surviving cells in the infarcted tissue are scarce and this circumstance is therefore consistent with the lack of capacitative response in healed infarction.

The mechanism by which a healed infarction possesses low resistance properties is not well known although it seems reasonable to link this electrical characteristic to the extracellular matrix of the infarct scar. The extracellular matrix, which increases during infarct healing [5,8,9], may afford a high ionic diffusibility and hence a low tissue electrical resistivity due to its particular biochemical composition. Indeed, extracellular matrix contains fibrous proteins (collagen, elastin, fibronectin, among others) immersed in an amorphous substance composed by water and electrically charged glycoproteins (proteoglycans) [9,10].

This aqueous phase permits diffusion of nutrients, metabolites and hormones between the blood and tissue cells [10]. The moment at which resistivity of the infarcted tissue falls to lower than normal values has not yet been determined. In the study by Fallert et al [5] this resistivity drop occurred between the first four hours of ischemia and one week after infarction but intermediate time frames were not explored.

Our study rules out the possibility that the low infarct resistivity was in fact a measuring error caused by a closer proximity of the impedance electrodes to the intracavitary blood in the thinned infarcted regions. Indeed, in vitro data indicate that the infarct scar continues to have lower resistivity than blood alone.

Electrical transmission in healed myocardial infarction

In accordance with the low resistance properties of the infarct scar this study demonstrates that the necrotic tissue is able to afford a good transmission of current pulses and of ST segment potential changes elicited by ischemia of contiguous peri-infarction myocardium. Voltage attenuation of current pulses across a transmural healed infarction is as low as that yielded by a high conductive 0.9% NaCl solution and both were comparable to the ST segment potential decay measured in the infarct scar. Therefore, present data support the concept that a healed myocardial infarction is a high conductive medium able to allow passive transmission of extracellular injury currents responsible for ST segment shift; the main sources of which are localized in the ischemic-normal border zone [2]. For this passive transmission, the necrotic scar would act as an expansion of the extracellular space without the need for any intracellular current pathway. Since injury currents may induce arrhythmias [11] a possibility remains to be investigated as to whether the low resistance fibrous tissue might allow conduction of these currents thus intervening in arrhythmogenesis. Also speculatively, remains the possibility of conduction of local currents generated by activation of neighboring excitable myocardium through the fibrous matrix.

Because the infarct scar lacks of capacitative cell membrane properties, the shape of the transmitted current pulses in the infarcted tissue was not distorted. By contrast, electrotonic conduction through unexcitable gaps in Purkinje fibers causes a deformation of action potential upstroke [12,13].

Electrical resistivity in acute ischemic peri-infarction myocardium

Our data demonstrate that the advent of an ischemic episode at the borders of a healed infarction induces a marked resistivity rise in the ischemic peri-infarction zone without altering the low resistivity values in the contiguous healed infarction. Therefore, hearts suffering an acute reinfarction are exposed to marked inhomogeneities in electrical impedance between normal, infarcted and acute ischemic myocardium.

Tissue resistivity rise after coronary occlusion has been reported in several species [5,14,15-19] and reflects the increase in extra- and intracellular electrical resistance that leads to cell-to-cell electrical uncoupling [15]. Cellular uncoupling is a consequence of the increase in gap junctional resistance caused by accumulation of intracellular Ca^{2+} [18], reduction of adenosine triphosphate content [20], and accumulation of amphipathic lipid metabolites [21] in the ischemic myocardium, among other things. The major determinants of myocardial impedance in the intact heart are intracellular and extracellular resistance, gap junction conductance and membrane capacitance [22,23,24]. The rise in tissue resistivity at 1 kHz follows a two-phase pattern [14]. The initial slowly rising phase lasts about 15 minutes and has been related to a rise in extracellular resistance [15] secondary to the collapse of the extracellular compartment caused by cessation of coronary perfusion and by osmotic cell swelling [25]. The second resistivity rise is apparent after 30 minutes of ischemia and has been attributed to increases in both intra and extracellular resistance leading to cell-to-cell electrical uncoupling.

Clinical implications

Studies in patients with autopsy-proven myocardial infarction [26] confirm that, like pigs with a 1-month-old coronary ligature, old coronary occlusion elicits transmural infarcts with collagen deposition and with an irregular band of surviving cells in the subendocardial and subepicardial myocardium. Based on this anatomical resemblance healed transmural myocardial infarcts in humans may also have a low electrical resistivity and this may permit transmission of local currents involved in the genesis of local ST segment potential changes and arrhythmias. Reelevation of ST segment in infarcted-related ECG leads is currently considered indicative of either left ventricular dysfunction [27-29] or ischemia of residual viable myocardium [30,31]. However, the low resistance of the infarct scar seen in this study strengthens a previous observation from our laboratory showing that reelevation of

ST segment in the infarcted region may simply indicate passive ST segment potential transmission from the ischemic peri-infarction zone [4]. The distinct impedance spectrum of normal and infarcted myocardium may settle the basis for the development of new technologies able to detect areas of healed infarction in patients either using intracavitary probes or using noninvasive tomographic systems.

REFERENCES

1. Samson WE, Scher AM. Mechanism of ST segment alteration during acute myocardial injury. Circ Res. 1960;8:780-787.

2 Kléber AG, Janse MJ, van Capelle FJL, Durrer D. Mechanism and time course of ST and TQ segment changes during acute regional ischemia in the pig heart determined by extracellular and intracellular recordings. Circ Res. 1978;42:603-613.

3 Cinca J, Janse MJ, Mórena H, Candell J, Valle V, Durrer D. Mechanism and time course of the early electrical changes during acute coronary artery occlusion. An attempt to correlate the early ECG changes in man to the cellular electrophysiology in the pig. Chest. 1980;77:499-505.

4 Cinca J, Bardají A, Carreño A, Mont Ll, Bosch R, Soldevilla A, Tapias A, Soler-Soler J. ST segment elevation at the surface of a healed transmural myocardial infarction in pigs. Conditions for passive transmission from the ischemic peri-infarction zone. Circulation. 1995;91:1552-1559.

5 Fallert MA, Mirotznik MS, Downing SW, Savage EB, Foster KR, Josephson ME, Bogen DK. Myocardial electrical impedance mapping of ischemic sheep hearts and healing aneurysms. Circulation. 1993;87:199-207.

6 Plonsey R, Barr RC. A critique of impedance measurements in cardiac tissue. Ann Biomed Eng. 1986;14:307-322.

7 Foster KR, Schwan HP. Dielectric properties of tissues and biological materials: critical review. Crit Rev Biomed Eng. 1989;17:25-104.

8 Jugdutt BI, Amy RWM. Healing after myocardial infarction in the dog: changes in infarct hydroxyproline and topography. J Am Coll Cardiol. 1986;7:91-102.

9 Ju H, Dixon IMC. Extracellular matrix and cardiovascular diseases. Can J Cardiol. 1996;12:1259-1267.

10 Alberts B, Bray D, Lewis J, Raff M, Roberts K, Watson JD. Cell adhesion, cell junctions and the extracellular matrix. In: Molecular biology of the cell. Ed: Robertson M. Garland Publishing. New York. 1989. pp:791-836.

11 Janse MJ, van Capelle FJL, Morsink H, Kléber AG, Wilms-Schopman F, Cardinal R, D'Alancourt CN, Durrer D. Flow of "injury" current and patterns of excitation during early ventricular arrhythmias in acute regional myocardial ischemia in isolated porcine and canine hearts: Evidence for two different arrhythmogenic mechanisms. Circ Res. 1980;47:151-165.

12 Jalife J, Moe GK. Excitation, conduction, and reflection of impulses in isolated bovine and canine cardiac Purkinje fibers. Circ Res. 1981;49:233-247.

13 Antzelevitch C, Moe GK. Electrotonically mediated delayed conduction and reentry in relation

to "slow responses" in mammalian ventricular conducting tissue. Circ Res. 1981;49:1129-1139.

14 Cinca J, Warren M, Carreño A, Tresànchez M, Armadans Ll, Gómez P, Soler-Soler J. Changes in myocardial electrical impedance induced by coronary artery occlusion in pigs with and without preconditioning. Correlation with local ST segment potential and ventricular arrhythmias. Circulation 1997;96: 3079-3086.

15 Kléber AG, Riegger CB, Janse MJ. Electrical uncoupling and increase of extracellular resistance after induction of ischemia in isolated, arterially perfused rabbit papillary muscle. Circ Res. 1987;61:271-279.

16 Cascio WE, Yan GX, Kleber AG. Passive electrical properties, mechanical activity, and extracellular potassium in arterially perfused and ischemic rabbit ventricular muscle. Circ Res. 1990;66:1461-1473.

17 Smith WT, Fleet WF, Johnson TA, Engle CL, Cascio WE. The Ib phase of ventricular arrhythmias in ischemic in situ porcine heart is related to changes in cell-to-cell electrical coupling. Circulation. 1995;92:3051-3060.

18 Dekker LRC, Fiolet JWT, VanBavel E, Coronel R, Opthof T, Spaan JAE, Janse MJ. Intracellular Ca^{2+}, intracellular electrical coupling, and mechanical activity in ischemic rabbit papillary muscle. Effects of preconditioning and metabolic blockade. Circ Res. 1996;79:237-246.

19 Owens LM, Fralix TA, Murphy E, Cascio WE, Gettes LS. Correlation of ischemia-induced extracellular and intracellular ion changes to cell-to-cell electrical uncoupling in isolated blood-perfused rabbit hearts. Circulation. 1996;94:10-13.

20 Sugiura H, Toyama J, Tsuboi N, Kamiya K, Kodama I. ATP directly affects junctional conductance between paired ventricular myocytes isolated from guinea pig heart. Circ Res. 1990;66:1095-1102.

21 Wu J, McHowat J, Saffitz JE, Yamada KA, Corr PB. Inhibition of gap junctional conductance by long-chain acylcarnitines and their preferential accumulation in junctional sarcolemma during hypoxia. Circ Res. 1993;72:879-889.

22 Gebhard MM, Gersing E, Brockhoff CJ, Schnabel A, Bretschneider HJ. Impedance spectroscopy: A method for surveillance of ischemic tolerance of the heart. Thorac Cardiovasc Surg. 1987;35:26-32.

23 van Oosterom A, de Boer RW, van Dam RT. Intramural resistivity of cardiac tissue. Med Biol Eng Comput. 1979;17:337-343.

24 Ellenby MI, Small KW, Wells RM, Hoyt DJ, Lowe JE. On-line detection of reversible myocardial ischemic injury by measurement of myocardial electrical impedance. Ann Thorac Surg. 1987;44:587-597.

25 Tranum-Jensen J, Janse MJ, Fiolet JWT, Krieger WJG, d'Alnoncourt CN, Durrer D. Tissue osmolality, cell swelling, and reperfusion in acute regional myocardial ischemia in the isolated porcine heart. Circ Res. 1981;49:364-381.

26 Fishbein MC, Maclean D, Maroko PR. The histopathologic evolution of myocardial infarction. Chest. 1978;73:843-849.

27 Lahiri A, Balasubramanian V, Millar Craig MW, Crawley J, Raftery EB. Exercise-induced ST segment elevation. Electrocardiographic, angiographic, and scintigraphic evaluation. Br Heart J 1980;43:582-588.

28 Dunn RF, Bailey IK, Uren R, Kelly DT. Exercise-induced ST-segment elevation. Correlation of thallium-201 myocardial perfusion scanning and coronary arteriography. Circulation 1980;61:989-995.

29 Chahine RA, Lowery MH, Bauerlein EJ. Interpretation of the exercise-induced ST-segment

elevation. Am J Cardiol 1993;72:100-102.

30 Margonato A, Chierchia SL, Xuereb RG, Xuereb M, Fragasso G, Cappelletti A, Landoni C, Lucignani G, Fazio F. Specificity and sensitivity of exercise-induced ST segment elevation for detection of residual viability: comparison with fluorodeoxyglucose and positron emission tomography. J Am Coll Cardiol. 1995;25:1032-1038.

31 Elhendy A, Fiorett PM. Stress-induced ST-segment elevation after a recent myocardial infarction:myocardial necrosis, viability or both?. Eur Heart J.1996;17:975-977.

Chapter 5

Detection of Healed Transmural Myocardial Infarction by Percutaneous Electrocatheter Measurement of Electrical Impedance Spectrum

Contents

INTRODUCTION

Measurement of myocardial electrical impedance (resistance and phase angle) with intramural electrodes in animals with acute [1,2] and chronic myocardial infarction [1,3] has shown that healed infarcted myocardium can be differentiated from acute ischemic and healthy tissue by its lower resistance and by its flat phase angle frequency spectrum [3]. The development of a system capable of measuring myocardial impedance with a percutaneous intracavitary catheter would allow on line recognition of areas of healed infarction in patients. In this study we describe a new intracardiac catheter method which permits in vivo on-line detection of chronic transmural myocardial infarction in pigs.

STUDY PROTOCOL AND DATA ANALYSIS

Data were obtained from 9 pigs with a healed transmural infarction. Myocardial impedance spectrum was measured with an intracardiac electrocatheter introduced into the left ventricle either directly in four open chest pigs (group I), or percutaneously in the remaining five closed chest animals (group II). Electrical impedance was measured between the proximal catheter electrode and a reference electrode placed either on the overlying epicardium (group I) or on the precordial region (group II). Reference electrode sizes were respectively 20x20x0.2 mm and 100x150x1 mm.

In group I (open chest), a 1/0 silk thread mounted on a 10-cm long needle was secured to the catheter tip and was used to pull the catheter from the left ventricular posterior wall towards the endocardium of the anterior region (Fig 2.6). After measuring tissue impedance, the guiding thread was cut and left in place to mark the recording site. In each pig, we explored at least 7 loci spaced 2 to 3 mm apart, extending from the infarction to the surrounding healthy myocardium.

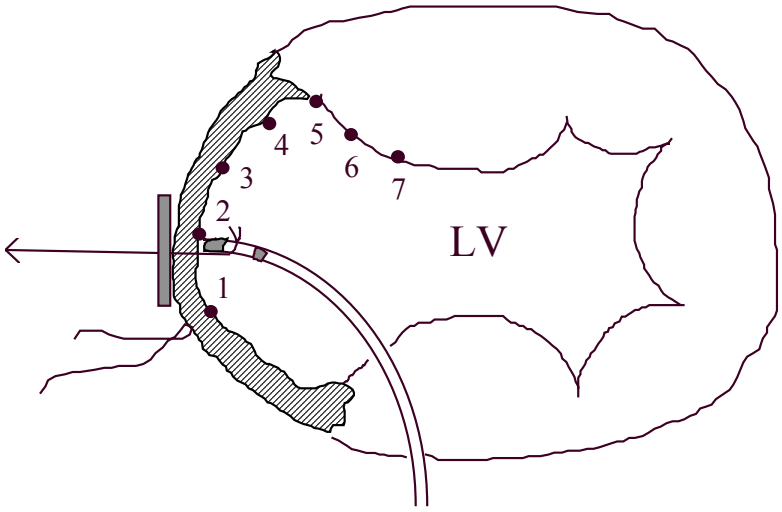

Fig 5.1 Technique of measuring tissue electrical impedance in a pig with a 2-month old transmural myocardial infarction (Masson's trichrome staining) using an electrocatheter (C) introduced into the left ventricle (LV) and an epicardial reference electrode (E). The catheter is directed towards the recording site by pulling a thread (arrow) secured to the catheter tip.

In group II (closed chest), the catheter was introduced into the left ventricle through the femoral artery under fluoroscopic control. This series was used to asses the possible methodological drawbacks that may occur in circumstances mimicking the clinical setting. The infarcted region was identified by its akinetic movement during left ventriculography. Moreover, a radiofrequency ablation lesion was produced at a site supposed to be in the necrotic area for later verification. Measures were taken in about 5 normal and 5 infarcted sites in each animal.

Data analysis: Changes in mean values of resistance and phase angle at each current frequency were calculated by applying the ANOVA test for repeated measures using sample values at 1, 10, 100, 1000 kHz . The same test was used to evaluate differences in resistance and phase angle between the two groups of pigs. The frequency that best differentiated infarcted from healthy myocardium was calculated by maximizing the inter to intraset distance ratio [4]. Group differences in the impedance values at these frequencies were assessed by the student's t test . A p value <0.05 was considered significant.

RESULTS

All pigs had a healed anterior transmural myocardial infarction with a thin subendocardial surviving cell layer of about 157±96 μm. Tissue impedance was measured in 31 sites in the open chest group (17 in the infarcted area, 9 in the normal myocardium, and 5 in the border zone) and in 48 sites in the closed chest series (26 in the akinetic region and 22 in areas with normal wall motion). The sentinel radiofrequency lesion was correctly located in the infarcted area in all 5 cases.

Myocardial impedance spectrum

Group I **:** As shown in Fig 5.2A, electrical resistance of normal myocardium decreased from 50±19 Ω at 1 kHz to 25±8 Ω at 1 MHz and phase angle decreased from 1.6±2.0 º at 1 kHz to a minimum of -15.3±4.9 º at 421 kHz (ANOVA: $p<0.001$). By contrast, resistance and phase angle of infarcted tissue had almost no frequency response. Moreover, the infarcted myocardium had a lower than normal resistance and a nearly zero phase angle at all frequencies ($p<0.001$) (Fig 5.2A). The frequencies that better differentiate normal from infarcted tissue were 1 kHz for the resistance and 316 kHz for the phase angle (Table 5.1).

Group II**:** The resistance and phase angle of normal myocardium showed a less apparent frequency response in closed than in open chest pigs (Fig 5.2B). Indeed, resistance decreased from 76±13 Ω at 1 kHz to 70±13Ω at 1 MHz, and phase angle decreased from -0.1±0.5 º at 1 kHz to a minimum of -2.8±1.7 º at 421 kHz. As occurs in open chest pigs, the infarcted myocardium differed from normal tissue by its lower resistance and nearly zero phase angle at all frequencies ($p<0.001$) (Fig 5.2B). As shown in Table 5.1, at the most discriminative frequency of 316 kHz, the infarction was recognized by its nearly zero phase angle.

Table 5.1 Electrical impedance of normal and healed infarcted myocardium at the most discriminative frequencies in pigs.

	Resistance (Ω) at 1 kHz		Phase angle (°) at 316 kHz	
	Normal	Infarction	Normal	Infarction
Open chest (n=4)	50±19	15±4*	-14.8±4.6	-2.5±1.9*
Closed chest (n=5)	76±13	64±13*	-2.7±1.4	+0.7±1.0*

* $p<0.001$ as compared to normal myocardium

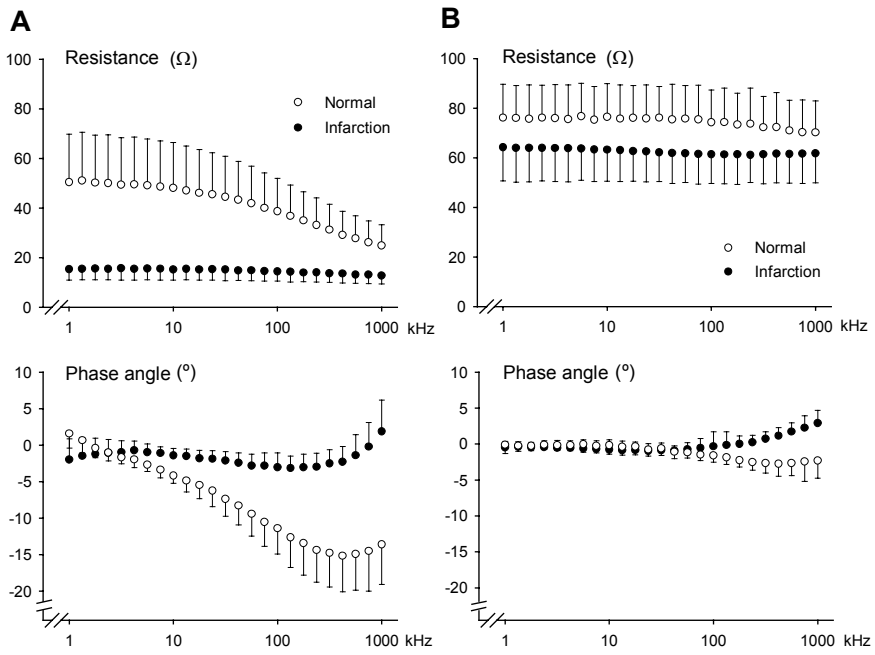

Fig 5.2 Changes in tissue electrical resistance and phase angle as a function of frequency in normal and healed infarcted myocardium in pigs with open (panel A) and closed chest (panel B). Symbols indicate mean values and bars the satandard deviation.

DISCUSSION

This study is the first to show that measurement of myocardial impedance spectrum with a percutaneous intracavitary contact electrocatheter allows in vivo recognition of transmural myocardial infarction by its close to zero phase angle at 316 kHz and by its low resistance at all frequencies. The finding that phase angle spectrum of the infarcted myocardium remains close to zero is presumably related to the low number of cells surviving in this region. Indeed, the capacitative properties of cell membranes are major determinants of the negative shift of phase angle spectrum [5]. The low electrical resistivity of the infarcted myocardium can be explained by the fact that the extracellular matrix generated during infarct healing [6] contains fibrous proteins, water, and electrically charged glycoproteins which favor ionic diffusibility and hence, confer a low electrical resistivity. In agreement with this view, we have previously observed that porcine infarct scar permits transmission of electrical pulses with a low amplitude attenuation [3] and also allows passive diffusion of ionic radiotracers ^{99m}technetium-tetrofosmin and ^{201}thallium chloride [7].

The open chest model shows that under the most favorable conditions (ie: when the catheter tip and reference electrode are well aligned and only myocardial tissue lies between them) the frequency response of tissue impedance of both healthy and infarcted myocardium is comparable to that seen when the more accurate 4-point intramural electrode technique is used in the same porcine model [3]. However, when closed chest pigs are used to mimic the clinical setting, the measured impedance shows a less marked frequency response and, in addition, the measured resistance of normal and infarcted myocardium shifts towards higher values. The attenuated frequency response of impedance in closed chest pigs is due to an averaging effect caused by the different impedance of the surrounding tissues [8]. Likewise, the high resistance of the lung (about 1500 Ωcm in pigs, unpublished personal data) would lead to an upright deviation of the measured resistance in the closed chest model. However, since the myocardium is in physical contact with the electrocatheter, the contribution of this tissue to the measured impedance is higher than that afforded by the surrounding tissues.

Anatomopathological features in patients with transmural myocardial infarction [9] share some correspondence with those in pigs thus it is conceivable that the present catheter technique would have clinical applicability. On line intracavitary catheter recognition of fibrous transmural infarction or areas of ventricular dysplasia would allow identification of sites in which application of energy sources would be ineffective or even hazardous (ie. radiofrequency ablation of

ventricular tachycardias in postinfarction patients or laser application for percutaneous myocardial revascularization).

REFERENCES

1. Fallert MA, Mirotznik MS, Downing SW, Savage EB, Foster KR, Josephson ME, Bogen DK. Myocardial electrical impedance mapping of ischemic sheep hearts and healing aneurysms. Circulation. 1993;87:199-207.
2. Cinca J, Warren M, Carreño A, Tresànchez M, Armadans L, Gómez P, Soler-Soler J. Changes in myocardial electrical impedance induced by coronary artery occlusion in pigs with and without preconditioning. Correlation with local ST segment potential and ventricular arrhythmias. Circulation 1997;96:3079-3086.
3. Cinca J, Warren M, Rodríguez-Sinovas A, Tresànchez M, Carreño A, Bragós R, Casas O, Domingo A, Soler-Soler J. Passive transmission of ischemic ST segment changes in low electrical resistance myocardial infarct scar in the pig. Cardiovasc Res 1998;40:103-112
4. Meisel WS. Computer oriented approaches to pattern recognition. Academic Press, New York 1972, pp 179-183
5. Foster KR, Schwan HP. Dielectric properties of tissues and biological materials: critical review. Crit Rev Biomed Eng 1989;17:25-104
6. Ju H, Dixon IMC. Extracellular matrix and cardiovascular diseases. Can J Cardiol 1996;12:1259-1267
7. Cinca J, Garcia-Burillo A, Carreño A, Castell J, Warren M, Candell-Riera J, Domingo A, Soler-Soler J. Differential uptake of myocardial perfusion radiotracers in normal, infarcted, and acutely ischemic peri-infarction myocardium. Cardiovasc Res 1998;38:91-97
8. Casas O, Bragós R, Riu PJ, Rosell J, Tresànchez M, Warren M, Rodríguez-Sinovas A, Carreño A, Cinca J. In vivo and in situ ischemic tissue characterization using electrical impedance spectroscopy. Ann NYAcad Sci 1999;873:51-58
9. Fishbein MC, Maclean D, Maroko PR. The histopathological evolution of myocardial infarction. Chest 1978;73:843-849

Chapter 6

Development of a Silicon Based Electrical Impedance Sensor for the Detection of Acute Ischemia in Arrested Hearts

Contents

INTRODUCTION

Myocardial ischemia alters cellular passive electrical properties [1] which comprise intracellular and extracellular resistances as well as membrane capacitance and resistance. Alterations in the passive electrical properties can be recorded in in vivo models as an increase in tissue electrical impedance [2-5]. Specifically, resistance measured at 1kHz with four-point intramural platinum electrodes depicts a slight abrupt increase during the first 2 to 4 minutes, and a slower increase during the ensuing 30 minutes [2,4]. These changes have been attributed to the initial collapse of the extracellular space caused by the occlusion of the coronary artery and to the ensuing increase in extracellular resistance caused by osmotic cell swelling [6,4]. After approximately 30 minutes of coronary occlusion tissue resistance increases sharply and reaches a plateau value after about 60 minutes. This second phase of the increase in tissue resistance has been related to the decrease in gap junction conductance which leads to cellular electrical uncoupling and which has been pointed out as a precursor of irreversible damage in myocytes [7-9]. On the other hand, changes in the phase angle measured at 1 kHz are not patent till after 17 minutes of coronary occlusion. As with resistance, a sharp decrease in phase angle is observed after about 30 minutes of coronary occlusion which has also been attributed to the occurrence of cellular electrical uncoupling. Changes in phase angle have been shown to be more specific in determining the onset of cellular electrical uncoupling.

Although recent technical advances in the field of cardiac surgery have decreased cardiac mortality, a high number of postoperative deaths can be attributed to inappropriate myocardial protective techniques applied during the operative phase of extracorporeal circulation. For technical reasons, the heart must be artificially arrested and therefore, the electrocardiogram (ECG), which is currently used to detect myocardial injury, becomes unreliable in this situation. This has arised the possibility of developing a specific sensor for the detection of ischemic myocardium by measuring the myocardial tissue impedance changes during cardiac arrest.

The aim of this study is to asses the ability of a specifically designed silicon impedance sensor in detecting the onset of myocardial ischemia by comparison with the measures obtained with the 4-point platinum electrodes used for impedance measurements in experimental studies.

STUDY PROTOCOL AND DATA ANALYSIS

In vitro data were obtained from four samples of explanted left ventricle (group I). Comparison between the measures obtained with the silicon needle and with the 4-point probes was achieved by inserting both electrodes side by side in the explanted tissue. Tissue impedance at 1 kHz was measured with each probe every 20 seconds during 2 hours of postmortem (Fig 6.1).

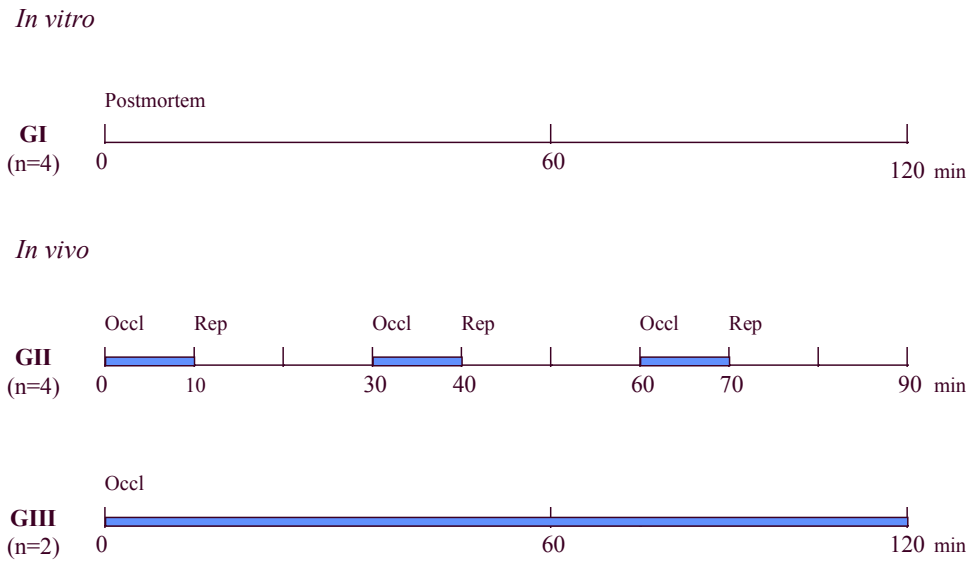

Fig 6.1 Schematic diagram depicting the in vitro and in vivo study protocols. In group I (GI), explanted myocardium electrical impedance was measured during postmortem. In group II pigs (GII), hearts were submitted to 10 minutes of LAD occlusion followed by 20 minutes of coronary reperfusion. This procedure was repeated three times. In group III pigs (GIII), hearts were submitted to 2 hours of LAD occlusion.

In vivo data were obtained from 6 pigs. In four pigs (group II), the LAD coronary artery was occluded during 10 minutes followed by 20 minutes of coronary reperfusion (Fig 6.1) to asses the performance of the silicon needle in the detection of the early changes in myocardial impedance after coronary occlusion.

This ischemia and reperfusion procedure was repeated three times. In two pigs (group III), the LAD coronary artery was occluded during two hours to asses the ability of the silicon needle in detecting the late changes of the ischemic myocardium electrical impedance. During LAD coronary occlusion and reperfusion, tissue impedance at 1 kHz was measured with each probe every 20 seconds. In all pigs, the normal myocardial impedance spectrum was measured at baseline with both the silicon needle and the 4-point platinum probe placed side to side.

RESULTS

Electrical impedance of explanted myocardium

As seen in Fig 6.2, resistivity and phase angle measured with both the silicon needle and the 4-point electrode depict comparable baseline values and a similar time course during 2 hours of postmortem.

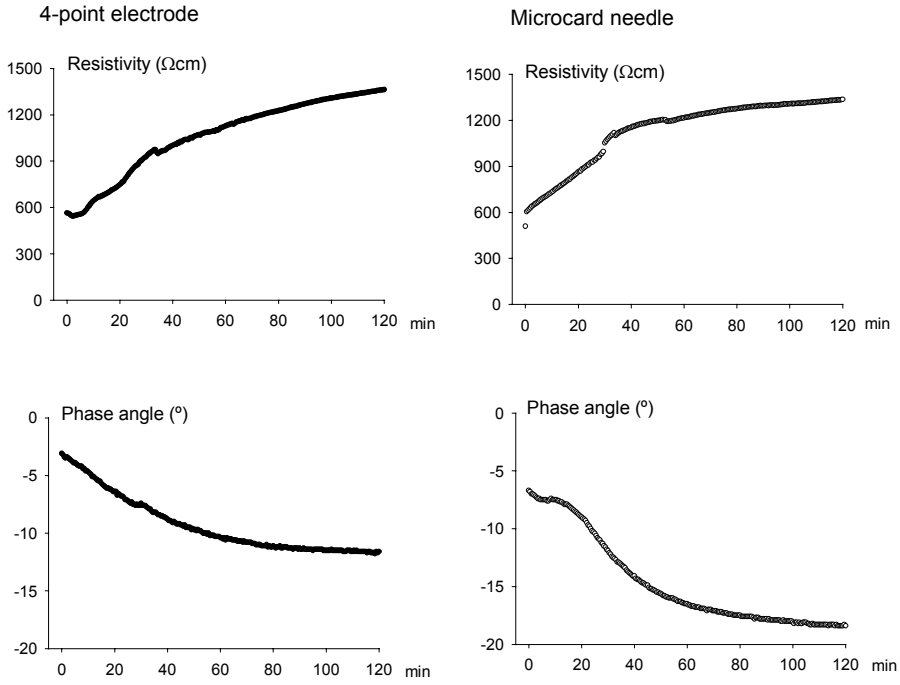

Fig 6.2 Evolution of the resistance and phase angle of explanted myocardium measured with the 4-point electrode and the silicon needle.

Electrical impedance of in vivo myocardium

Fig 6.3 shows the impedance spectrum of in vivo normal myocardium measured with the 4-point platinum electrodes and with the silicon needle. The impedance values obtained with both electrodes are similar.

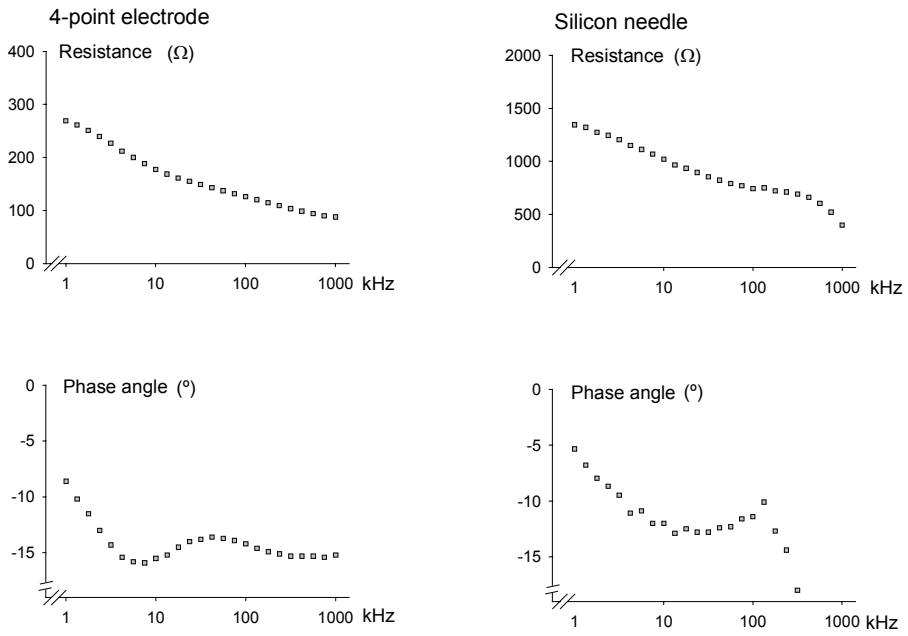

Fig 6.3 Resistance and phase angle spectra of *in vivo* normal myocardium measured with the 4-point probe and with the silicon needle.

However, measurement of tissue resistivity and phase angle at 1 kHz with the silicon sensor during LAD coronary occlusion in groups II and III, resulted in constant values during the whole period of ischemia. By contrast, impedance measurements performed with the 4-point probe resulted in the expected increase

of both myocardial resistance and phase angle after the onset of coronary occlusion in both groups.

DICUSSION

This study proves that the silicon impedance sensor is capable of measuring electrical impedance of myocardial tissue. Specifically, measurements of resistivity and phase angle of the explanted ventricle measured with both the silicon sensor and the 4-point probe depict comparable values, and a parallel evolution during the first two hours of postmortem. Furthermore, in vivo measurement of the normal myocardium impedance spectrum with both probes also results in similar values.

However, the silicon impedance sensor in its present form is not valid for the detection of the onset of myocardial ischemia since measures of both myocardial resistivity and phase angle during LAD coronary occlusion depict erratic values without a clear trend. The variability in the myocardial impedance measures could be caused by the large amount of bleeding that the needles produce when they are inserted into the myocardium. Since blood has a low resistivity [10] it could act as a short circuit between the four platinum electrodes of the silicon needle and the myocardium. In comparison to the silicon sensor, the standard 4-point needles produce less bleeding. In addition, the configuration of the 4-point probes also favours that the injected current pathway crosses larger volumes of myocardium even if bleeding does occur. By contrast, the planar disposition of the silicon needle platinum pads favours the deposition of blood between the pads and the myocardium. The traumatic effect caused by the silicon needles could be due to the sharp contour which the RIE (reactive ion etching) produces when the needles are cut. This problem could be solved by specifically designing a rugged contour of the needle. This solution is under development.

REFERENCES

1 Kleber AG, Riegger CB, Janse MJ. Electrical uncoupling and increase in extracellular resistance after induction of ischemia in isolated, arterially perfused rabbit papillary muscle. Circ Res 1987;61:271-279

2 Smith WT, Fleet WF, Johnson TA, Engle CL, Cascio WE. The Ib phase of ventricular arrhythmias in ischemic in situ porcine heart is related to changes in cell-to-cell electrical coupling. Circulation. 1995;92:3051-3060.

3 Ellenby MI, Small KW, Wells RM, Hoyt DJ, Lowe JE. On-line detection of reversible myocardial ischemic injury by measurement of myocardial electrical impedance. Ann Thorac Surg.1987;44:587-597.

4 Cinca, J., Warren, M., Carreño, A., Tresànchez, M., Armadans, L., Gómez, P., Soler-Soler, J. Changes in myocardial electrical impedance induced by coronary artery occlusion in pigs with and without preconditioning. Correlation with local ST segment potential and ventricular arrhythmias.Circulation. 1997; 96:3079-3086

5 van Oosterom A, de Boer RW, van Dam RTh. Intramural resistivity of cardiac tissue. Med Biol Eng Comput. 1979; 17: 337-343

6 Tranum-Jensen J, Janse MJ, Fiolet JWT, Krieger WJG, d'Alnoncourt CN, Durrer D. Tissue osmolality, cell swelling, and reperfusion in acute regional myocardial ischemia in the isolated porcine heart. Circ Res 1981;382:193-211

7 Murry CE, Jennings RB, Reimer KA. Preconditioning with ischemia: a delay of lethal cell injury in ischemic myocardium. Circulation 1986;74:1124-1136

8 Reimer KA, Lowe JE, Rasmussen MM, Jennings RB. The wavefront phenomenon os ischemic cell death. I. Myocardial infarct size vs duration of coronary occlusion in dogs. Circulation 1977;56:786-794

9 Hano T. Cellular electrical uncoupling and protection of ischemic myocardium. Thesis. Amsterdam 1993.

10 Bao JZ, Davis CC, Schmukler RE. Impedance spectroscopy of human erythrocytes: System calibration and nonlinear modeling. IEEE Trans Biomed Eng. 1993;40:364-378.

Chapter 7

Conclusions

1. The first half hour of acute ischemia is characterized by an immediate rise in tissue resistivity, whereas phase angle does not shift until 17 minutes of coronary occlusion have elapsed. Both resistivity and phase angle depict a sharp increase after 34 and 30 minutes of coronary occlusion, respectively, and reach plateau values after about 1 hour of ischemia. The beginning of the sharp increase in tissue impedance which has been attributed to the occurrence of cell to cell uncoupling is better delineated by the changes in phase angle than by the changes in resistivity.

2. Healed infarcted myocardium is characterized by an approximately 50% lower than normal tissue resistivity and a close to zero phase angle value. Furthermore, both variables depict a lack of frequency response in the 1 kHz to 1Mhz range.

3. The peak incidence of phase Ib ventricular arrhythmias temporally coincides with the sharp increase of tissue resistivity and phase angle in non precondtioned pigs. Myocardial preconditioning delays the maximum slope of the sharp increase of tissue resistivity and phase angle occurring during LAD occlusion, but the overall magnitude of the changes remains unaltered. In addition, a parallel delay of the peak of phase Ib arrhythmias is observed in the preconditioned hearts. This fact supports the hypothesis that cellular uncoupling might play a determinant role in the genesis of these arrhythmias.

4. The sharp rise in tissue resistivity is not accompanied by a decrease in epicardial ST segment elevation. However this does not rule out a possible role of cellular uncoupling in the decrease of the injury currents since cell to cell uncoupling likely takes place unhomogenously during a wide time interval. The low resistivity of the infarcted tissue is responsible for the enhanced transmission of current pulses applied across the necrotic myocardium in both in vitro and in vivo experimental conditions. This result supports the hypothesis that during periinfarction ischemia the ST segment elevation measured in epicardial electrodes overlying the infarcted tissue devoid of viable cells, is by passive electrical transmission of the injury currents that are generated in the border of the ischemic and normal tissue.

5. Measurement of myocardial impedance with a contact intracavitary percutaneous catheter permits differentiation of areas of transmural infarction from normal tissue by their particular impedance spectrum. Furthermore, phase angle measured at 316 kHz is the parameter that best differentiates both types of tissues.

6. The silicon based impedance sensor is capable of measuring the changes in myocardial resistivity and phase angle of explanted samples of ventricular tissue. However, the sensor in its present form does not allow the in vivo detection of the onset of acute ischemia by measurement of myocardial tissue electrical impedance.

In summary, both acute ischemic myocardium and the infarct scar are characterized by having specific values of tissue impedance. Therefore, measurement of infarcted myocardium electrical impedance could become an important diagnostic tool under various clinical circumstances. Furthermore, the altered passive electrical properties of these tissues play relevant roles in the pathogenesis of acute ischemic arrhythmias and of the transmission of injury currents across the necrotic scar.